약학박사 학위논문

Phenylboronic acid-decorated chondroitin sulfate A-based nanoparticles for solid tumor targeting and penetration

암 조직 표적화 및 침투를 위한 페닐보론산이 수식된 콘드로이틴황산염 기반 나노입자에 대한 연구

2016년 8월

서울대학교 대학원

약학과 약제과학 전공

이 재 영

ABSTRACT

Phenylboronic acid-decorated chondroitin sulfate A-based nanoparticles for solid tumor targeting and penetration

Jae-Young Lee

Department of Pharmaceutical Sciences

The Graduate School

Seoul National University

For effective chemotherapy, it is crucial for anti-cancer drugs to gain adequate access to tumor tissues. Despite numerous efforts to improve tumor targeting including drug-loaded nanoparticles (NPs), the homogeneous distribution of the drug molecules across the entire tumor tissue—particularly in the hypoxic region distant from functioning blood vessels—is not readily achieved due to unfavorable tumor microenvironments. In this thesis work, we hypothesized that the tumor-targetable chondroitin sulfate A (CSA)-based NP system with phenylboronic acid (PBA) moiety added (targeting the hypoxic region of tumors) may achieve enhanced tumor targeting and penetration of anticancer drugs, thereby improving anticancer efficacy. To test the validity of our hypothesis, we designed NPs that consist of PBA-functionalized amphiphilic chondroitin sulfate A (CSA) derivatives.

Briefly, deoxycholic acid (DOCA) was conjugated to the CSA backbone *via* ethylenediamine (EDA) linker, followed by the introduction of (3-aminomethylphenyl)boronic acid (AMPB) to CSA-DOCA. Successful synthesis of the developed graft copolymers was verified using proton nuclear magnetic resonance spectroscopy (^{1}H-NMR). The amphiphilic CSA-DOCA and CSA-DOCA-AMPB conjugates were loaded with doxorubicin (DOX). The resulting self-assembled NPs displayed an average diameter of approximately 200 nm with narrow size distribution, negative zeta potential, and spherical morphology. With the relatively high drug entrapment efficiency (approximately 80%), the developed NPs exhibited an increased DOX release at acidic pH (pHs 5.5 and 6.8) compared to at pH 7.4. Further experiments using confocal laser scanning microscopy and flow cytometry indicated that the developed NPs have an enhanced cellular uptake, penetration into spheroids and enhanced cytotoxic effects, likely *via* the CSA-CD44 and PBA-sialic acid interactions. Using near-infrared fluorescence (NIRF) imaging in mouse xenograft models, we also observed that the developed NPs have an improved tumor targeting and drug penetration *in vivo*, potentially leading to improved anti-tumor efficacy and reduced systemic toxicity of DOX. In summary, our results showed that the CSA-DOCA-AMPB NPs can achieve improved tumor targeting and drug penetration, thereby a promising nanoplatform potentially applicable to the treatment of various solid cancers.

Keywords: chondroitin sulfate A; tumor targeting; tumor penetration; anti-cancer drug delivery system; nanoparticles.

Student Number: 2011-21757

Contents

List of Tables

List of Figures

1. Introduction

1.1. Polymeric nanoparticles for anti-cancer drug delivery

Over the past few decades, technologies for polymeric nanoparticles (NPs) have made enormous strides together with the advances in polymer sciences. A great deal of researches have been carried out to develop elaborate NPs for various purposes, including drug delivery [1, 2] and medical imaging [3, 4]. Based on these previous reports, polymeric NPs are typically categorized according to their characteristic structural features. Among many kinds of polymeric NP formulations (i.e., nanocapsules, polymersomes, and dendrimers), polymeric micelles and nanogels were adopted in this study due to their excellent physicochemical properties for an anti-cancer drug delivery, which include appropriate size distribution, good loading capacity, in vivo safety, and the potential for functionalization [5]. Particularly, their nano-size can take advantage of the so-called enhanced permeability and retention (EPR) effect [6], which will be discussed in detail in section 1.5.

Polymeric micelles are usually defined as micelles made from amphiphilic block copolymers, which form nanostructures spontaneously in aqueous condition [7]. Typically, the hydrophobic parts of polymers are assembled, forming the single or multiple core(s) of micelles, while the hydrophilic parts are arranged outside to form a shell [5]. Meanwhile, nanogels are made up of cross-linked hydrophilic polymers; the cross-linking points can be covalent bonds or hydrophobic aggregations [8]. Sometimes, it is hard to clearly differentiate one from the other [9,

10]. When an amphiphilic polymer made from graft-copolymerization of hydrophobic moieties on a hydrophilic backbone is exposed to aqueous environment, it will spontaneously assembled ("self-assembled") to form NPs. The NPs developed from this polymer are likely to form a hydrophilic shell structure anchored to hydrophobic multicores, which can work as cross-linking points from a different perspective. In fact, the NPs formed by amphiphilic graft copolymers are ambiguously defined either as "polymeric micelles" or "nanogels" in the literature [11, 12]. Therefore, a designation, 'self-assembled NPs,' will be used, rather than 'polymeric micelles' or 'nanogels' in this thesis.

1.2. Self-assembled nanoparticle system

The self-assembled NPs, based on amphiphilic graft copolymers, have been widely investigated for anti-cancer drug delivery due to their capacity to entrap water-insoluble anti-cancer agents [5]. Theoretically, the drugs are loaded during the self-assembly of NPs, which begins with aggregation of amphiphilic polymer chains over the critical concentration in an aqueous condition [13]. The resulting nano-structures possess the two main supramolecular structures, an outer shell and inner multicores, which provide the distinctive features of the self-assembled NPs [13].

The shell forms a hydrophilic surface and makes the NPs hard to be recognized and eliminated by the mononuclear phagocyte system, also known as the reticuloendothelial system (RES), which in turn facilitates highly prolonged circulation in the blood stream when intravenously administered [14]. Also, the shell can serve as a barrier against hostile biological circumstances, such as enzymatic

degradation [5]. Furthermore, it can be utilized for cancer targeting and imaging with the conjugation of diverse functional moieties onto the surface. Many studies of self-assembled NPs have employed polysaccharides, including hyaluronic acid [15], chitosan [16], heparin [17], and pullulan [11], as a hydrophilic shell for their biomedically advantageous properties, which will be discussed in section 1.3.

On the other hand, the inner multicores provide hydrophobic cavities, which can be loaded with water-insoluble cargo molecules, thereby improving their solubility and/or absorption [13]. According to previous reports, many kinds of hydrophobic molecules, including cholesterol [18], fatty acids [16, 17], poly(ε-caprolactone) [19], poly(lactic-co-glycolic acid) [20], L-histidine [12], and acetic anhydride [21], were employed to synthesize amphiphilic polysaccharides. In this study, deoxycholic acid (DOCA), a bile acid, was used to make an amphiphilic graft copolymer, and its wide variety of usage can also be found in other research articles [11, 22, 23]. Moreover, clinical application of DOCA was approved by the U.S. Food and Drug Administration in 2015 for the treatment of submental fat (Kybella®; deoxycholic acid injection, 10 mg/mL) [24], which attests the relatively low toxicity of DOCA.

1.3. Polysaccharides for drug delivery and tumor targeting

Polysaccharides are carbohydrate polymers with linear or branched chain structure composed of monosaccharides linked together *via* glycosidic bonds. Polysaccharides are present in all living organisms and they fulfill a set of functional roles, such as constituting the body structure and serving as long-term energy storage

[25]. Recently, polysaccharides have attracted a great deal of attention in the field of pharmaceutical sciences for their characteristic material properties suitable for drug delivery systems [25-27]: polysaccharides seldom have and immunogenicity concerns; the glycosidic linkage renders them not only chemically-stable but also biodegradable *in vivo* by the hydrolytic enzymes; and they also possess functional groups, such as –OH, –COOH, and $–NH_2$, which are amenable to chemical modifications.

Apart from the reactive functional groups, polysaccharides can also possess negatively charged sulfate groups at various positions of sugar moieties [27]. These sulfated polysaccharides, including chondroitin sulfate, heparin/heparan sulfate, dermatan sulfate, keratan sulfate, dextran sulfate, carrageenans, fucoidans, and ulvan, are widely utilized in nanotechnological and pharmaceutical fields for their unique physico-chemical properties, along with the advantages mentioned above [25, 27]. In particular, the sulfated polysaccharides with animal origin, such as chondroitin sulfate, are located outside the plasma membrane and play key roles in cellular adhesion and cell-cell interaction [28]. They are also able to entrap endogenous molecules and serve as reservoir [29]. Similarly, the formulations prepared with those kinds of materials possibly mimic the cellular adhesion/interaction mechanisms and can be loaded with cargo molecules with high efficiency [25]. Based on these advantages, chondroitin sulfate was employed in this thesis work to fabricate a doxorubicin-loaded nanoparticle for tumor targeting.

1.4. Chondroitin sulfate and CD44 targeting

Chondroitin sulfate (CS) is one of the major glycosaminoglycans (GAGs) found in bones, cartilages, skin, extracellular matrix (ECM), nerve tissue, and blood vessels. CS consists of repeating disaccharide units of N-acetylgalactosamine (GalNAc) and glucuronic acid (GlcA) with sulfation [29]. There are four types of CS depending on the position of sulfate group(s) [30]: chondroitin-4-sulfate (CSA), Chondroitin-6-sulfate (CSC), Chondroitin-2,6-sulfate (CSD), and Chondroitin-4,6-sulfate (CSE). Particularly, CSA is extracted from mammalian tissues, such as bovine and porcine cartilages, and commercially available as sodium salts [30]. With numerous biological functions [29], including anti-coagulant, anti-thrombogenic, anti-oxidant, anti-atherosclerosis, and anti-inflammatory activities, CS has been widely used in biomedical approaches for cartilage repair and wound dressing [31]. Moreover, CS is involved in intracellular signal transduction, cell-cell recognition, and regulation of cell division and morphogenesis [28]. Most importantly, as a constituent of ECM, CS can interact with the cell surface receptor, CD44, which facilitates CS to serve as a tumor-homing moiety [28, 32].

CD44 is a family of transmembrane glycoproteins expressed on the various types of cells, such as lymphoid cells, myeloid cells, fibroblasts, epithelial cells, and endothelial cells, and is involved in cell adhesion and migration [33]. CD44 is able to bind with GAGs (including CS), collagen (type I and VI), laminin, and fibronectin [28, 33]. This binding ability of CD44, can assist cells to adhere to or to crawl along the ECM [34, 35]. CD44 comprises the extracellular link domain, membrane proximal stalk domain, transmembrane region, and cytoplasmic tail [36]. The link domain (amino acid [AA] 32–132) and the stalk domain (AA 150–158) play major roles in GAG binding [33, 37]. Furthermore, the binding ability can be modulated

according to the isoforms of CD44 and the extent of glycosylation; the insertion of variable exonic sequences into the stalk domain *via* tissue-specific alternative mRNA splicing determines the CD44 isoforms [35, 38]. Under physiological conditions, the cell adhesion and migration *via* CD44 are closely related to embryogenesis, tissue remodeling, wound healing, and leukocyte migration [33]. However, under the pathological conditions, particularly cancer, CD44 is overexpressed on the surface of cancer cells and associated with cancer cell growth and metastasis [34]. A number of recent studies extensively exploited this property of cancer cells to develop formulations based on CS for tumor-targeted drug delivery [30].

1.5. Tumor-targeting strategies and microenvironment of solid tumor

Despite the recent major advances in the anti-cancer therapy, a complete cure for cancer still has a long way to go. Frequent occurrences of drug resistance and tumor relapse have brought a wide variety of anti-cancer agents into failure [39]. When administered, the drugs are distributed not only to tumor lesion but also to the normal organs and tissues, which leads to the off-target accumulation of toxic anti-cancer agents. Therefore, unwanted side effects have been inevitable to achieve therapeutic concentrations in tumor. To overcome this challenge, two approaches have been actively explored; passive- and active-targeting strategies.

The passive-targeting strategy is based on the enhanced permeability and retention (EPR) effect, initially proposed by Matsumura and Maeda in 1986 [6]. Most of solid tumor tissues have leaky vasculature and impaired lymphatics, so that macromolecules large enough to avoid renal clearance (> 40 kDa) could extravasate

(endothelial pore size: 10–1000 nm) from the blood vessels and accumulate within the interstitial space of tumor [40]. Based on the leaky characteristics of tumor blood vessel, a variety of strategies using nano-sized formulations have been developed to achieve their tumor-selective accumulation [40, 41].

The active-targeting strategy utilizes tumor-specific ligands to improve targeting specificity. In a typical active-targeting strategy, tumor-specific ligands are introduced to nano-carriers, and each ligand interacts with the corresponding cell-surface molecule overexpressed in cancer cells [42]. This specific interaction results in the preferential accumulation in the tumor tissue and subsequent internalization into cancer cells through receptor-mediated endocytosis [43]. In this work, the interaction between the CS shell of the developed nanoparticles and the CD44 receptors overexpressed in the cancer cells was exploited for tumor targeting.

In spite of the enhanced tumor-targeting *via* the two strategies mentioned above, the highly complicated and heterogeneous characteristics of the tumor microenvironment often compromise the efficacy of treatments [44, 45]. Cancer cells tend to proliferate faster than blood vessel cells, resulting in a reduced vascular density within tumor [45]. Literally, some cancer cells are located far from the functioning blood vessels, thereby without sufficient access to oxygen and nutrients [46]. This hypoxic condition induces glucose fermentation, and concomitant metabolic wastes may lower the pH of extracellular region [45]. Moreover, the poorly organized vasculature and immature lymphatics of the tumor tissue break the balance of the flow of fluid, thereby causing an increased interstitial fluid pressure (IFP) and reduced convection [47]. The change in ECM structure and composition, and the higher packing density of cancer cells are also characteristics of tumors [45,

48]. These unfavorable properties of the tumor microenvironment are obstacles for the homogeneous drug delivery to the cancer cells located far from the blood vasculature [46].

1.6. Penetration into solid tumor using sialic acid and phenylboronic acid interaction

The homogeneous distribution of anti-cancer agents throughout the whole tumor tissue is of great importance [44]. Particularly, a poor accessibility of these agents into tumor stem cells (TSCs), which are involved in tumor regeneration, easily leads to tumor relapse [49]. Recently, various strategies targeting tumor-microenvironment to overcome the unfavorable barriers and deliver anti-cancer agents in sufficient amount to whole cancer cells, including TSCs, have been studied [44, 46, 47].

In this work, a strategy targeting sialic acids (SAs), carbohydrate antigens of cancer cells, was adopted. These sugar epitopes are overexpressed on the cancer cell surface glycan chains, of which expression was found to be increased particularly in hypoxic regions of solid tumors [50]. As mentioned in the previous section, the hypoxic conditions occur in the region distant from functioning blood vessels, implying SA-targeting could be an efficient tumor penetration strategy [45]. Moreover, hypoxic cancer cells often have great potential to develop resistance to anti-cancer agents and are thought to have more TSC-like properties [45, 49]. Therefore, this targeting strategy will increase the chances of complete cancer eradications, due to the enhanced delivery efficiency of anti-cancer agent to the deep

hypoxic regions in tumor tissues.

In an attempt to exploit the aberrant glycophenotypes of tumors, a phenylboronic acid (PBA) decoration was employed. PBA functional group can interact with SA to form stable six-membered ring complexes [51]. Although PBA is able to form complex with other sugars, such as glucose, mannose, and galactose, its trigonal binding is usually unstable and readily hydrolyzed at the lower pH values than the p*K*a values of those sugars [52]. The acidic tumor microenvironment, due to the hypoxic fermentation, compromises the complex stability other than that with SA [45]. This high affinity of SA with PBA is attributed to the additional metastable binding sites and intramolecular stabilization effect through B–O and B–N interactions [52]. Additionally, PBA is free from toxicity and immunogenicity concerns, which surely are advantageous properties for *in vivo* use [53].

1.7. Spheroid model: an evaluation tool for tumor penetration

Multicellular spheroids are three-dimensionally (3D) cultured cancer cell aggregates, of which morphology is spherical with a mean diameter under 1 mm [45]. Usually, spheroids are prepared by suspension culture in spinner, and they grow without attachment to culture plates or supporting materials [54, 55]. Compared to 2D cultured cells (monolayer model), the spheroids mimic the *in vivo* environment more closely. For example, when an anti-cancer agent is administered to solid tumors, it will diffuse into the tumor microenvironment, building-up a large gradient in drug concentration in reverse proportion to the distance from blood vessels, whereas in an *in vitro* experiment with the monolayer culture model, all cancer cells will be

exposed to the same amount of drug with the same manner [45]. This large discrepancy accounts for the poor clinical translation of the results from 2D cultured cells. The spheroid model, however, reflects the features of solid tumors; it develops concentration gradients of nutrients and oxygen, ECM, and tight junctions between cells [56]. In addition, the cells in the outer region of spheroids proliferate faster than that of core region, which is in accordance with the tumor cells adjacent to blood vessels, which grow faster [45]. These properties make the spheroid model become a useful tool for the evaluation of the penetration efficiency of drugs or formulations. Also, this model can more accurately predict the anti-tumor efficacy in *in vivo* situation than the 2D culture model, by reflecting not only the tumor microenvironment but also cell contact effect [57]. Thus, in this work, the tumor penetration efficiency and anti-tumor efficacy of the developed PBA-decorated CS-based NPs were evaluated in the spheroid model.

2. Materials and Methods

2.1. Materials

Chondroitin sulfate A (CSA; 37 kDa average molecular weight), deoxycholic acid (DOCA), ethylenediamine (EDA), (3-aminomethylphenyl)boronic acid hydrochloride (AMPB), *N*-ethyl-*N*′-(3-dimethylaminopropyl)carbodiimide hydrochloride (EDC), *N*-hydroxysuccinimide (NHS), triethylamine (TEA), agarose, and deuterium oxide (D_2O) were purchased from Sigma-Aldrich Co. (St. Louis, MO, USA). Doxorubicin hydrochloride (DOX·HCl) was obtained from Boryung Pharmaceutical Co., Ltd. (Seoul, Korea). The near-infrared fluorescent dye, FCR-675 (Cy5.5-amine), was purchased from BioActs (Incheon, Korea). Dimethyl sulfoxide-d_6 (DMSO-d_6) was purchased from Cambridge Isotope Laboratories Inc. (Andover, MA, USA). DMSO was bought from DAEJUNG chemicals & metals Co., Ltd. (Seoul, Korea). Formamide and *N*,*N*-dimethylformamide (DMF) were purchased from Junsei Chemical Co., Ltd. (Tokyo, Japan). Dulbecco's modified Eagle's medium (DMEM), RPMI 1640 cell culture medium, penicillin, streptomycin, and fetal bovine serum (FBS) were obtained from Gibco Life Technologies, Inc. (Carlsbad, CA, USA). All other reagents were of analytical grade.

2.2. Synthesis and characterization of CSA-DOCA conjugate

Synthesis of DOCA-conjugated CSA (CSA-DOCA) was carried out through EDC/NHS-mediated amide bond formation. DOCA was modified with EDA

to form aminoethyldeoxycholamide (EtDOCA) for further reaction with the carboxylic acid group of CSA. In brief, DOCA (1.177 g) was dissolved in methanol (MeOH; 5 mL). After hydrochloric acid (36.5–38.0%; 184 μL) was added, the mixture was stirred for 6 h at 60 °C under reflux. The pale-yellow colored solution was then concentrated using a rotary evaporator and dried under vacuum. The resulting white powder was washed with ice-cold water and lyophilized to obtain methyldeoxycholate (DOCA-OMe). DOCA-OMe was dissolved in EDA (50 molar equivalents). The solution was stirred for 8 h at 120 °C under reflux. The resulting yellowish solution was precipitated with an excess amount of water. The mixture was filtered and the filtrate, EtDOCA, was washed with water thrice and freeze-dried. Then, CSA was modified with EtDOCA, a hydrophobic moiety, to produce amphiphilic CSA-DOCA. Briefly, CSA (100 mg) was dissolved in formamide (20 mL) at 80 °C and cooled to room temperature. EDC (61.3 or 122.6 mg) and NHS (36.8 or 73.6 mg) were added and the mixture was stirred for 20 min at room temperature to activate the carboxylic acid group of CSA. EtDOCA (34.8 or 69.6 mg) dissolved in DMF (20 mL) was slowly added to the CSA solution. The mixture was stirred for 20 h at room temperature, dialyzed against methanol for 1 day, a water/methanol mixture (25–75%, v/v) for 1 day, and water for 1 day. After lyophilization, the products—CSA-DOCA conjugates with different EtDOCA/CSA feed ratios—were stored at 2~8 °C for further experiments.

For the evaluation of DOCA content in CSA-DOCA, ^{1}H-nuclear magnetic resonance (^{1}H-NMR; Varian FT-500 MHz; Varian Inc., Palo Alto, CA, USA) analysis was used. CSA-DOCA was dissolved in a DMSO-d_6 and D_2O mixture (3:1, v/v) for ^{1}H-NMR analysis. The DOCA weight percentage (w/w, %) in CSA-DOCA

was calculated using a simple linear regression method with ^{1}H-NMR spectra of DOCA/CSA physical mixtures (w/w; 0.05, 0.1, 0.2, and 0.5). The regression line was constructed based on the correlation between the weight ratio (DOCA/CSA) of the physical mixtures and the ratio of corresponding ^{1}H-NMR peak area (0.6/1.8 ppm).

2.3. Preparation and characterization of DOX-loaded CSA-DOCA NPs

DOX (base form) was prepared by removing HCl according to the previous report [58]. Briefly, DOX·HCl (100 mg) was dissolved in DMSO (10 mL) containing TEA (0.12 mL). After stirred for 12 h at room temperature, the resulting solution was lyophilized. The dark-red colored powder, DOX, was used as a hydrophobic model drug in this work.

To prepare DOX-loaded CSA-DOCA (CSA-DOCA/DOX) NPs, DOX (1 mg) and CSA-DOCA (7 mg) were dissolved in a mixture of DMSO and double deionized water (DDW) (1 mL; 1:1, v/v). The solvent was evaporated under a N_2 gas stream for 5 h at 70 °C. The drug and polymer composite film was reconstituted with DDW (1 mL) and filtered through a syringe filter with 0.45 μm pore size (Minisart RC 15, Sartorius Stedim Biotech GmbH, Goettingen, Germany). DOX entrapment efficiency (EE) was measured by dissolving the CSA-DOCA/DOX NPs with DMSO. The DOX content was analyzed using a high-performance liquid chromatography (HPLC) (Waters Co., Milford, MA, USA), equipped with a reverse phase C18 column (Xbridge RP18, 250 mm × 4.6 mm, 5 μm; Waters Co.), a separation module (Waters e2695), and a fluorescence detector (Waters 2475). The mobile phase was

composed of 10 mM potassium phosphate buffer (pH 2.5) and acetonitrile containing 0.1% TEA (71:29, v/v). The flow rate was set at 1.0 mL/min, and the injection volume was 20 μL. The eluent was monitored at the excitation and emission wavelengths of 470 and 565 nm, respectively. The morphology of the CSA-DOCA/DOX NPs was observed by transmission electron microscopy (TEM; JEM 1010; JEOL, Tokyo, Japan). The samples were stained with 2% (w/v) phosphotungstic acid solution, placed on a copper grid coated with carbon film, and dried at room temperature for 30 min. The particle size, polydispersity index, and zeta potential of the developed NPs were measured by an electrophoretic light scattering (ELS) method (ELS-Z; Otsuka Electronics, Tokyo, Japan) according to the manufacturer's protocol.

To investigate the self-aggregation behavior of CSA-DOCA, the critical aggregation concentration (CAC) was determined by measuring the fluorescence intensity with pyrene as a fluorescence probe. Aliquots (0.3 mL) of pyrene solutions in acetone were added to tubes and the organic solvent was evaporated under nitrogen (N_2) gas stream for 1 h at 60 °C. Various concentrations of CSA-DOCA solutions (5.0×10^{-4} to 1.0×10^{-1} mg/mL) were added to obtain the final pyrene concentration of 6.0×10^{-7} M. The emission fluorescence intensities of pyrene at 373 nm and 384 nm was measured at an excitation wavelength of 335 nm using a spectrofluorometer (FP-6500, Jasco Co., Tokyo, Japan). For the determination of CAC, the fluorescence intensity ratio at 373 nm to 384 nm was calculated and plotted against the logarithm of the CSA-DOCA concentration.

2.4. In vitro cytotoxicity tests of CSA-DOCA conjugate in MDA-

MB-231 cells

MDA-MB-231 cells (human breast adenocarcinoma cell line; Korean Cell Line Bank, Seoul, Korea) were cultured in RPMI 1640, containing 300 mg/L of L-glutamine, supplemented with 10% (v/v) heat inactivated FBS, 1% (v/v) penicillin (100 U/mL), and streptomycin (0.1 mg/mL). Cells were maintained in a 5% CO_2 atmosphere with 95% relative humidity at 37 °C and trypsinized at 70–80% confluency for the following experiment. The cytotoxicity of CSA-DOCA conjugate was evaluated using a 3-(4,5-dimethyl-2-yl)-5-(3-carboxymethoxyphenyl)-2-(4-sulfophenyl)-2H-tetrazolium (MTS)-based assay. MDA-MB-231 cells were seeded onto 96-well plates at a density of 1.0×10^4 cells per well and incubated with various concentrations (2, 5, 10, 20, 50, and 100 μg/mL) of CSA-DOCA conjugate. After incubating for 24, 48, or 72 h at 37 °C, the cells were treated with CellTiter 96 AQueous One Solution Cell Proliferation Assay Reagent (Promega Corp., Madison, WI, USA) and incubated for an additional 4 h at 37 °C according to the manufacturer's manual. The absorbance was measured at a wavelength of 490 nm using a UV/Vis spectrophotometer (EMax Precision Microplate Reader, Molecular Devices Corp., Sunnyvale, CA, USA).

2.5. In vitro cellular uptake studies of DOX-loaded CSA-DOCA NPs in MDA-MB-231 and NIH3T3 cells

The cellular uptake efficiency and cellular distribution of the DOX-loaded CSA-DOCA NPs were evaluated by confocal laser scanning microscopy (CLSM).

MDA-MB-231 (Korean Cell Line Bank) cells were cultured with the same culture medium mention in section 2.4. NIH3T3 (mouse embryonic fibroblast cell line; Korean Cell Line Bank) cells were cultured with DMEM supplemented with 10% (v/v) heat inactivated FBS and 1% (v/v) penicillin (100 U/mL) and streptomycin (0.1 mg/mL). Cells were maintained in a 5% CO_2 atmosphere and 95% relative humidity at 37 °C and were harvested for the following experiments at 70–80% confluency. For the CLSM observation, MDA-MB-231 or NIH3T3 cells were seeded on culture slides (BD Falcon, Bedford, MA, USA) at a density of 1.0×10^5 cells per well (surface area: 1.7 cm^2 per well) and incubated for 24 h at 37 °C. Free DOX or DOX-loaded NPs were added at a DOX concentration of 5 μg/mL. To confirm the inhibitory effect of CSA on the cellular uptake of NPs, free CSA solution (0.05 or 0.5 mg/mL) was co-treated with NPs. After incubating for 0.5, 2, or 6 h (only 6 h for NIH3T3 cells), the cells were washed with phosphate-buffered saline (PBS; pH 7.4) for three times and fixed with a 4% (v/v) formaldehyde solution for 10 min. After the samples were dried, the VECTASHIELD mounting medium with 4′,6-diamidino-2-phenylindole (DAPI; H-1200, Vector laboratories, Inc. CA, USA) was loaded onto the culture slides. Subsequently, they were observed using CLSM (LSM 710, Carl-Zeiss, Thornwood, NY, USA).

2.6. Biodistribution of DOX-loaded CSA-DOCA NPs

Near infrared fluorescence (NIRF) imaging technique was employed to evaluate the biodistribution of the CSA-DOCA/DOX NPs. Cy5.5, a fluorescence probe, was conjugated to CSA-DOCA *via* amide bond formation. In brief, CSA-

DOCA (50 mg) was dissolved in a mixture of DMSO and DDW (25 mL; 1:1, v/v). The carboxylic acid group of CSA-DOCA was activated with EDC (168.1 mg) and NHS (20.5 mg). Cy5.5 (0.1 mg; FCR-675, amine-functionalized form), dissolved in 0.1 mL of DMSO, was slowly added and stirred for 1 day. The mixture was dialyzed for 2 days against DDW to remove the unreacted Cy5.5, EDC, and NHS. After lyophilization, the cyan-colored product, Cy5.5-CSA-DOCA, was obtained. The DOX-loaded Cy5.5-CSA-DOCA NPs were were prepared according to the method in section 2.3. To make an MDA-MB-231 tumor-xenografted mouse model, female BALB/c nude mice (5 weeks old, Charles River, Wilmington, MA, USA) were reared in a light-controlled room maintained at 22 ± 2 ℃ with 55 ± 5% relative humidity (Animal Center for Pharmaceutical Research, College of Pharmacy, Seoul National University, Seoul, Korea). The experimental protocols for the animal study were approved by the Animal Care and Use Committee of the College of Pharmacy (Seoul National University). An MDA-MB-231 cell suspension (1.5×10^6 cells in 0.1 mL cell culture media) was injected into the back of the mice. When the tumor reached a volume of 150−200 mm^3, the NIRF imaging was performed. The tumor volume (V, mm^3) was calculated by the following formula: $V = 0.5 \times \text{longest diameter} \times (\text{shortest diameter})^2$. For verifying the tumor targetability of the developed NPs, Cy5.5-CSA-DOCA/DOX NPs (0.18 mL) with or without free CSA solution (5 mg per mice) were injected into the tail vein of the mouse. *In vivo* NIRF images were taken by using Optix MX3 (ART Advanced Research Technologies Inc., Saint-Laurent, QC, Canada). Cy5.5 was excited with the laser diode at 670 nm wavelength. Whole-body images were taken at 1, 3, 6, and 24 h post-injection.

2.7. Synthesis and characterization of CSA-DOCA-AMPB conjugate

Synthesis of CSA-DOCA-AMPB was performed using EDC/NHS-mediated amide bond formation. CSA-DOCA (100 mg) was dissolved in a co-solvent of DMSO and water (20 mL; 3:1, v/v). EDC (23.0 or 46.0 mg) and NHS (13.8 or 27.4 mg) were added. The mixture was stirred for 20 min to activate the carboxylic acid group of CSA-DOCA. AMPB (7.5 or 15.0 mg) dissolved in a co-solvent of DMSO and water (20 mL; 3:1, v/v) was added dropwise to the activated CSA-DOCA solution. The mixture was stirred for 20 h at room temperature, dialyzed against water for 2 days, and lyophilized. The resulting white powder, CSA-DOCA-AMPB, was stored at 2–8 ℃ for further experiments.

For the determination of AMPB content in CSA-DOCA-AMPB, ^{1}H-NMR (Varian FT-500 MHz) was used. CSA-DOCA, AMPB, and CSA-DOCA-AMPB were dissolved in a mixture of DMSO-d_6 and D_2O (3:1, v/v) for ^{1}H-NMR analysis. A simple linear regression method based on the relationship between the weight ratio of AMPB/CSA-DOCA physical mixtures (w/w; 0.01, 0.02, 0.05, and 0.10) and the ratio of ^{1}H-NMR peak area (7.7/1.8 ppm) was employed.

To further confirm the conjugation of AMPB to CSA-DOCA, the fluorescence intensity of AMPB was measured from CSA-DOCA-AMPB. CSA-DOCA and CSA-DOCA-AMPB were dissolved in the mixture of methanol and DDW (1:1, v/v) at 20 μM concentration. A corresponding amount of AMPB was dissolved in a solvent with the same composition, of which concentration was determined according to the AMPB content in CSA-DOCA-AMPB calculated by

the ^{1}H-NMR analysis. The fluorescence emission spectrum of each compound was monitored using a spectrofluorometer (FP-6500, Jasco Co.) at an excitation wavelength of 270 nm. The fluorescence emission was scanned in the range of 280–500 nm. Band width values for the excitation and emission wavelengths were 3 nm and 5 nm, respectively.

2.8. Preparation and characterization of DOX-loaded CSA-DOCA-AMPB NPs

To prepare CSA-DOCA/DOX and CSA-DOCA-AMPB/DOX NPs, DOX (1 mg) and each polymer (7.5 mg) were dissolved in a mixture of DMSO and water (1 mL; 1:1, v/v), and the solvent was evaporated under an N_2 gas stream for 5 h at 70 °C. The drug and polymer composite film was resuspended in DDW (1 mL) and filtered through a syringe filter (0.45 μm pore size; Minisart RC 15). To measure the EE of DOX, the NPs were dissolved with DMSO, and the DOX content was analyzed using high-performance liquid chromatography (HPLC) system mentioned in section 2.3. The morphology of the DOX-loaded NPs was observed using TEM (JEM 1010). The samples were stained with 2% (w/v) phosphotungstic acid solution, placed on the copper grid coated with carbon film, and dried at room temperature. The particle size, polydispersity index, and zeta potential of the NPs were measured using electrophoretic light scattering (ELS-Z) according to the manufacturer's protocol. To evaluate the stability of the developed NPs, the changes in their mean diameters were monitored in PBS (pH 7.4) and serum (50% FBS) conditions for 24 h.

2.9. In vitro release tests

The DOX release behaviors of CSA-DOCA/DOX and CSA-DOCA-AMPB/DOX NPs were evaluated. Aliquots (150 μL) of the NP dispersions were loaded into dialysis tubes (mini-GeBAflex tubes; Gene Bio-Application Ltd., Kfar Hanagide, Israel) with a molecular weight cut-off (MWCO) of 14 kDa. Each tube was immersed into a release medium (10 mL; PBS) with various pH values (pH 7.4 for CSA-DOCA/DOX NPs and pH 5.5, 6.8, or 7.4 for CSA-DOCA-AMPB/DOX NPs) and agitated at 50 rpm at 37 °C. Aliquots (200 μL) of the release media were collected at predetermined times (1, 2, 4, 6, 8, 24, 48, 72, 96, and 120 h), and the same volume of fresh medium was replenished at each time point. The released amount of DOX was determined using the HPLC method mentioned in section 2.3.

2.10. In vitro cytotoxicity tests of CSA-DOCA and CSA-DOCA-AMPB conjugates in A549 cells

A549 cells (human lung adenocarcinoma cell; Korean Cell Line Bank) were cultured in RPMI 1640, containing 300 mg/L of L-glutamine, supplemented with 10% (v/v) heat inactivated FBS, 1% (v/v) penicillin (100 U/mL), and streptomycin (0.1 mg/mL). Cells were maintained in a 5% CO_2 atmosphere with 95% relative humidity at 37 °C and trypsinized at 70–80% confluency for the following cytotoxicity studies. The cytotoxicity of the CSA-DOCA and CSA-DOCA-AMPB conjugates was evaluated using an MTS-based assay. A549 cells were seeded onto 96-well plates at

a density of 1.0×10^4 cells per well and incubated with various concentrations (1, 2, 5, 10, 20, 50, and 100 μg/mL) of each conjugate. After incubating for 24, 48, or 72 h at 37 °C, the cells were treated with CellTiter 96 AQueous One Solution Cell Proliferation Assay Reagent (Promega Corp.) and incubated for an additional 4 h at 37 °C. The absorbance was measured at a wavelength of 490 nm using a UV/Vis spectrophotometer (EMax Precision Microplate Reader, Molecular Devices Corp.).

2.11. In vitro cellular uptake studies in 2D-cultured A549 cells

A549 cells were cultured in the same conditions described in the previous section. To exclude the effect of possible cytotoxicity of AMPB and SA on cellular uptake, the cell viability was first evaluated after incubating AMPB and SA at their experimental concentration (500 μM for both compounds). A549 cells were seeded onto 96-well plates at a density of 1.0×10^4 cells per well and incubated with each compounds for various time periods (1, 6, 24, 48, 72, and 96 h). The cell viability was measured using the MTS-based assay described in section 2.11.

Cellular distribution and uptake efficiency of DOX were assessed using CLSM. A549 cells were seeded onto 4-chamber culture slides (BD Falcon) at a density of 1.0×10^5 cells per well (surface area: 1.7 cm^2 per well) and incubated 24 h at 37 °C. The DOX solution or DOX-loaded NP suspension (as DOX, 100 μM) was added to the cells. To verify the PBA-SA interaction, SA (500 μM) was pre-incubated with the NP suspension, or AMPB (500 μM) was pre-incubated with the cells prior to adding the NP suspension to the cells. Cells were incubated for 1 h, washed with PBS (pH 7.4) thrice, and fixed in 4% (v/v) formaldehyde solution for

10 min. After the samples were dried, the VECTASHIELD mounting medium with DAPI (Vector laboratories, Inc.) was loaded onto the culture slides. Cells were observed using CLSM (LSM 710, Carl-Zeiss).

Cellular uptake efficiency was quantitatively analyzed using flow cytometry. A549 cells were seeded onto 6-well plates at a density of 6.0×10^5 cells per well. After incubating for 24 h at 37 °C, cell culture media were replaced with DOX solution or DOX-loaded NPs (as DOX, 100 μM) and incubated for 15 or 60 min. SA (500 μM) or AMPB (500 μM) was pre-incubated using the same method above. After washing with PBS (pH 7.4) three times, the cells were trypsinized and centrifuged. The cell pellets were resuspended with PBS including FBS (2%, v/v). The cellular uptake efficiency of DOX was quantitatively determined by a FACSCalibur fluorescence-activated cell sorter (FACS^{TM}) equipped with CELLQuest software (Becton Dickinson Biosciences, San Jose, CA, USA).

2.12. In vitro tumor penetration studies in 3D-cultured A549 spheroids

For the preparation of the A549 spheroid model, A549 cells were seeded onto round-bottomed 96-well plates coated with a thin layer of agarose (2% [w/v] in Hank's balanced salt solution) at a density of 500 cells per well, and cultured in the same medium as described in section 2.10. The cells were incubated in 5% CO_2 atmosphere with 95% relative humidity at 37 °C with gentle agitation, and the culture medium was replaced every other day. A549 spheroids were harvested after 5–7 days when reaching a diameter of around 300 μm. To evaluate the tumor penetration of

the CSA-DOCA/DOX and CSA-DOCA-AMPB/DOX NPs, the NPs were labeled with Cy5.5 and their distribution within the A549 spheroid was observed using CLSM. Cy5.5-amine was conjugated to CSA-DOCA and CSA-DOCA-AMPB with the same synthetic method described in section 2.6, except for the increased Cy5.5 to polymer feed ratio (0.2 mg to 50 mg). Cy5.5-tagged CSA-DOCA/DOX or CSA-DOCA-AMPB/DOX NPs were incubated with the A549 spheroids for 0.5, 4, and 24 h at a Cy5.5 concentration of 5 μg/mL; the Cy5.5 concentration was determined using a fluorescence spectrophotometer (SpectraMax M5 multi-mode microplate reader, Molecular Devices Corp.) at excitation and emission wavelengths of 675 nm and 700 nm, respectively. SA (500 μM) was pre-incubated with the NP suspension and AMPB (500 μM) was pre-incubated with the spheroids prior to adding the NP suspension to the spheroids. After incubating, the spheroids were washed with PBS (pH 7.4) thrice and fixed with 4% (v/v) formaldehyde solution for 10 min. The spheroids were then placed onto a coverslip bottom dish and embedded in a 2% agarose solution. The Z-stack images were taken using CLSM (LSM 710, Carl-Zeiss).

2.13. In vitro anti-tumor efficacy tests in 2D-cultured A549 cells

A549 cells were cultured in the same conditions described in section 2.10. For the evaluation of *in vitro* anti-tumor efficacy, A549 cells were seeded onto 96-well plates at a density of 1.0×10^4 cells per well and treated with the free DOX or DOX-loaded NPs at various DOX concentrations (0.1, 0.2, 0.5, 1, 2, 5, and 10 μg/mL). After incubating for 24, 48, or 72 h at 37 °C, the cells were treated with

CellTiter 96 AQueous One Solution Cell Proliferation Assay Reagent (Promega Corp.) and incubated for an additional 4 h at 37 °C. The absorbance was measured at a wavelength of 490 nm using a UV/Vis spectrophotometer (EMax Precision Microplate Reader, Molecular Devices Corp.). IC_{50} values were calculated using CompuSyn software (Version 1.0; ComboSyn, Inc., NJ, USA).

2.14. In vitro anti-tumor efficacy tests in 3D-cultured A549 spheroids

A549 spheroids were cultured in the same conditions described in section 2.12. When the diameter of spheroids reached around 300 μm, DOX solution or DOX-loaded NPs (corresponding to 50 μg/mL DOX concentration) was added. SA (500 μM) was pre-incubated with the NP suspension, or AMPB (500 μM) was pre-incubated with the spheroids prior to adding the NP suspension to the spheroids. After 24 h of incubation, the drug solution or drug-loaded NP suspension was replaced with fresh cell culture media. Morphology of the A549 spheroids was observed using optical microscopy (IX70, Olympus, Tokyo, Japan) over 4 days. The volume (V, mm^3) of spheroid was calculated with the following formula: $V = 0.5 \times \text{longest diameter} \times (\text{shortest diameter})^2$.

2.15. Biodistribution of DOX-loaded CSA-DOCA-AMPB NPs

The biodistribution of CSA-DOCA/DOX and CSA-DOCA-AMPB/DOX NPs was evaluated in the A549 tumor-xenografted mouse model using the NIRF

imaging system described in section 2.6. Female BALB/c nude mice (5-weeks-old, Charles River, Wilmington, MA, USA) were injected with A549 cell suspension (2 × 10^6 cells in 0.1 mL cell culture media) on the lower dorsal region, close to the hind limb. The Mice were maintained in a light-controlled room kept at a temperature of 22 ± 2 °C with a relative humidity of 55 ± 5% (Animal Center for Pharmaceutical Research). The experimental protocols for the animal study were approved by the Animal Care and Use Committee of the College of Pharmacy (Seoul National University). NIRF imaging was performed on the mice with tumor volumes of 150−200 mm^3. The tumor volume (V, mm^3) was calculated using the following formula: V = 0.5 × longest diameter × (shortest diameter)^2. The Cy5.5-conjugated CSA-DOCA/DOX or CSA-DOCA-AMPB/DOX NPs were injected into the tail vein of the mouse at a dose of 0.12 mg/kg (Cy5.5 amount per body weight) and the fluorescence intensity of whole body region were scanned at 1, 3, 6, and 24 h post-injection. A laser diode with a wavelength of 670 nm was used for the excitation of Cy5.5. At 24 h post-injection, the mice were euthanized, and their organs (liver, kidneys, spleen, heart, and lungs) and tumors were dissected, of which fluorescence intensities were also monitored to evaluate the distribution of NPs.

To compare the penetration and retention of NPs in tumor tissue, volumetric data were generated using OptiView 3D Reconstruction module (version 3.2; ART Advanced Research Technologies Inc.), which can construct fluorescence intensity in 3D space from time-resolved fluorescence measurements. The fluorescence intensity of the region of interest (ROI) (i.e. the tumor tissue) was reconstructed three-dimensionally, and the penetration into the tumor tissue was estimated by comparing the sliced planes of the ROI.

2.16. In vivo anti-tumor efficacy tests

The anti-tumor efficacy of the CSA-DOCA/DOX and CSA-DOCA-AMPB/DOX NPs was evaluated in the A549 tumor-xenografted mouse model. The animal model was prepared with the same method mentioned in the previous section. The experimental protocols used in these animal studies were approved by the Animal Care and Use Committee of the College of Pharmacy (Seoul National University). After the tumor volume reached 50–100 mm^3, the tumor size and the body weight were measured. The tumor volume (mm^3) was calculated using the formula described in the previous section. The experimental groups were as follows: control (no-treatment), DOX solution-treated, CSA-DOCA/DOX NP-treated, and CSA-DOCA-AMPB/DOX NP-treated. DOX (at a dose of 5 mg/kg) was injected intravenously on day 4, 7, 9, and 11. The tumor volume and body weight of the mice were measured for 24 days.

Tumors and hearts of the mice were dissected at the end of the test, and fixed with 4% (v/v) formaldehyde for histological staining. After paraffin embedding and sectioning (6 μm), the tissues were deparaffinized and hydrated with ethanol. The tumor and heart sections were stained with hematoxylin and eosin (H&E). For tumor sections, the apoptotic effect was also evaluated by a terminal deoxynucleotidyl transferase dUTP nick end labeling (TUNEL) assay. Chromogen diaminobenzene (DAB) was incubated for color development, and DNA fragmentation resulting from apoptotic signaling cascades was detected.

2.17. Statistical analysis

All experiments in this study were performed at least three times, and the data are presented as mean ± standard deviation (SD). Statistical analyses were carried out using the two-tailed t-test or analysis of variance (ANOVA) with *post-hoc* test (IBM SPSS Statistics software, version 21.0; IBM Corp, Armonk, NY, USA), and $p < 0.05$ was considered significantly different.

3. Results

3.1. Synthesis and characterization of CSA-DOCA conjugate

For the synthesis of CSA-DOCA conjugate, DOCA was conjugated to CSA with an EDA linker *via* amide bond formation (Fig. 2). DOCA-OMe was first synthesized using the Fischer–Speier esterification method [59], where DOCA and MeOH was refluxed at an elevated temperature (60 °C) in the presence of an acid catalyst (HCl). The formation of the methyl ester was confirmed by ^{1}H-NMR (Fig. 3). In the spectrum of DOCA-OMe, the signals indicating carboxylic acid group (a; 11.9 ppm [1H, -COO*H*]) and methoxy group (c, 3.6 ppm [3H, -COOCH_3]) disappeared and appeared, respectively, compared with the spectrum of DOCA. The methoxy group, as a leaving group, was then replaced with EDA by nucleophilic substitution. The formation of EtDOCA was confirmed by the signals indicating the amide group (d, 7.7 ppm [1H, -CON*H*CH_2-]) and ethylene group (e, 3.0 ppm [2H, -NHCH_2-]; f, 2.5 ppm [2H, -CH_2NH_2]). Afterwards, CSA-DOCA was conjugated with EtDOCA through amide bond formation using EDC and NHS coupling reaction. As shown in the ^{1}H-NMR spectrum of CSA-DOCA (Fig. 4B), the signals indicating the C-18 methyl group (b, 0.6 ppm) and the ethylene group (2.5–3.0 ppm) of EtDOCA imply successful introduction of DOCA to CSA. To calculate the DOCA content, a simple linear regression method with ^{1}H-NMR spectra of DOCA/CSA physical mixtures was used (Fig. 5). Representative signals of C-18 methyl group of DOCA (b, 0.6 ppm) and *N*-acetyl protons of CSA (g, 1.8 ppm) were used to plot the regression line, where the X and Y axes represent the weight ratio of DOCA to CSA

and the integration ratio of their characteristic peaks, respectively. The average content of the DOCA introduced in CSA-DOCA was calculated to be 8.92 or 11.5% (w/w) for the one with the low or high EtDOCA/CSA feed ratio, respectively (Table 1).

3.2. Preparation and characterization of DOX-loaded CSA-DOCA NPs

The amphiphilic CSA-DOCA was prepared *via* the modification of hydrophilic CSA with a hydrophobic DOCA, which is able to self-assemble in an aqueous condition. The CAC values of CSA-DOCA measured with the help of fluorescence probe, pyrene, was 5.53 μg/mL. DOX, a hydrophobic drug, was loaded into the CSA-DOCA NPs by a solvent-evaporation method. The DOX-loaded NPs made from the CSA-DOCA with the low DOCA content showed more advantageous properties for tumor-targeted drug delivery than those with the high DOCA content in terms of particle size, polydispersity index, and EE (Table 2). Therefore, only the CSA-DOCA NPs from the polymer with the low DOCA content were used for the following experiments. The developed NPs showed a mean diameter of around 230 nm with narrow size distribution. After the DOX loading with high EE (> 85%), the zeta potential value of the NPs was slightly increased to be -21.52 ± 1.06 mV compared with that of the blank (drug-free) NPs (-23.07 ± 1.17 mV). The spherical shapes of blank and DOX-loaded NPs were observed by TEM imaging (Fig. 7). The mean diameter values of the developed NPs from the TEM images correspond with those measured by the ELS method.

3.3. In vitro cytotoxicity tests of CSA-DOCA conjugate

The cytotoxicity of the blank CSA-DOCA NPs was evaluated in MDA-MB-231 cells using an MTS-based assay (Fig. 8). The cell viability (%) was measured after incubating the various concentrations of CSA-DOCA (up to 100 μg/mL) for 24, 48, and 72 h. As shown in Fig. 8, a negligible cytotoxicity was observed in all experimental conditions (cell viability > 95.9%), which guarantees the safe *in vivo* application of CSA-DOCA, as well as the absence of misleading effects from the cytotoxicity on the results of the following experiments.

3.4. In vitro cellular uptake studies of DOX-loaded CSA-DOCA NPs in MDA-MB-231 and NIH3T3 cells

The intracellular distribution of the CSA-DOCA/DOX NPs was evaluated using CLSM observation (Fig. 9). MDA-MB-231 and NIH3T3 were employed as CD44 positive and negative cell lines, respectively, to confirm the interaction between the CSA shell of the developed NPs and the CD44 receptors on the cell surface. The free CSA was used as a competitive inhibitor for the interaction. Fig. 9 shows the fluorescence intensity of the cells after the cellular uptake study. The red fluorescence intensity (indicating DOX uptake) in the NP-treated groups was increased as the incubation time extended from 0.5 to 6 h. After 6 h of incubation with the CSA-DOCA/DOX NPs, the DOX uptake in MDA-MB-231 cells was obviously decreased by the CSA co-treatment. The uptake inhibitory effect of free

CSA in MDA-MB-231 cells became stronger as its concentration increased. However, the co-treatment of free CSA made no difference in the cellular uptake of the CSA-DOCA/DOX NPs in NIH3T3 cells. In addition, the lower uptake efficiency of CSA-DOCA/DOX NPs was observed in NIH3T3 cells compared with that of MDA-MB-231 cells.

3.5. Biodistribution of DOX-loaded CSA-DOCA NPs

Biodistribution of the DOX-loaded CSA-DOCA NPs was investigated using NIRF imaging technique (Fig. 10). Cy5.5-tagged NPs were intravenously administered to the MDA-MB-231 tumor-xenografted mouse model. Based on the result of the cellular uptake studies in section 3.5, it was expected that the *in vivo* tumor disposition of CSA-DOCA NPs could be enhanced *via* the CSA-CD44 interaction and hampered by a pre-treatment of free CSA. As evidenced by Fig. 10, the average fluorescence intensity of tumor region was more than 1.31-folds higher in the group without CSA pre-treatment than in the group with CSA pre-treatment throughout the monitoring period ($p < 0.05$). Moreover, at 24 h post-injection, the enhanced accumulation of CSA-DOCA NPs to the tumor than to the other organs was barely observed when the free CSA was pre-administered.

3.6. Synthesis and characterization of CSA-DOCA-AMPB conjugate

CSA-DOCA-AMPB was successfully synthesized by conjugating AMPB

to CSA-DOCA through the amide bond formation using the EDC/NHS coupling reaction (Fig. 11). The product from the high AMPB/CSA-DOCA feed ratio precipitated during the dialysis step in water, indicating its aggregation, rather than the formation of self-assembled NPs, in an aqueous condition. Therefore, only the product with the low AMPB/CSA-DOCA feed ratio was selected for the further experiments (Table 3).

The characteristic peaks of AMPB (j and k, 7.3-7.4 ppm; h and i, 7.6-7.7 ppm) in the ^{1}H-NMR spectrum of CSA-DOCA-AMPB indicate successful synthesis of CSA-DOCA-AMPB (Fig. 12). To calculate the AMPB content, a simple linear regression method with ^{1}H-NMR spectra of AMPB/CSA-DOCA physical mixtures was used. Representative signals of AMPB (7.7 ppm; the 2- and 6-positions of the phenyl ring) and CSA-DOCA (0.6 ppm; the C-18 methyl group of DOCA) were used to construct the regression line, whereby the X and Y axes represent the weight ratio and the integration ratio of the peaks, respectively (Fig. 13). The AMPB content in CSA-DOCA-AMPB was 2.35% (w/w) according to the ^{1}H-NMR data (Table 3).

The conjugation of AMPB to CSA-DOCA was further confirmed by measuring the fluorescence of AMPB. The inset of Fig. 14 shows the concentration-dependent emission spectra of AMPB, where the maximum emission was observed at 297 nm. A linear correlation between the maximum fluorescence intensity and the concentration of AMPB was revealed (data not shown). The emission spectra of CSA-DOCA-AMPB also exhibited its maximum emission at the same wavelength value. Moreover, the fluorescence intensity of CSA-DOCA-AMPB was comparable to that of free AMPB of the corresponding concentration (calculated by ^{1}H-NMR analysis). This consistency in the emission fluorescence intensities supported the

successful attachment of AMPB to the CSA-DOCA conjugate.

3.7. Preparation and characterization of DOX-loaded CSA-DOCA-AMPB NPs

The CSA-DOCA-AMPB/DOX NPs, as well as the CSA-DOCA/DOX NPs as control group, were prepared using the same solvent evaporation method in section 3.2, except for the slight change in the drug-to-polymer weight ratio. After the reconstitution of the drug-polymer composite with DDW, the DOX-loaded NPs with nano-sized mean diameters (206–229 nm), negatively-charged zeta potentials (-24.58 to -20.10 mV), narrow size distributions (evaluated from the low polydispersity index values), and high drug entrapment efficiency values (70–80%), were prepared (Table 4 and Fig. 15A). Spherical shapes of the NPs were observed by TEM imaging (Fig. 15B).

The stability of CSA-DOCA and CSA-DOCA-AMPB NPs was evaluated in the high ionic strength condition (PBS; pH 7.4) and the serum condition (FBS; 50%, v/v) to show the robust design of the developed formulation. Both of the formulations maintained their initial nano-sized mean diameters and size distribution profiles during the 24 h of incubation in PBS or FBS, implying their good stability in the presence of salts and serum proteins (Fig. 16).

3.8. In vitro release tests

The drug release behavior from the developed NPs was evaluated under

different pH conditions (Fig. 17). Sustained DOX release profiles from the formulations were observed for 5 days. In the physiological pH condition (pH 7.4), the released amounts of DOX from the formulations at day 5 were 38.3 ± 3.0% and 37.2 ± 1.1% for the CSA-DOCA/DOX and CSA-DOCA-AMPB/DOX NPs, respectively. The AMPB decoration of CSA-DOCA NPs made no significant difference in the DOX release pattern ($p > 0.05$). In acidic pH conditions, the CSA-DOCA-AMPB NPs showed enhanced drug release profiles; on day 5, the released amounts of DOX at pH 5.5 and pH 6.8 were 1.91- and 1.26-fold higher than that at pH 7.4 ($p < 0.05$). The increased DOX release under the acidic conditions could be attributed to the enhanced DOX solubility and the reduced interaction between DOX and the NP structure.

3.9. In vitro cytotoxicity tests of CSA-DOCA and CSA-DOCA-AMPB conjugates in A549 cells

The cytotoxicity of the CSA-DOCA and CSA-DOCA-AMPB conjugates was assessed in A549 cells (Fig. 18). The cell viability (%) at various concentrations of each polymer (1–100 μg/mL) after 24, 48, and 72 h of incubation was measured using the MTS-based assay. As can be seen in Fig. 18, both polymers showed a negligible cytotoxicity in all the experimental conditions (cell viability > 96.0%), which ensures their safe *in vivo* application.

3.10. In vitro cellular uptake studies in 2D-cultured A549 cells

The cytotoxicity of SA and AMPB was evaluated in A549 cells prior to carry out the cellular uptake studies. SA and AMPB exhibited a negligible cytotoxicity in all experimental conditions (cell viability > 94.3%), implying there was no possible misleading effects from the cytotoxicity on the results of the following experiments (Fig. 19B).

The DOX uptake was evaluated in 2D-cultured A549 cells using CLSM and flow cytometry. As shown in Fig. 19A and 20, the fluorescence intensity of the CSA-DOCA-AMPB NP-treated group was higher than that of the CSA-DOCA NP-treated group ($p < 0.05$), indicating the PBA modification of the NPs improved their cellular uptake efficiency. Moreover, the DOX uptake of the CSA-DOCA-AMPB NP-treated group was drastically decreased by the intervention of free SA or AMPB ($p < 0.05$), indicating the interaction between SA and PBA could be a possible mechanism for the enhanced cellular uptake of the CSA-DOCA-AMPB NPs. In the CSA-DOCA NP-treated group, however, no significant uptake inhibitory effects from SA and AMPB was observed. Nonetheless, both NP-treated groups exhibited a higher cellular uptake efficiency than drug solution-treated group due to the receptor-mediated endocytosis [60].

3.11. In vitro cellular uptake studies in 3D-cultured A549 spheroids

The tumor penetrating ability of the developed NPs was evaluated using the A549 tumor spheroid model. The internalization of the Cy5.5-CSA-DOCA/DOX and Cy5.5-CSA-DOCA-AMPB/DOX NPs into the spheroid was observed and quantified using CLSM. Fig. 21, the Z-stack images of the spheroids, clearly showed

that the NPs (red color; fluorescence intensity of Cy5.5) internalized deeper into the core of spheroids as the incubation time elapsed. As shown in Fig. 22, the mean fluorescence intensity of the Z-stack image was stronger in the CSA-DOCA-AMPB NPs-treated group than in the CSA-DOCA NPs-treated group ($p < 0.05$). The enhancement in penetration efficiency of the CSA-DOCA-AMPB NPs disappeared after the pre-treatment of SA or AMPB ($p < 0.05$), which is in good accordance with the result in section 3.10.

3.12. In vitro anti-tumor efficacy tests in 2D-cultured A549 cells

In vitro anti-tumor efficacy of the developed NPs was assessed in 2D-cultured A549 cells using the MTS-based assay. As shown in Fig. 23, the rank-order of cytotoxicity after 48 or 72 h incubation was CSA-DOCA-AMPB/DOX NPs > CSA-DOCA/DOX NPs > DOX solution, which corresponds with that of cellular uptake efficiency (section 3.10). The IC_{50} value of each formulation was significantly different from each other after 48 or 72 h of incubation ($p < 0.05$) (Table 5). The 24 h incubation groups showed too low toxicity at the experimental DOX concentrations to calculate the IC_{50} values.

3.13. In vitro anti-tumor efficacy tests in 3D-cultured A549 spheroids

The *in vitro* anti-tumor efficacy was evaluated by measuring the alteration in the volume of A549 spheroid after the treatment of each formulation. As shown

in Fig. 24, the spheroid growth was inhibited after the DOX solution or DOX-loaded NP treatment, whereas the control group (no treatment) increased 4.34-folds in volume after the 4 days of incubation. Compared with DOX solution-treated group, the mean spheroid volumes of CSA-DOCA/DOX NP- and CSA-DOCA-AMPB/DOX NP-treated groups at day 4 were reduced to 73.0% and 47.8%, respectively ($p < 0.05$); the rank-order of the anti-tumor efficacy measured in spheroid model was the same with that in 2D-culture model. By the pre-treatment of SA or AMPB, the spheroid growth inhibitory effect of the CSA-DOCA-AMPB/DOX NPs was compromised, showing the similar effect of the CSA-DOCA NPs. This implies the enhanced spheroid penetration efficiency (see section 3.11) was closely related to the improved anti-tumor efficacy of the CSA-DOCA-AMPB/DOX NPs in the spheroid model.

3.14. Biodistribution of DOX-loaded CSA-DOCA-AMPB NPs

Biodistribution of CSA-DOCA-AMPB/DOX NPs after an intravenous administration was evaluated in A549 tumor-xenografted mouse model using NIRF imaging technique (Fig. 25–27). Cy5.5-conjugated NPs were injected into the mouse tail vein and the fluorescence intensity was measured for 24 h. The Cy5.5-CSA-DOCA/DOX NPs were used as a control group of this experiment. As shown in Fig. 25, the average fluorescence intensity of tumor region in the Cy5.5-CSA-DOCA-AMPB/DOX NP-treated group was at least 1.68-fold higher than that in the Cy5.5-CSA-DOCA/DOX NP-treated group throughout the monitoring period ($p < 0.05$). Moreover, the fluorescence intensity of the tumor region was higher than any other

organs in the whole body images from both groups at 24 h post-injection. This enhanced accumulation of the developed NPs to tumor was further confirmed by *ex vivo* experiment. Fig. 26 shows that both NPs were mainly accumulated in liver and kidneys, as well as tumor. However, the fluorescence intensity ratios of tumor-to-liver and tumor-to-kidneys were 1.78-fold and 1.35-fold higher in Cy5.5-CSA-DOCA-AMPB/DOX NP-treated group than that in Cy5.5-CSA-DOCA/DOX NP-treated group ($p < 0.05$), respectively, indicating the AMPB modification of CSA-DOCA NPs improved their tumor targetability.

Furthermore, the *in vivo* tumor penetration efficiency of the developed NPs was assessed using the 3D image analysis program. By reconstructing the volume data and fluorescence intensity of the tumor region, the NP disposition inside the tumor was compared between the two groups. As shown in Fig. 27, the Cy5.5-CSA-DOCA-AMPB/DOX NP-treated group exhibited 3.1-fold higher fluorescence intensity in the sliced plane of tumor region than the Cy5.5-CSA-DOCA/DOX NP-treated group ($p < 0.05$), implying more efficient tumor penetration and/or retention of the PBA-functionalized NPs.

3.15. In vivo anti-tumor efficacy tests

The *in vivo* anti-tumor efficacy of the developed NPs was evaluated by measuring the tumor growth after intravenous administration of each formulation into the A549 tumor-xenografted mouse model (Fig. 28). The tumor volume and body weight were monitored for 24 days. As shown in Fig. 28A, the tumor volume of the CSA-DOCA-AMPB/DOX NP-treated group at day 24 was smaller than those

of the other groups ($p < 0.05$). However, the CSA-DOCA/DOX NP-treated group showed no significant difference in tumor volume compared to DOX solution-treated group, implying a mere enhancement in tumor targetability was not enough to achieve the improved *in vivo* anti-tumor efficacy in this investigation. Moreover, the increased apoptosis was observed in CSA-DOCA-AMPB/DOX NP-treated group, compared to the other groups (Fig. 29A and 29C). Although the body weight values of all groups exhibited no significant difference ($p > 0.05$), the mean body weight of the DOX solution-treated group was slightly lower than those of the other groups. This implies the tumor-targeting strategy using the developed NP formulation could reduce the systemic toxicity of DOX, which is supported by the histological assay result (Fig. 29B); the reduced cardiac toxicity of DOX was observed when administered as the NP formulations.

4. Discussion

In this study, the CSA-DOCA-AMPB/DOX NPs were prepared and evaluated in terms of the solid tumor targeting and penetration, based on the CSA-CD44 interaction and the PBA-SA complexation, respectively (Fig. 1). For the preparation of the NPs, CSA was hydrophobically modified with DOCA as a first step to form an amphiphilic graft copolymer, namely CSA-DOCA. Among the four types of CS mentioned in section 1.4, CSA was selected due to its mammalian origins, such as from bovine and porcine connective tissues, whereas CSC and CSE are usually extracted from shark and squid, respectively [30]. CSA has carboxylic acid and hydroxyl groups which can easily undergo chemical modifications; there have been various studies, in which CS was conjugated with the hydrophobic molecules, including prednisolone [61], cholesterol [62], histamine [63], L-lactide [64], poly(ε-caprolactone) [19], and acetic anhydride [65], to develop self-assembled NPs. For the synthesis of CSA-DOCA, the carboxylic acid functional groups from CSA and DOCA were linked together using EDA, a diamine linker, *via* amide bond formation. Though both of the CSA-DOCAs with different DOCA contents formed NPs in the aqueous environment, only the CSA-DOCA with the low DOCA content was selected for the further experiments because of its better physicochemical properties mentioned in section 3.2.

The self-assembly behavior of the CSA-DOCA conjugate was evaluated by measuring its CAC value in the aqueous condition. The CAC value of CSA-DOCA was much lower than the critical micelle concentration of low-molecular-weight surfactants [66]. Considering the dilution in biological fluids after the *in vivo*

administration, this low CAC value guarantees the structural stability of the CSA-DOCA NPs. Additionally, the negative zeta potential values of the developed NPs also support the formation of the shell structure with CSA, containing the negatively-charged carboxylate and sulfate groups. After loading DOX to the CSA-DOCA NPs using the solvent-evaporation method, their physicochemical properties, including the mean diameter, polydispersity index, and zeta potential values showed no significant difference ($p > 0.05$) from those of the blank CSA-DOCA NPs. Interestingly, the EE of DOX was higher than expected from the previous studies with polymeric micelles and nanogels [5]. This could be attributed to the electrostatic interaction between the amine group of DOX and carboxylate and sulfate groups of CSA, as well as the hydrophobic interaction with DOCA [67]. The slight increase in zeta potential values after DOX loading also accords well with this result. The spherical morphology of the developed NPs was also maintained after the DOX loading.

In the *in vitro* cytotoxicity test, CSA-DOCA revealed a negligible cytotoxicity in the physiologically-meaningful concentration range. As mentioned earlier, both CSA and DOCA are almost free from toxicity and considered as safe materials for *in vivo* applications [24, 30]. A lot of evidence from the previous studies support that the polysaccharide-based drug delivery systems have relatively low toxicity and good biocompatibility [25, 27]. The result of CSA-DOCA can guarantee the absence of misleading effects from the cytotoxicity of the polymer itself on the results of the following experiments.

The cellular uptake studies of the CSA-DOCA/DOX NPs were then carried out to evaluate their tumor targetability. The interaction between CS and CD44

receptor has been reported in the previous report [28]. In order to verify whether the CSA in the NP structure can serve as a tumor targeting moiety, the MDA-MB-231, human breast adenocarcinoma cells, and NIH3T3, mouse embryonic fibroblast cells, were adopted as the CD44 positive and negative cell lines, respectively. As expected, the cellular uptake of the CSA-DOCA/DOX NPs were inhibited in the MDA-MB-231 cells with the co-treatment of the free CSA, whereas no inhibitory effect was observed in the NIH3T3 cells. This confirmed the interaction between the CSA shell of the NPs and the CD44 receptors expressed on the cancer cell surface during the cellular uptake of the CSA-DOCA NPs. Meanwhile, the degrees of DOX uptake were somewhat different between the DOX solution-treated group and the DOX-loaded NP-treated group. This could be attributed to the difference in the cellular uptake mechanism; according to the previous reports, the DOX solution passively diffuses into the cells, whereas the DOX-loaded NPs were taken up by the cells *via* receptor-mediated endocytosis [68].

To further confirm the CSA-CD44 interaction in the *in vivo* condition, the tumor disposition was evaluated after the intravenous injection of the developed NPs to the MDA-MB-231 tumor-xenografted mouse model. With the 24 h of the NIRF imaging study, it was demonstrated that the CSA-DOCA/DOX NPs were predominantly distributed to the tumor than to the other organs, and this tumor targetability was decreased with the co-administration of free CSA. This indicates the interaction between CSA and CD44, as well as the EPR effect from the NP structure itself, can contribute to the *in vivo* tumor targeting of CSA-DOCA/DOX NPs.

After the successful preparation and evaluation of the CSA-DOCA/DOX

NPs, the PBA functional group was introduced to the CSA-DOCA backbone *via* amide bond formation between the amine group of AMPB and the carboxylic acid group of CSA for tumor penetrating performances. The synthesized CSA-DOCA-AMPB conjugate was also capable of self-assembling into NPs in the aqueous environment. CSA-DOCA-AMPB NPs were then loaded with DOX using the same solvent evaporation method, resulting in similar physicochemical properties with those of the CSA-DOCA/DOX NP in terms of the mean diameter, the polydispersity index, the zeta potential value, and the EE. Among them, the mean diameter is one of the key factors that determine the *in vivo* fate of NPs; it has been reported that NPs with around 200 nm of the mean diameter can take the best advantage of EPR effect, leading to accumulation in the tumor region without being eliminated by the RES [40]. Meanwhile, the NPs encounter a variety of blood components like plasma proteins after their intravenous administration, which can cause the aggregation of the NPs. The aggregates much larger than 200 nm would reduce the tumor targetability and cause off-target side effects in normal tissues and organs. The developed NPs in this study, however, maintained their initial particle sizes in the PBS and serum conditions for at least 24 h, which guarantees their prolonged circulation in blood stream, providing the efficient passive targeting.

In addition, a sustained drug release behavior of NPs is another advantageous characteristic for the anti-cancer drug delivery system. Until the NPs being delivered to the tumor region, it is desirable for the loaded drug to be retained in the NPs, rather than to be released and cause the unwanted systemic toxicity. On the other hand, after the NPs being distributed to the tumor site and taken up by the tumor cells, the loaded drug should be released to exert its anti-cancer effect. In this

study, the developed NPs exhibited sustained release patterns of DOX for 5 days, and its release was markedly increased at the acidic environment (pH 5.5 and 6.8) compared to that at the neutral condition (pH 7.4). As mentioned in section 1.5, the hypoxic tumor microenvironment induces the glycolysis and lactic acid fermentation, and the metabolic wastes acidify the extracellular region of tumors (pH 6.5-6.9). Additionally, the endolysosomal system, to which the NPs taken up by the cancer cells will initially be exposed, also provides an acidic environment (pH 5.5). This implies the developed NPs would exhibit enhanced drug release in the tumor than in the blood pool or normal tissues (pH 7.4). This enhanced release profile of DOX from developed NPs in acidic condition could be obtained not only from increased solubility of DOX, but also from the reduced interaction between DOX and CSA. Under the acidic pH condition, the protonated carboxylic acid groups in CSA are increased and the electrostatic interaction between the amine group of DOX could be decreased, leading to the enhanced DOX release [67].

The cellular uptake efficiency of the CSA-DOCA-AMPB/DOX NPs was then evaluated in the A549 cells. As mentioned in section 1.6, the PBA functional group can interact with the SA group on the surface of cancer cells forming the hexagonal complex. Accordingly, in the 2D-cultured model, the DOX uptake of the CSA-DOCA-AMPB/DOX NP-treated group was enhanced compared to that of the CSA-DOCA/DOX NP-treated group. To verify this interaction between the CSA-DOCA-AMPB/DOX NPs and A549 cells, the NPs were pre-treated with the free SA to make their PBA groups ineffective, while the A549 cells were pre-incubated with the free AMPB to block their surface SA groups. Noteworthy is that this blockade of PBA-SA interaction with the pre-treatment of AMPB or SA, decreased the DOX

uptake level of the CSA-DOCA-AMPB/DOX NPs to the degree of that of the CSA-DOCA/DOX NPs. This implies the interaction between PBA and SA plays a key role in the cellular uptake of CSA-DOCA-AMPB/DOX NPs. Additionally, the effect of AMPB-modification on tumor penetration performance was investigated in the 3D-cultured A549 spheroid model. Cy5.5 was conjugated to the developed NPs and its fluorescence emission was observed to evaluate the NP distribution to the spheroids, as the DOX distribution could not give the accurate information about the NP localization. More specifically, the experiment was carried out over 24 h, which is an enough time for the loaded DOX to be released significantly out of the NPs to the spheroids, leading to a poor colocalization of DOX and NPs in the spheroids. Moreover, the wavelength of the DOX emission fluorescence is not long enough to completely pass through the body of spheroids. As expected from the result of the cellular uptake study with the 2D-cultured A549 cells, the NP penetration efficiency was higher in the PBA-modified NP-treated group than in the unmodified NP-treated group. Moreover, the tumor penetration of CSA-DOCA-AMPB/DOX NPs was impeded by the pre-treatment of free SA or AMPB. This indicates the interaction between PBA and SA is a main reason for the enhancement in the spheroid penetration, which is in good accordance with the previous reports on the PBA-functionalized NPs [50, 52, 69].

As described in section 1.5, the homogeneous distribution of anti-cancer agents to the whole tumor region could be one of the key factors for the curative cancer treatment. Though the developed NPs showed a qualified success in terms of homogeneous NP distribution, the enhancement in tumor penetration of the PBA-modified NPs clearly exhibited the improved anti-cancer efficacy in A549 cells.

Interestingly, in the 2D-cultured A549 cells, the rank-order of cytotoxicity of the tested formulations was in the same order of their cellular uptake efficiency. As each of the blank formulations showed negligible cytotoxicity, the increased anti-cancer efficacy of the developed NPs could be attributed to their enhanced cellular uptake *via* the CSA-CD44 and the AMPB-SA interactions. Similarly, the increased spheroid penetration efficiency of the developed NPs caused the enhanced spheroid growth inhibition; the spheroid growth inhibitory effect of the CSA-DOCA-AMPB/DOX NPs was higher than that of the CSA-DOCA/DOX NPs, and the superiority in anti-cancer efficacy of the PBA-modified formulation was decreased with the pre-treatment of AMPB or SA. Thus, again this can be explained by the interaction between the PBA groups of the developed NPs and the SA groups on the A549 cell surface.

To evaluate the *in vivo* tumor targetability and penetration efficiency, the A549 tumor-xenografted mouse model was employed and the distribution of the Cy5.5-tagged NPs after intravenous administration were observed using the NIRF imaging technique. As expected, the tumor disposition of the AMPB-conjugated NPs were much increased, compared with that of the unconjugated NPs. This indicates that the PBA functionalization provides another driving force for the tumor-targeting to the CSA-DOCA/DOX NPs, in addition to the CSA-CD44 interaction. Given that the co-treatment of free SA or AMPB inhibited the cellular uptake of CSA-DOCA-AMPB/DOX NPs in A549 cells, the PBA-SA interaction could contribute to the increased accumulation of the PBA-modified NPs to the A549 tumors in the *in vivo* situation. Moreover, according to the volumetric data of the Cy5.5 fluorescence intensity in tumor, the CSA-DOCA-AMPB/DOX NPs showed improved distribution

inside the tumor than the CSA-DOCA/DOX NPs, as expected from the *in vitro* data with the A549 spheroids. The PBA groups on the CSA-DOCA-AMPB/DOX NPs could make it possible for the NPs to overcome the unfavorable properties of the tumor microenvironment, which are described in section 1.5, and be retained in the tumor region for a prolonged time by interacting with SA.

This enhancement in tumor targeting and penetrating performances added up to the improvement in the *in vivo* therapeutic outcome of the developed NPs. Indeed, the CSA-DOCA-AMPB/DOX NPs exhibited better anti-tumor efficacy than the other groups in the A549 tumor xenografted mouse model. Noteworthy is that the CSA-DOCA/DOX NPs revealed almost the same tumor growth inhibitory effect compared to bare DOX, notwithstanding their improved *in vitro* anti-cancer efficacy and *in vivo* tumor targetability. Meanwhile, the adverse side effects of DOX in terms of loss in body weight and cardiotoxicity were alleviated in both of the CSA-DOCA/DOX NP- and CSA-DOCA-AMPB/DOX NP-treated groups. In other words, the CSA-DOCA/DOX NPs were readily accumulated to the tumor region than to the other organs and tissues, showing the decreased the systemic toxicity, but they failed to achieve any better anti-tumor efficacy than the drug alone. This clearly means that the efficient penetration of cancer therapeutics inside the tumor, as well as the gross tumor targeting to tumor regions, is of great importance in cancer therapy. Therefore, the CSA-DOCA-AMPB/DOX NPs with their decent tumor targeting and penetrating performances, can be a promising nanoplatform for the treatment of solid tumors.

5. Conclusion

In this study, the PBA-functionalized CSA-DOCA graft copolymer-based NPs were prepared for solid tumor targeting and penetration. DOCA, as a hydrophobic moiety, was introduced to the hydrophilic CSA backbone, followed by the conjugation of AMPB. The resulting amphiphilic CSA-DOCA and CSA-DOCA-AMPB conjugates were loaded with DOX to form the self-assembled NPs of around 200 nm mean diameter with narrow size distribution, negative zeta potential, and spherical morphology. With the relatively high EE, the developed NPs exhibited an enhanced DOX release at acidic pH (pH 5.5 and 6.8) than at physiological pH (pH 7.4). In the 2D-cultured cell monolayer and 3D-cultured spheroid models, the CSA-DOCA-AMPB/DOX NPs exhibited improved cellular uptake and spheroid penetration, respectively, *via* the CSA-CD44 and PBA-SA interactions. The *in vivo* tumor targeting and penetrating performances of the CSA-DOCA-AMPB/DOX NPs were evaluated using NIRF imaging in the tumor-xenografted mouse model, of which successful demonstration added up to the improvement in their anti-cancer efficacy compared with that of the CSA-DOCA NPs or bare DOX. In conclusion, the CSA-DOCA-AMPB/DOX NPs with the tumor targeting and penetrating performances have a great potential for the treatment of solid tumors.

6. References

[1] Elsabahy M, Wooley KL. Design of polymeric nanoparticles for biomedical delivery applications. Chemical Society reviews. 2012;41:2545-61.

[2] Hubbell JA, Chilkoti A. Nanomaterials for Drug Delivery. Science. 2012;337:303-5.

[3] Tang J, Sheng Y, Hu H, Shen Y. Macromolecular MRI contrast agents: Structures, properties and applications. Progress in Polymer Science. 2013;38:462-502.

[4] Doane TL, Burda C. The unique role of nanoparticles in nanomedicine: imaging, drug delivery and therapy. Chemical Society Reviews. 2012;41:2885-911.

[5] Kowalczuk A, Trzcinska R, Trzebicka B, Müller AHE, Dworak A, Tsvetanov CB. Loading of polymer nanocarriers: Factors, mechanisms and applications. Progress in Polymer Science. 2014;39:43-86.

[6] Matsumura Y, Maeda H. A new concept for macromolecular therapeutics in cancer chemotherapy: mechanism of tumoritropic accumulation of proteins and the antitumor agent smancs. Cancer Research. 1986;46:6387-92.

[7] Zhulina EB, Borisov OV. Theory of block polymer micelles: Recent advances and current challenges. Macromolecules. 2012;45:4429-40.

[8] Yallapu MM, Jaggi M, Chauhan SC. Design and engineering of nanogels for cancer treatment. Drug Discovery Today. 2011;16:457-63.

[9] Kabanov AV, Vinogradov SV. Nanogels as pharmaceutical carriers: finite networks of infinite capabilities. Angewandte Chemie (International ed in English). 2009;48:5418-29.

[10] Tahara Y, Akiyoshi K. Current advances in self-assembled nanogel delivery systems for immunotherapy. Advanced Drug Delivery Reviews. 2015;95:65-76.

[11] Na K, Park KM, Jo EA, Lee KS. Self-organized pullulan/deoxycholic acid nanogels: Physicochemical characterization and anti-cancer drug-releasing behavior. Biotechnology and Bioprocess Engineering. 2006;11:262-7.

[12] Qiu L, Li Z, Qiao M, Long M, Wang M, Zhang X, Tian C, Chen D. Self-assembled pH-responsive hyaluronic acid–g-poly(l-histidine) copolymer micelles for targeted intracellular delivery of doxorubicin. Acta Biomaterialia. 2014;10:2024-35.

[13] Palao-Suay R, Gómez-Mascaraque LG, Aguilar MR, Vázquez-Lasa B, Román JS. Self-assembling polymer systems for advanced treatment of cancer and inflammation. Progress in Polymer Science. 2016;53:207-48.

[14] Davis ME, Chen ZG, Shin DM. Nanoparticle therapeutics: an emerging treatment modality for cancer. Nature Reviews Drug Discovery. 2008;7:771-82.

[15] Cho HJ, Yoon HY, Koo H, Ko SH, Shim JS, Lee JH, Kim K, Kwon IC, Kim DD. Self-assembled nanoparticles based on hyaluronic acid-ceramide (HA-CE) and Pluronic® for tumor-targeted delivery of docetaxel. Biomaterials. 2011;32:7181-90.

[16] Termsarasab U, Cho HJ, Kim DH, Chong S, Chung SJ, Shim CK, et al. Chitosan oligosaccharide-arachidic acid-based nanoparticles for anti-cancer drug delivery. International Journal of Pharmaceutics. 2013;441:373-80.

[17] Kim DH, Termsarasab U, Cho HJ, Yoon IS, Lee JY, Moon HT, et al. Preparation and characterization of self-assembled nanoparticles based on low-molecular-weight heparin and stearylamine conjugates for controlled delivery of docetaxel.

International Journal of Nanomedicine. 2014;9:5711-27.

[18] Akiyoshi K, Kobayashi S, Shichibe S, Mix D, Baudys M, Wan Kim S, Sunamoto J. Self-assembled hydrogel nanoparticle of cholesterol-bearing pullulan as a carrier of protein drugs: Complexation and stabilization of insulin. Journal of Controlled Release. 1998;54:313-20.

[19] Lin YJ, Liu YS, Yeh HH, Cheng TL, Wang LF. Self-assembled poly(epsilon-caprolactone)-g-chondroitin sulfate copolymers as an intracellular doxorubicin delivery carrier against lung cancer cells. International Journal of Nanomedicine. 2012;7:4169-83.

[20] Ling G, Zhang P, Zhang W, Sun J, Meng X, Qin Y, Deng Z. Development of novel self-assembled DS-PLGA hybrid nanoparticles for improving oral bioavailability of vincristine sulfate by P-gp inhibition. Journal of Controlled Release. 2010;148:241-8.

[21] Pitombeira NAO, Veras Neto JG, Silva DA, Feitosa JPA, Paula HCB, de Paula RCM. Self-assembled nanoparticles of acetylated cashew gum: Characterization and evaluation as potential drug carrier. Carbohydrate Polymers. 2015;117:610-5.

[22] Lee KY, Jo WH, Kwon IC, Kim Y-H, Jeong SY. Physicochemical characteristics of self-aggregates of hydrophobically modified chitosans. Langmuir. 1998;14:2329-32.

[23] Lee KY, Jo WH, Kwon IC, Kim Y-H, Jeong SY. Structural determination and interior polarity of self-aggregates prepared from deoxycholic acid-modified chitosan in water. Macromolecules. 1998;31:378-83.

[24] Rubin R. FDA okays drug to reduce double chins. Journal of the American

Medical Association. 2015;313:2115.

[25] Swierczewska M, Han HS, Kim K, Park JH, Lee S. Polysaccharide-based nanoparticles for theranostic nanomedicine. Advanced Drug Delivery Reviews. 2016;99, Part A:70-84.

[26] Raemdonck K, Martens TF, Braeckmans K, Demeester J, De Smedt SC. Polysaccharide-based nucleic acid nanoformulations. Advanced Drug Delivery Reviews. 2013;65:1123-47.

[27] Liu Z, Jiao Y, Wang Y, Zhou C, Zhang Z. Polysaccharides-based nanoparticles as drug delivery systems. Advanced Drug Delivery Reviews. 2008;60:1650-62.

[28] Fujimoto T, Kawashima H, Tanaka T, Hirose M, Toyama-Sorimachi N, Matsuzawa Y, Miyasaka M. CD44 binds a chondroitin sulfate proteoglycan, aggrecan. International Immunology. 2001;13:359-66.

[29] Raveendran S, Yoshida Y, Maekawa T, Kumar DS. Pharmaceutically versatile sulfated polysaccharide based bionano platforms. Nanomedicine: Nanotechnology, Biology and Medicine. 2013;9:605-26.

[30] Zhao L, Liu M, Wang J, Zhai G. Chondroitin sulfate-based nanocarriers for drug/gene delivery. Carbohydrate Polymers. 2015;133:391-9.

[31] Nair LS, Laurencin CT. Biodegradable polymers as biomaterials. Progress in Polymer Science. 2007;32:762-98.

[32] Favretto ME, Wallbrecher R, Schmidt S, van de Putte R, Brock R. Glycosaminoglycans in the cellular uptake of drug delivery vectors – Bystanders or active players? Journal of Controlled Release. 2014;180:81-90.

[33] Marhaba R, Zoller M. CD44 in cancer progression: adhesion, migration and growth regulation. Journal of Molecular Histology. 2004;35:211-31.

[34] Naor D, Nedvetzki S, Golan I, Melnik L, Faitelson Y. CD44 in cancer. Critical Reviews in Clinical Laboratory Sciences. 2002;39:527-79.

[35] Skelton TP, Zeng C, Nocks A, Stamenkovic I. Glycosylation provides both stimulatory and inhibitory effects on cell surface and soluble CD44 binding to hyaluronan. The Journal of Cell Biology. 1998;140:431-46.

[36] Bajorath J, Greenfield B, Munro SB, Day AJ, Aruffo A. Identification of CD44 residues important for hyaluronan binding and delineation of the binding site. Journal of Biological Chemistry. 1998;273:338-43.

[37] Peach RJ, Hollenbaugh D, Stamenkovic I, Aruffo A. Identification of hyaluronic acid binding sites in the extracellular domain of CD44. Journal of Cell Biology. 1993;122:257-64.

[38] Naor D, Sionov RV, Ish-Shalom D. CD44: structure, function, and association with the malignant process. Advances in Cancer Research. 1997;71:241-319.

[39] Kirtane AR, Kalscheuer SM, Panyam J. Exploiting nanotechnology to overcome tumor drug resistance: Challenges and opportunities. Advanced Drug Delivery Reviews. 2013;65:1731-47.

[40] Fang J, Nakamura H, Maeda H. The EPR effect: Unique features of tumor blood vessels for drug delivery, factors involved, and limitations and augmentation of the effect. Advanced Drug Delivery Reviews. 2011;63:136-51.

[41] Maeda H. Toward a full understanding of the EPR effect in primary and metastatic tumors as well as issues related to its heterogeneity. Advanced Drug Delivery Reviews. 2015;91:3-6.

[42] Glasgow MD, Chougule MB. Recent developments in active tumor targeted multifunctional nanoparticles for combination chemotherapy in cancer

treatment and imaging. Journal of Biomedical Nanotechnology. 2015;11:1859-98.

[43] Zhong Y, Meng F, Deng C, Zhong Z. Ligand-directed active tumor-targeting polymeric nanoparticles for cancer chemotherapy. Biomacromolecules. 2014;15:1955-69.

[44] Al-Abd AM, Aljehani ZK, Gazzaz RW, Fakhri SH, Jabbad AH, Alahdal AM, Torchilin VP. Pharmacokinetic strategies to improve drug penetration and entrapment within solid tumors. Journal of Controlled Release. 2015;219:269-77.

[45] Minchinton AI, Tannock IF. Drug penetration in solid tumours. Nature Reviews Cancer. 2006;6:583-92.

[46] Marcucci F, Corti A. How to improve exposure of tumor cells to drugs — Promoter drugs increase tumor uptake and penetration of effector drugs. Advanced Drug Delivery Reviews. 2012;64:53-68.

[47] Ernsting MJ, Murakami M, Roy A, Li S-D. Factors controlling the pharmacokinetics, biodistribution and intratumoral penetration of nanoparticles. Journal of Controlled Release. 2013;172:782-94.

[48] Holback H, Yeo Y. Intratumoral drug delivery with nanoparticulate carriers. Pharmaceutical Research. 2011;28:1819-30.

[49] Plaks V, Kong N, Werb Z. The cancer stem cell niche: How essential is the niche in regulating stemness of tumor cells? Cell Stem Cell. 2015;16:225-38.

[50] Kim J, Lee YM, Kim H, Park D, Kim J, Kim WJ. Phenylboronic acid-sugar grafted polymer architecture as a dual stimuli-responsive gene carrier for targeted anti-angiogenic tumor therapy. Biomaterials. 2016;75:102-11.

[51] Varki A. Sialic acids as ligands in recognition phenomena. FASEB Journal. 1997;11:248-55.

[52] Deshayes S, Cabral H, Ishii T, Miura Y, Kobayashi S, Yamashita T, Matsumoto A, Miyahara Y, Nishiyama N, Kataoka K. Phenylboronic acid-installed polymeric micelles for targeting sialylated epitopes in solid tumors. Journal of the American Chemical Society. 2013;135:15501-7.

[53] Cambre JN, Sumerlin BS. Biomedical applications of boronic acid polymers. Polymer. 2011;52:4631-43.

[54] Mikhail AS, Eetezadi S, Ekdawi SN, Stewart J, Allen C. Image-based analysis of the size- and time-dependent penetration of polymeric micelles in multicellular tumor spheroids and tumor xenografts. International Journal of Pharmaceutics. 2014;464:168-77.

[55] Ong S-M, Zhao Z, Arooz T, Zhao D, Zhang S, Du T, Wasser M, Noort D, Yu H. Engineering a scaffold-free 3D tumor model for in vitro drug penetration studies. Biomaterials. 2010;31:1180-90.

[56] Sutherland RM. Cell and environment interactions in tumor microregions: the multicell spheroid model. Science. 1988;240:177-84.

[57] Olive PL, Durand RE. Drug and radiation resistance in spheroids: cell contact and kinetics. Cancer and Metastasis Reviews. 1994;13:121-38.

[58] Cho HJ, Yoon IS, Yoon HY, Koo H, Jin YJ, Ko SH, Shim JS, Kim K, Kwon IC, Kim DD. Polyethylene glycol-conjugated hyaluronic acid-ceramide self-assembled nanoparticles for targeted delivery of doxorubicin. Biomaterials. 2012;33:1190-200.

[59] Fischer E, Speier A. Darstellung der Ester. Berichte der Deutschen Chemischen

Gesellschaft. 1895;28:3252-8.

[60] Jin YJ, Termsarasab U, Ko SH, Shim JS, Chong S, Chung SJ, Shim CK, Cho HJ, Kim DD. Hyaluronic acid derivative-based self-assembled nanoparticles for the treatment of melanoma. Pharmaceutical Research. 2012;29:3443-54.

[61] Onishi H, Isoda Y, Matsuyama M. In vivo evaluation of chondroitin sulfate-glycyl-prednisolone for anti-arthritic effectiveness and pharmacokinetic characteristics. International Journal of Pharmaceutics. 2013;456:113-20.

[62] Yu C, Gao C, Lü S, Chen C, Huang Y, Liu M. Redox-responsive shell-sheddable micelles self-assembled from amphiphilic chondroitin sulfate-cholesterol conjugates for triggered intracellular drug release. Chemical Engineering Journal. 2013;228:290-9.

[63] Yu C, Gao C, Lü S, Chen C, Yang J, Di X, Liu M. Facile preparation of pH-sensitive micelles self-assembled from amphiphilic chondroitin sulfate-histamine conjugate for triggered intracellular drug release. Colloids and Surfaces B: Biointerfaces. 2014;115:331-9.

[64] Lee CT, Huang CP, Lee YD. Preparation of amphiphilic poly(L-lactide)-graft-chondroitin sulfate copolymer self-aggregates and its aggregation behavior. Biomacromolecules. 2006;7:1179-86.

[65] Park W, Park S-j, Na K. Potential of self-organizing nanogel with acetylated chondroitin sulfate as an anti-cancer drug carrier. Colloids and Surfaces B: Biointerfaces. 2010;79:501-8.

[66] Phillips JN. The energetics of micelle formation. Transactions of the Faraday Society. 1955;51:561-9.

[67] Xi J, Zhou L, Dai H. Drug-loaded chondroitin sulfate-based nanogels:

preparation and characterization. Colloids and Surfaces B, Biointerfaces. 2012;100:107-15.

[68] Misra R, Sahoo SK. Intracellular trafficking of nuclear localization signal conjugated nanoparticles for cancer therapy. European Journal of Pharmaceutical Sciences. 2010;39:152-63.

[69] Wang X, Zhen X, Wang J, Zhang J, Wu W, Jiang X. Doxorubicin delivery to 3D multicellular spheroids and tumors based on boronic acid-rich chitosan nanoparticles. Biomaterials. 2013;34:4667-79.

Table 1 The feed ratio of EtDOCA to CSA and the DOCA content in CSA-DOCA conjugates.

Product name	Feed ratio (EtDOCA/CSA) weight ratio	^{1}H-NMR peak area ratio	Calculated DOCA/CSA weight ratio	DOCA content in CSA-DOCA (%; w/w)
CSA-DOCA (low DOCA content)	34.8 mg/100 mg	0.168	0.0979	8.92
CSA-DOCA (high DOCA content)	69.6 mg/100 mg	0.224	0.130	11.5

Table 2 Characterization of the CSA-DOCA NPs.

Composition	Mean diameter (nm)	Polydispersity index	Zeta potential (mV)	Entrapment efficiency (%)
Blank CSA-DOCA NPs (low DOCA content)	228.2 ± 7.6	0.19 ± 0.03	-23.07 ± 1.17	-
DOX-loaded CSA-DOCA NPs (low DOCA content)	233.7 ± 7.0	0.22 ± 0.02	-21.52 ± 1.06	85.5 ± 7.9
DOX-loaded CSA-DOCA NPs (high DOCA content)	273.8 ± 4.1	0.24 ± 0.02	-26.94 ± 0.57	78.2 ± 2.4

The weight ratio between polymer and drug was 7:1.

Data are presented as mean ± SD (n = 3).

Table 3 The feed ratio of AMPB to CSA-DOCA and the AMPB content in CSA-DOCA-AMPB conjugate.

Product name	Feed ratio (AMPB/CSA-DOCA) weight ratio	^{1}H-NMR peak area ratio	Calculated AMPB/CSA-DOCA weight ratio	AMPB content in CSA-DOCA-AMPB (%; w/w)
CSA-DOCA-AMPB (low AMPB content)	7.5 mg/100 mg	0.265	0.0235	2.30
CSA-DOCA-AMPB (high AMPB content)	15.0 mg/100 mg	Precipitation occurred during dialysis against water		

Table 4 Characterization of the CSA-DOCA-AMPB NPs.

Composition	Mean diameter (nm)	Polydispersity index	Zeta potential (mV)	Entrapment efficiency (%)
DOX-loaded CSA-DOCA NPs	228.9 ± 2.0	0.22 ± 0.01	-22.58 ± 1.82	80.9 ± 0.2
DOX-loaded CSA-DOCA-AMPB NPs	205.8 ± 8.2	0.21 ± 0.01	-20.97 ± 0.75	71.7 ± 0.2

The weight ratio between polymer and drug was 7.5:1.

Data are presented as mean ± SD (n = 3).

Table 5 IC_{50} values of the DOX solution and DOX-loaded NPs in A549 cells.

Group	IC_{50} (μM)	
	48 h[a]	72 h[a]
DOX solution	6.52 ± 0.23	5.96 ± 0.42
CSA-DOCA/DOX NPs	5.01 ± 0.25	4.23 ± 0.08
CSA-DOCA-AMPB/DOX NPs	4.20 ± 0.18	3.06 ± 0.28

Data are presented as the mean ± SD (n = 6).

[a] All data are significantly different from each other ($p < 0.05$).

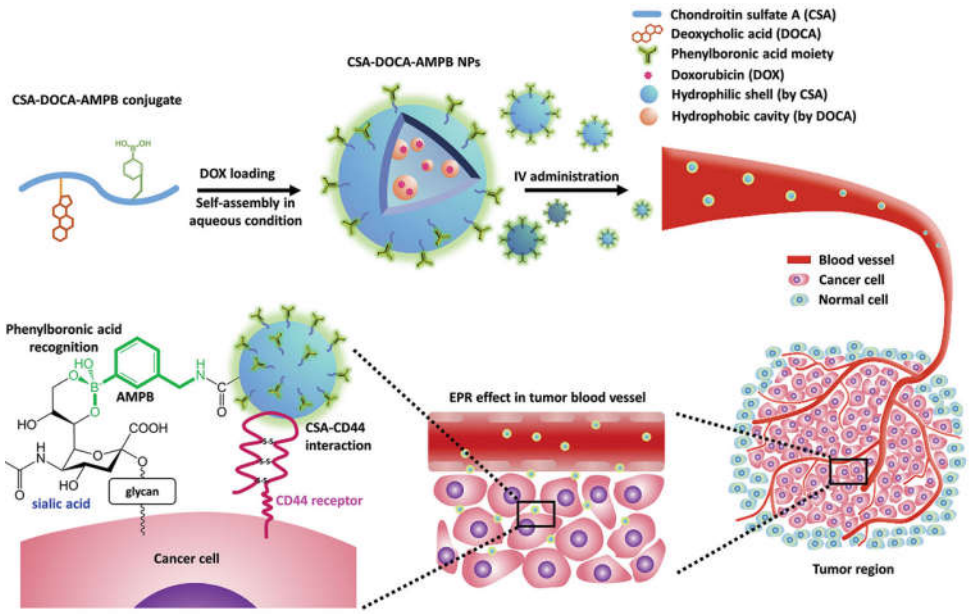

Figure 1 Schematic illustration of the strategy for solid tumor targeting and penetration using CSA-DOCA-AMPB/DOX NPs.

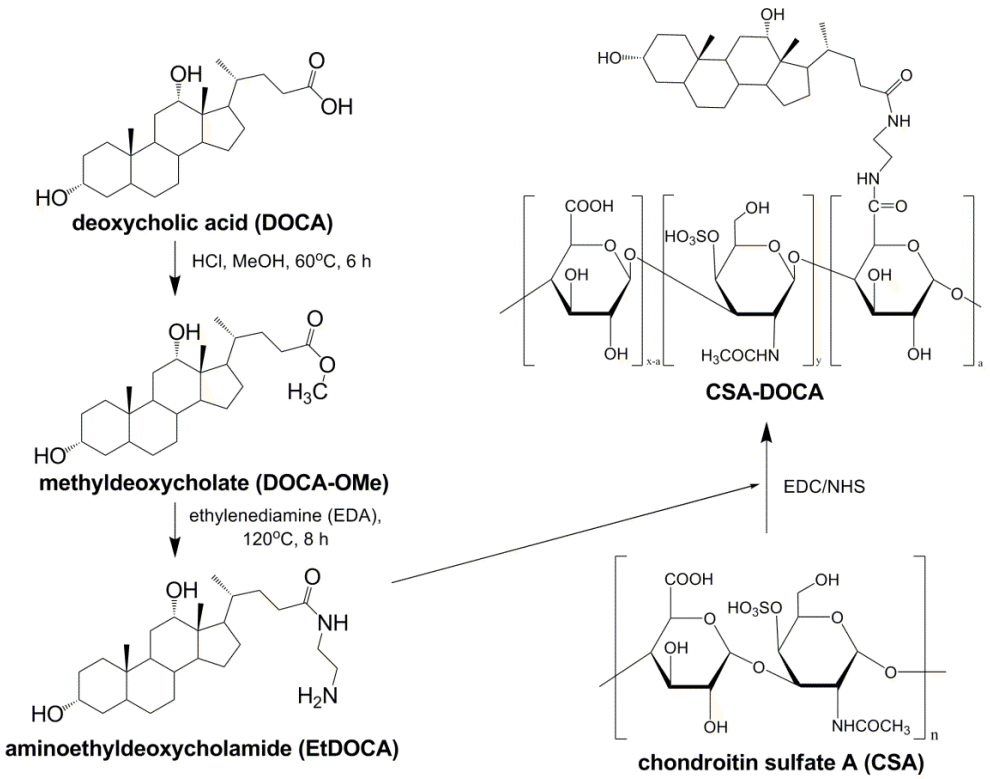

Figure 2 Synthetic scheme of CSA-DOCA.

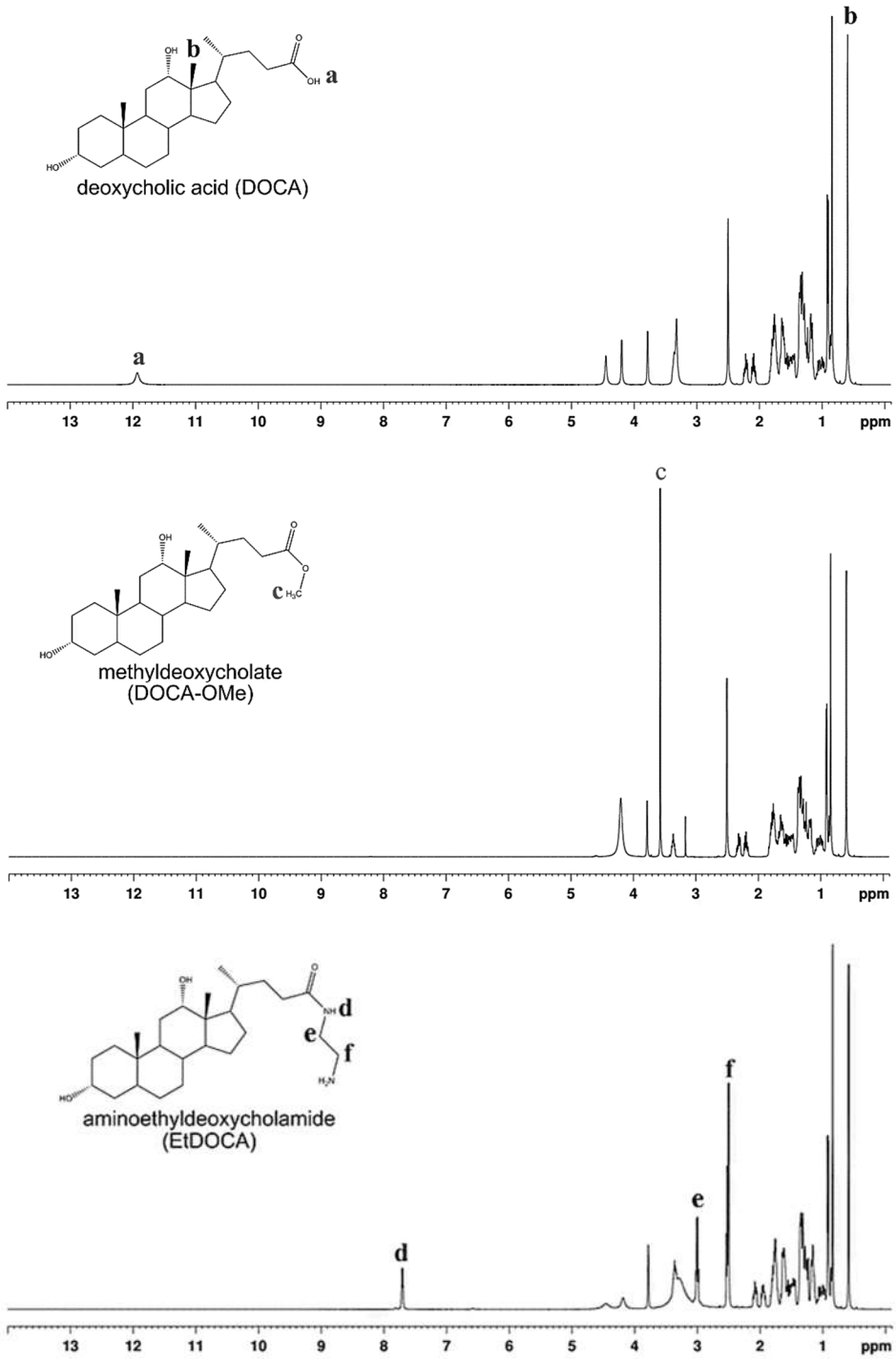

Figure 3 ^{1}H-NMR spectra of DOCA and its derivatives. All the compounds were dissolved in DMSO-d_6 for the NMR analysis.

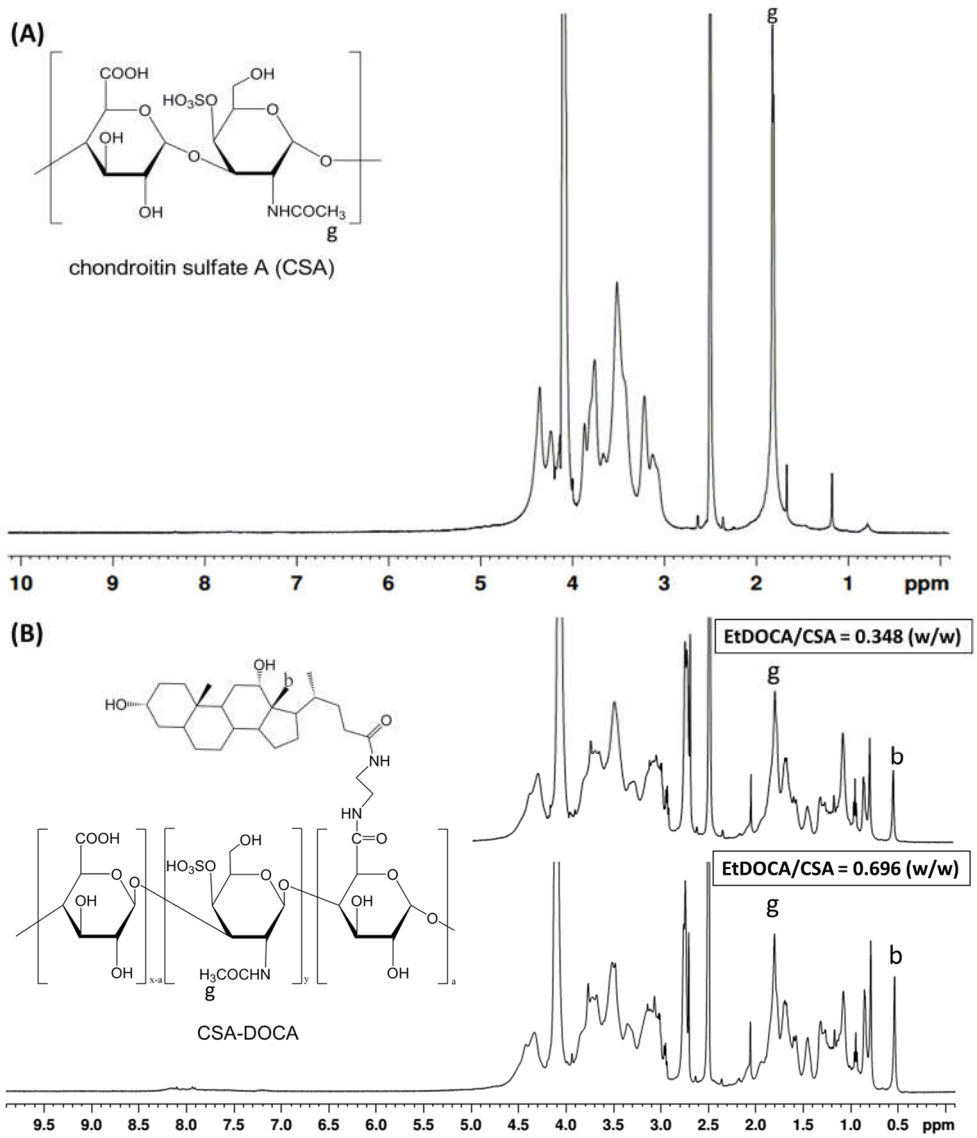

Figure 4 ^{1}H-NMR spectra of CSA (A) and CSA-DOCA conjugates with different EtDOCA/CSA feed ratios (B). All the compounds were dissolved in DMSO-d_6 and D_2O mixture (3:1, v/v).

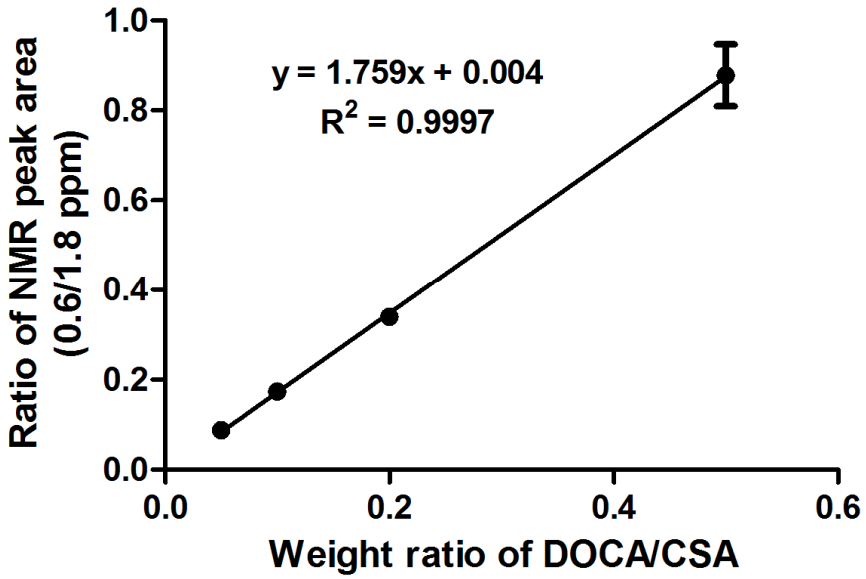

Figure 5 The calibration curve for the determination of DOCA content in CSA-DOCA was constructed based on the relationship between the ratio of ^{1}H-NMR peak area (0.6/1.8 ppm) and the weight ratio (DOCA/CSA) of their physical mixtures. Each point represents the means ± SD (n = 3).

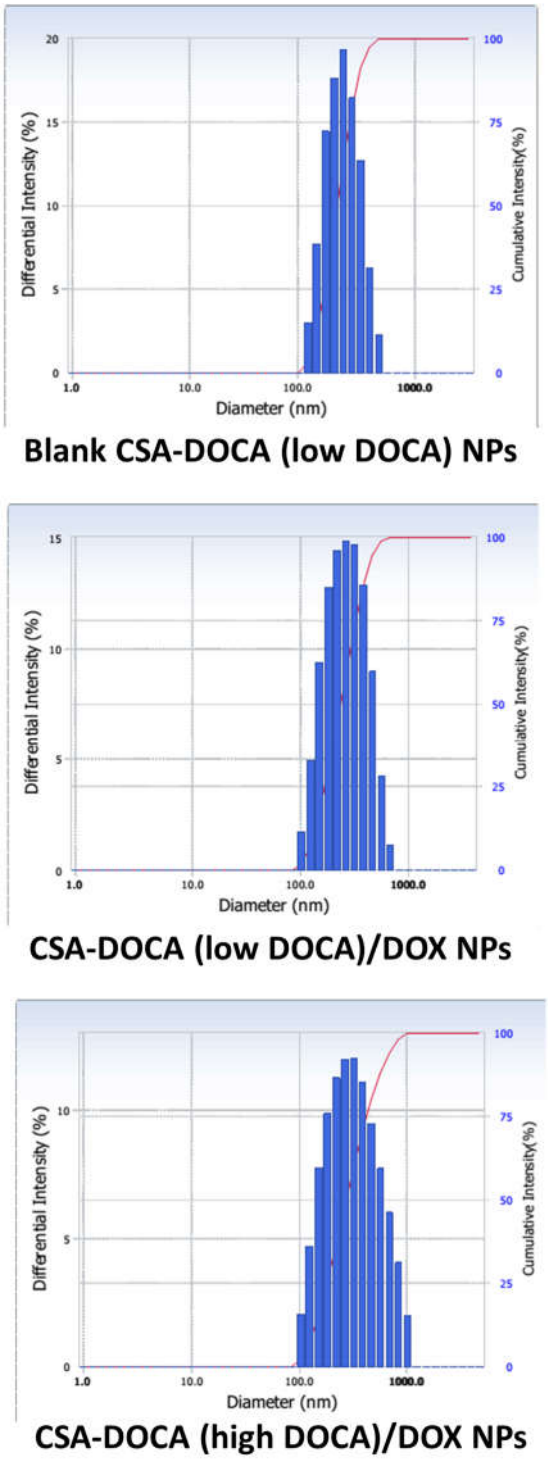

Figure 6 The size distribution diagrams of the CSA-DOCA NPs.

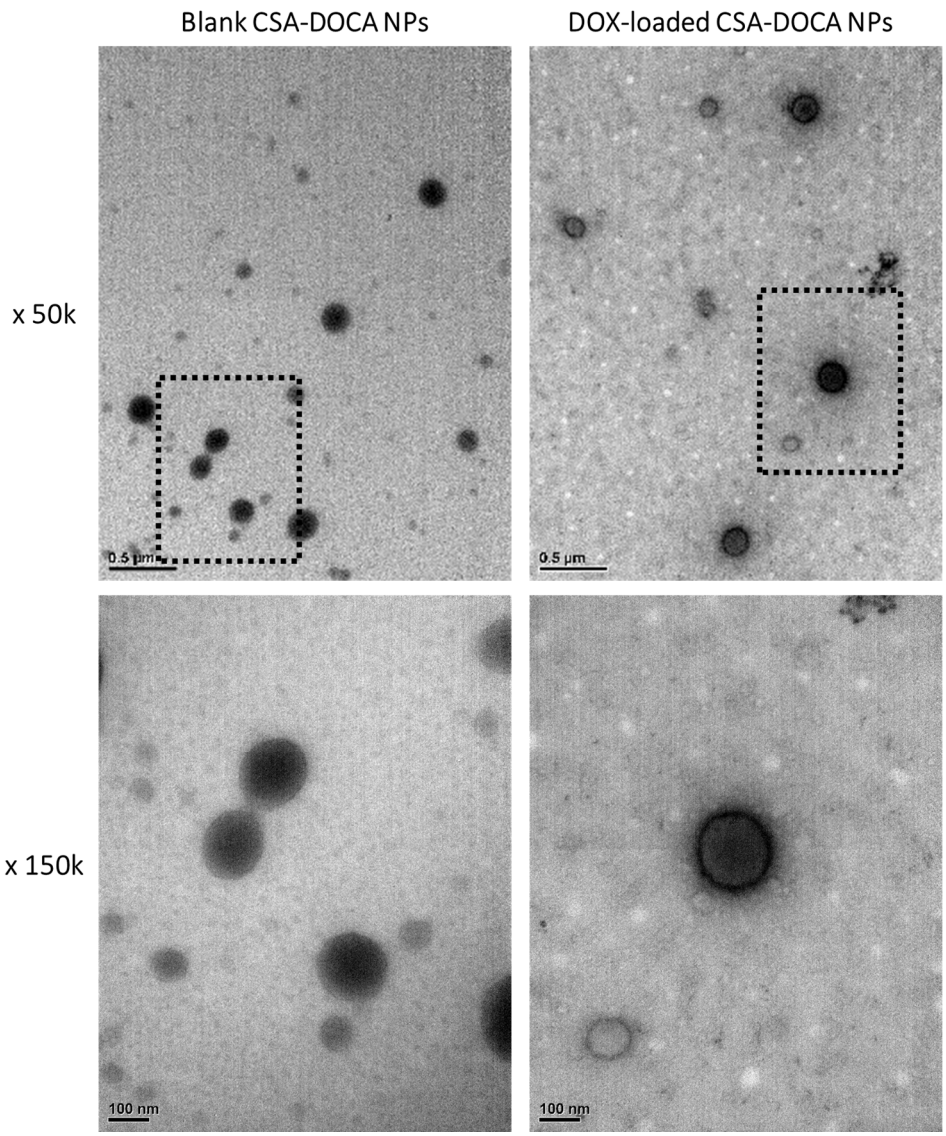

Figure 7 TEM image of the CSA-DOCA NPs. Each image in the lower panel corresponds to the region inside the dashed border in the upper panel image. The lengths of the scale bars in the ×50 k and ×150 k images are 0.5 μm and 100 nm, respectively.

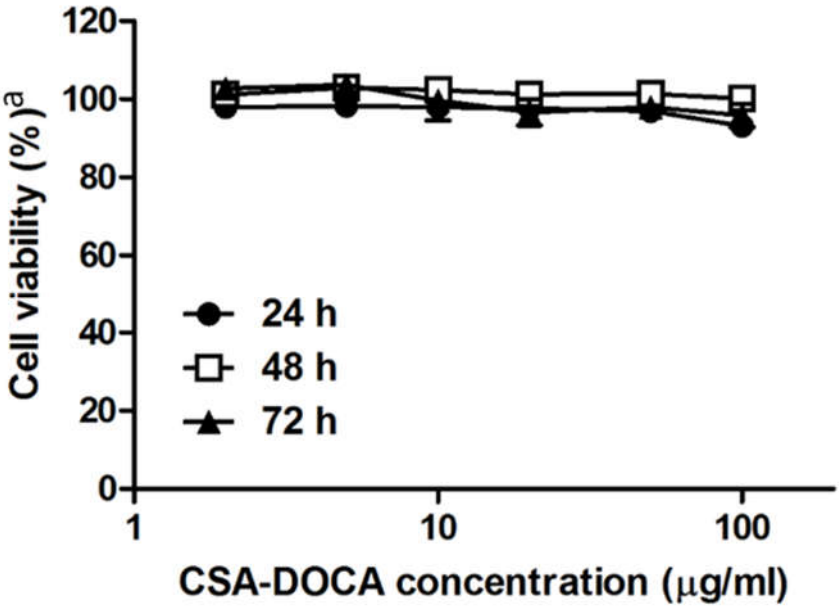

[a]Cell viability (%)$=\frac{\text{Absorbance}^{b}\text{ of NP-treatment group}}{\text{Absorbance}^{b}\text{ of no-treatment group}}$

[b]Absorbance of water-soluble formazan at a wavelength of 490 nm.

Figure 8 *In vitro* cytotoxicity test of blank CSA-DOCA NPs in MDA-MB-231 cells using an MTS-based assay. Data are presented as means ± SD (n = 6).

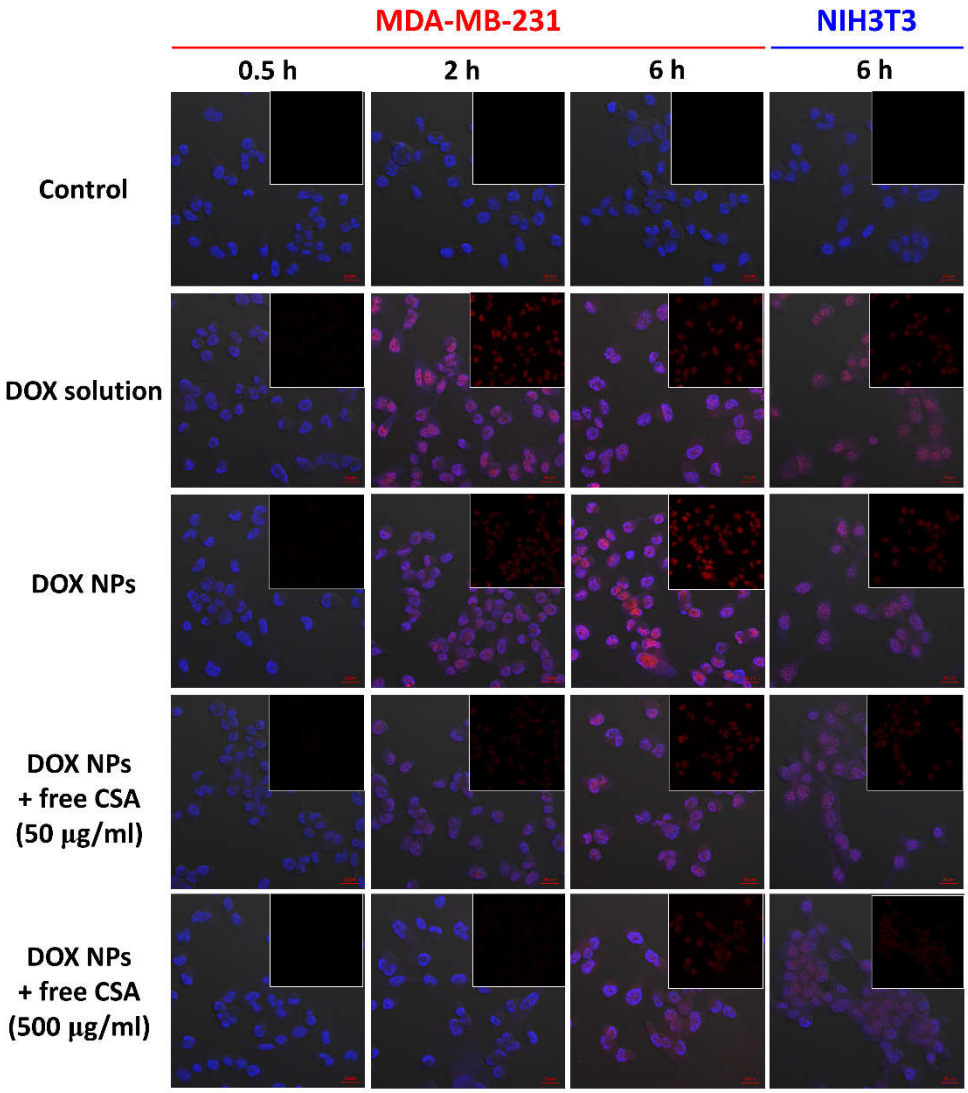

Figure 9 CLSM images of MDA-MB-231 and NIH3T3 cells after incubation with free DOX or DOX-loaded NPs. DAPI was used for the staining of nuclei. The inset images represent the DOX fluorescence channel only. The length of scale bar is 20 μm.

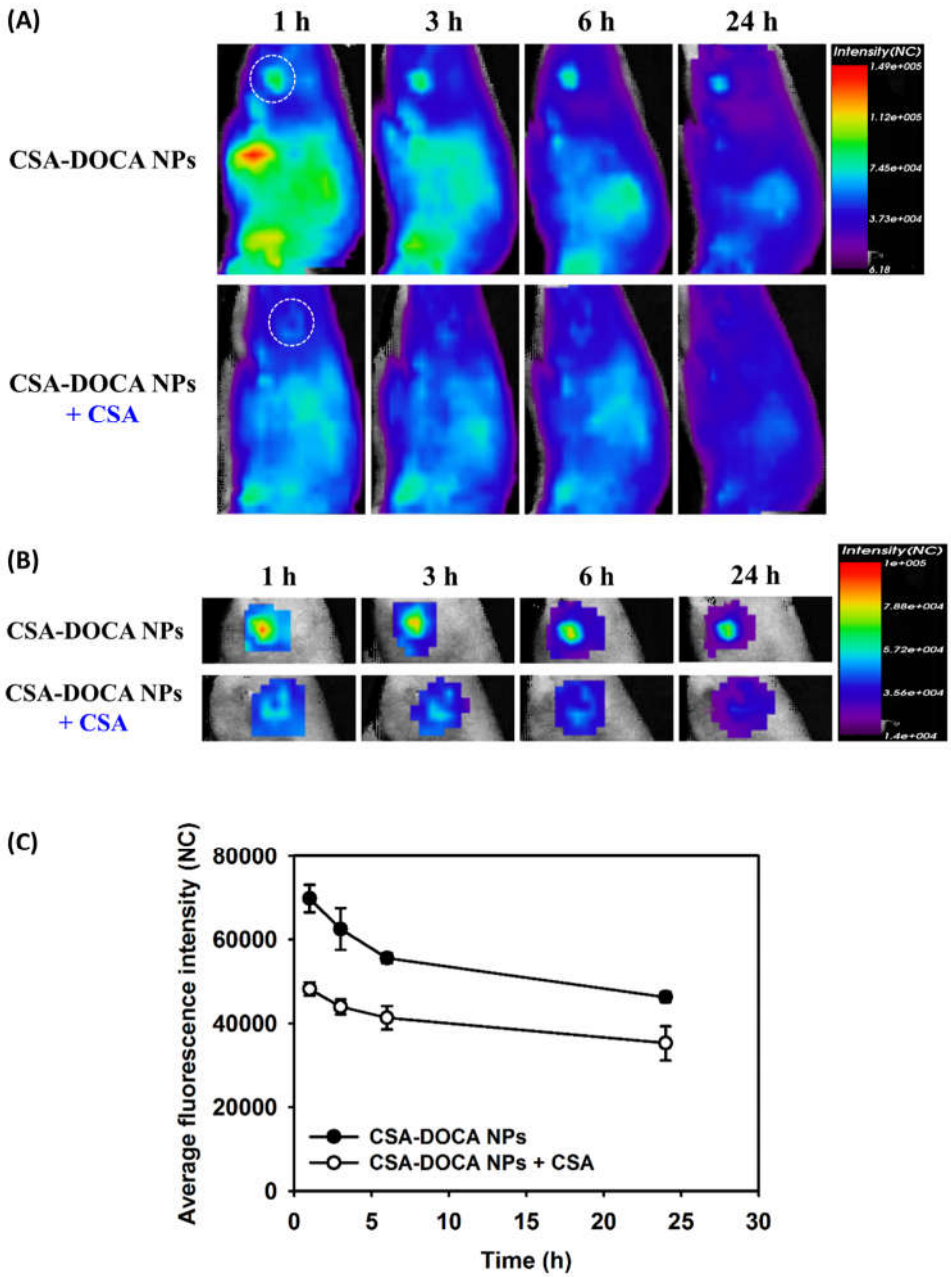

Figure 10 *In vivo* NIRF imaging after intravenous injection of Cy5.5-labeled CSA-DOCA NPs in MDA-MB-231 tumor-xenografted mouse model. The pre-treatment with free CSA was employed to evaluate the CD44-targetability of CSA-DOCA NPs. The fluorescence images for whole body (A) and tumor region (B) were presented. Time-dependent profile of average fluorescence intensity in the tumor region (C) was plotted. Each point represents the mean ± SD (n = 3).

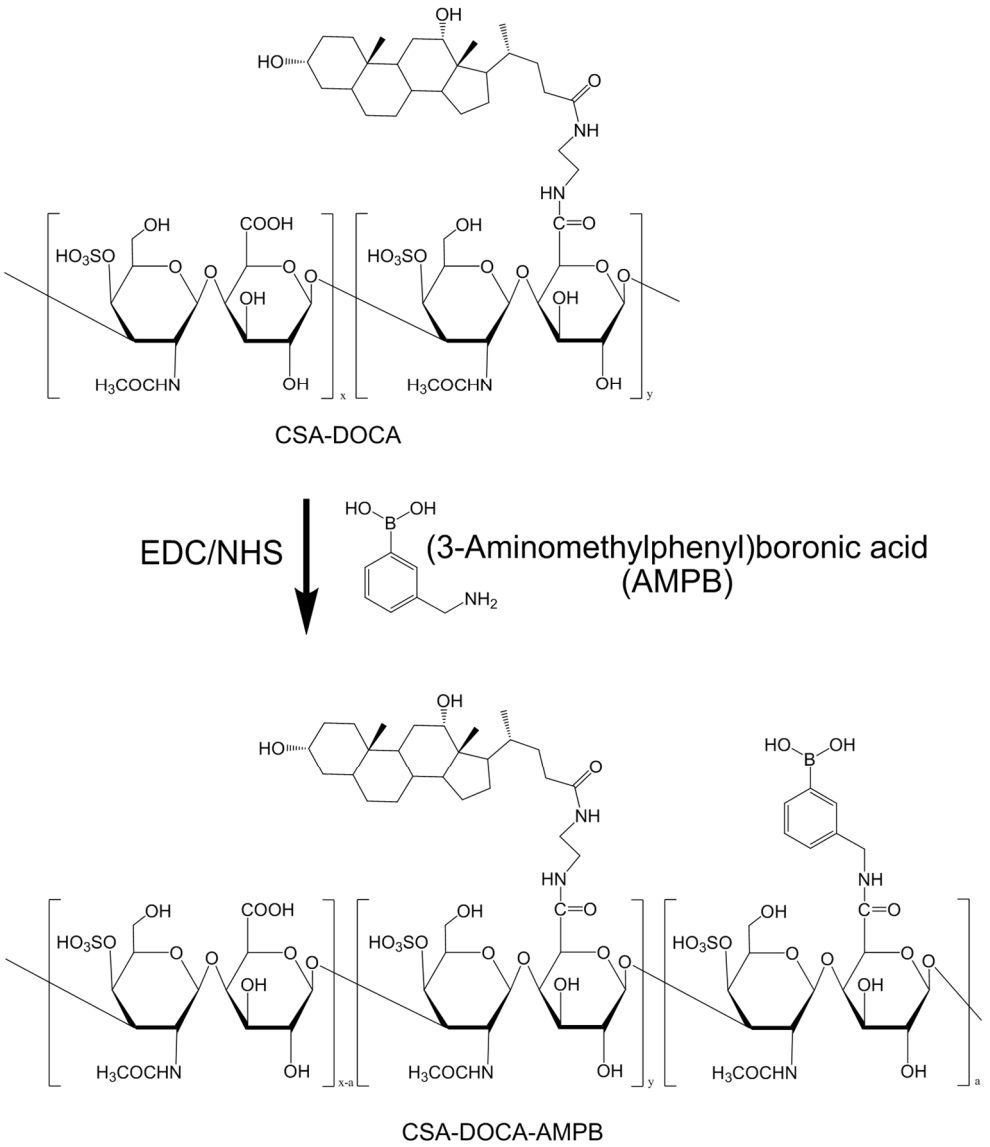

Figure 11 Synthetic scheme of CSA-DOCA-AMPB.

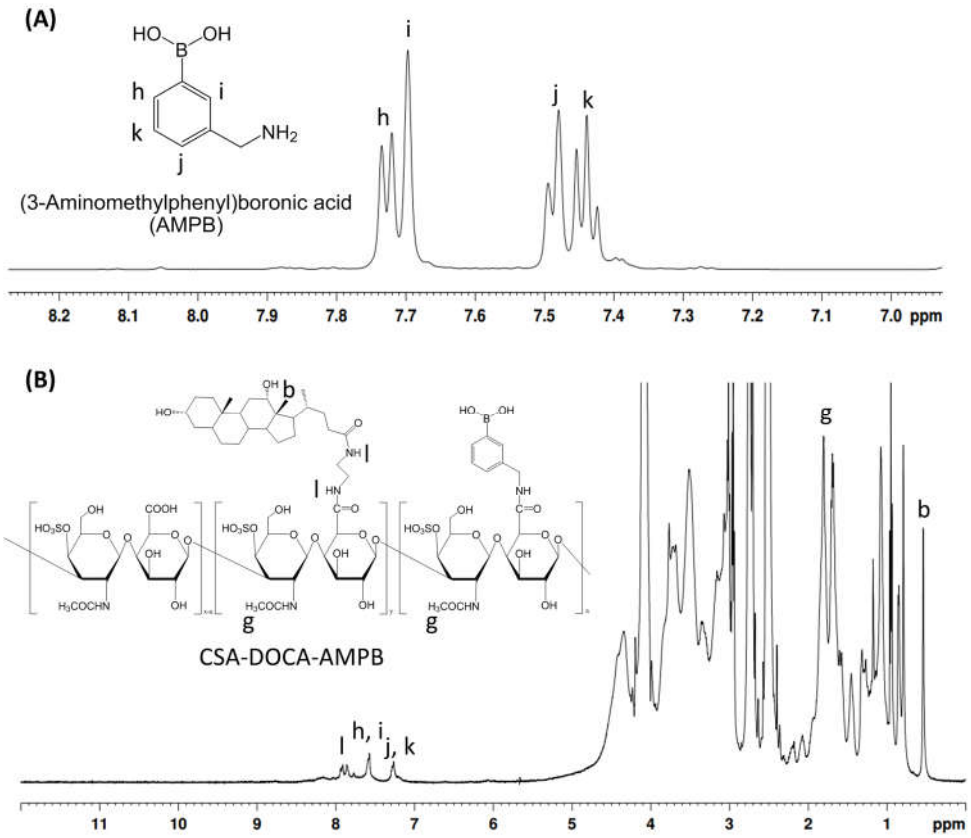

Figure 12 ^{1}H-NMR spectra of AMPB (A) and CSA-DOCA-AMPB (B). For the NMR analyses, AMPB and CSA-DOCA-AMPB were dissolved in D_2O and DMSO-d_6/D_2O mixture (3:1, v/v), respectively.

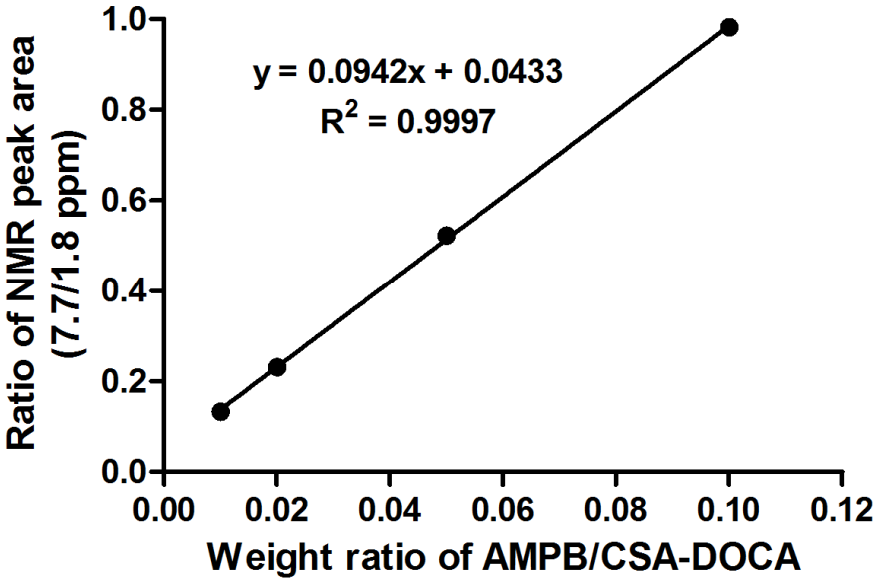

Figure 13 The calibration curve was plotted as the ratio of ^{1}H-NMR peak area (7.7/1.8 ppm) against the weight ratio of AMPB/CSA-DOCA in physical mixtures to determine the AMPB content in CSA-DOCA-AMPB.

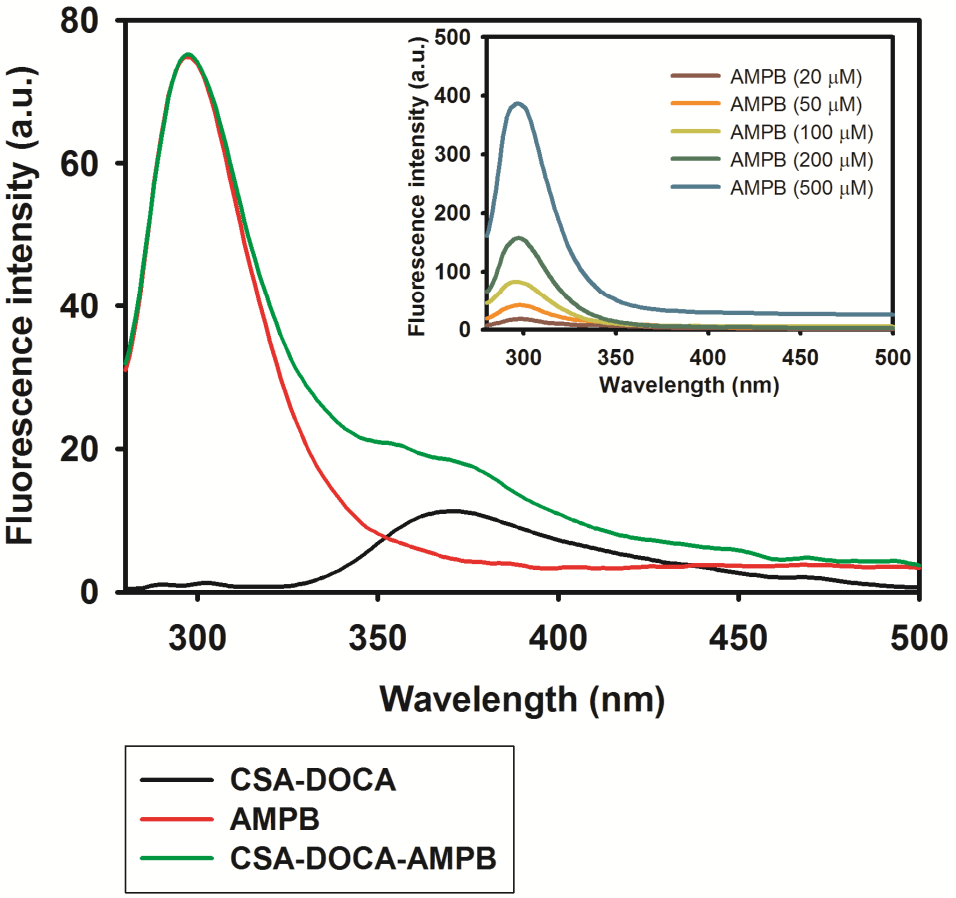

Figure 14 The fluorescence emission spectra of CSA-DOCA, AMPB, and CSA-DOCA-AMPB at an excitation wavelength of 270 nm are presented. The emission spectra of AMPB at various concentrations (20–500 μM) are also shown in the inset image.

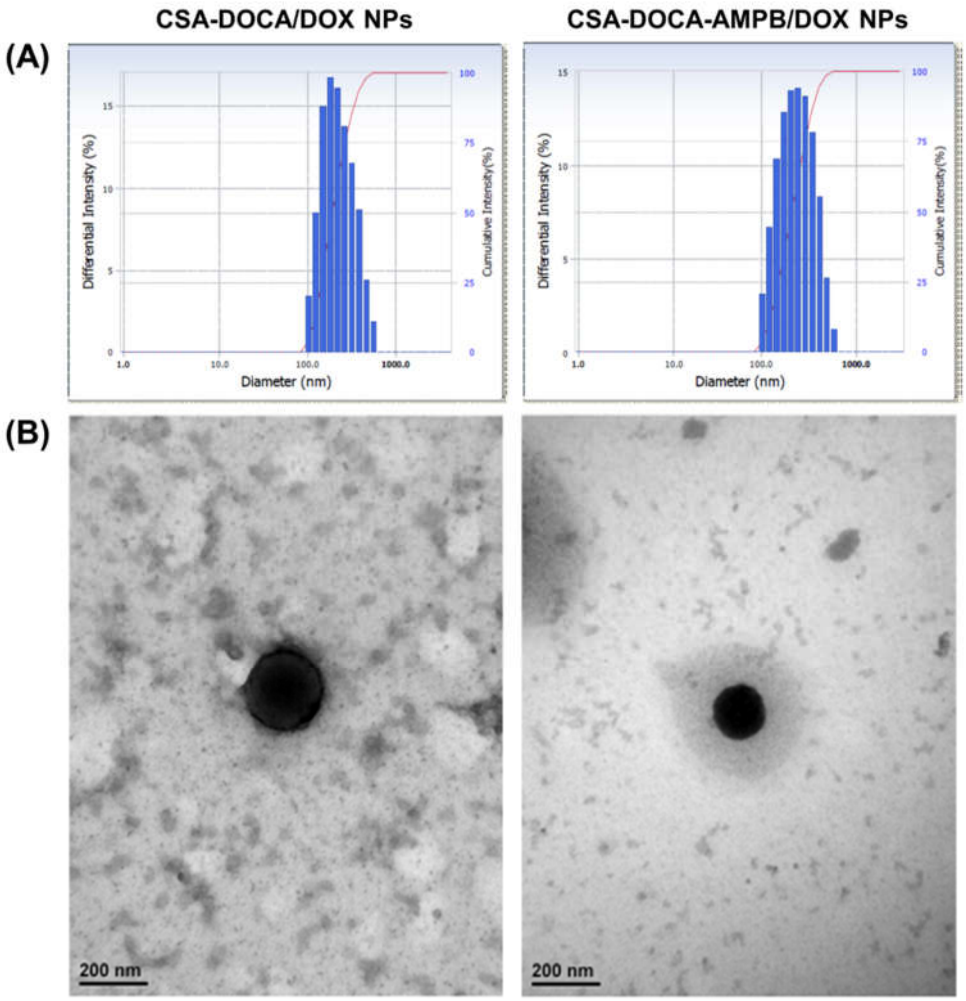

Figure 15 Characterization of CSA-DOCA/DOX NPs and CSA-DOCA-AMPB/DOX NPs. Size distribution diagrams (A) and TEM images (B) of the developed NPs are presented. The length of scale bar is 200 nm.

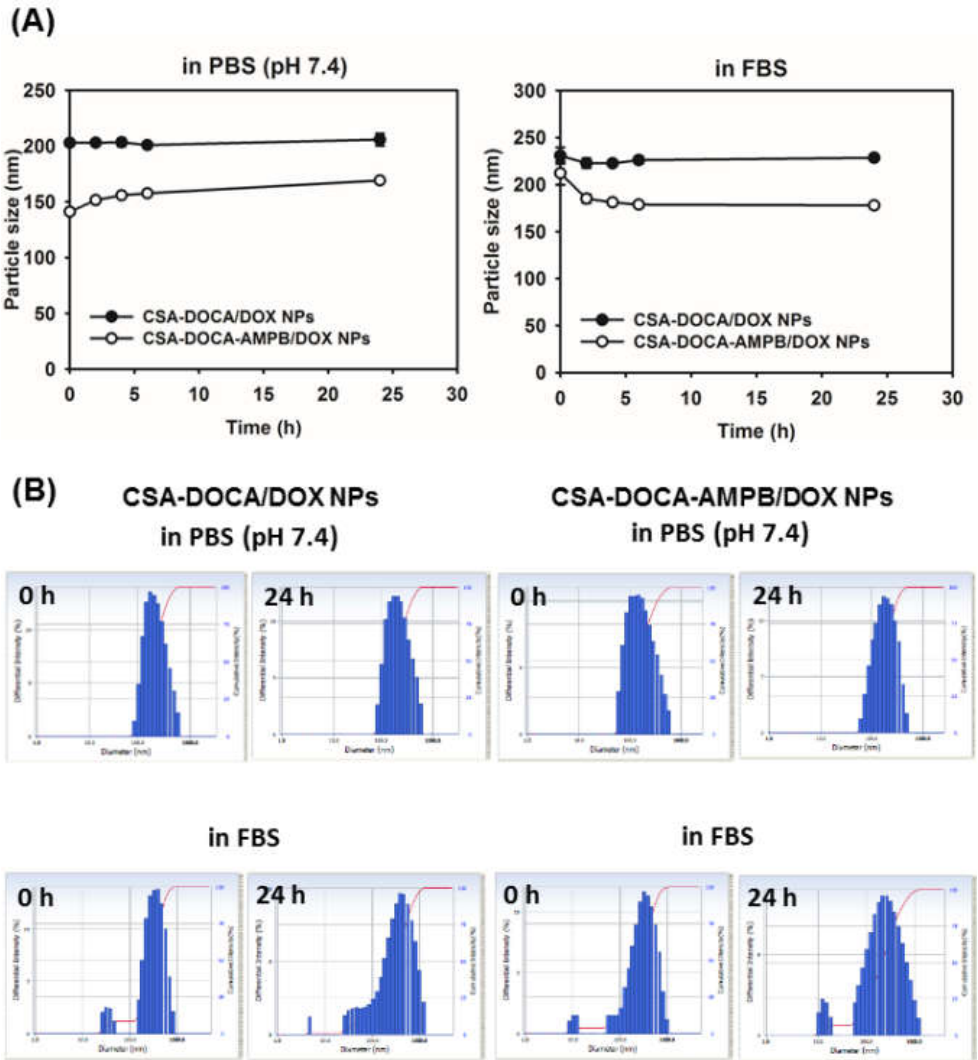

Figure 16 *In vitro* stability of the developed NPs was evaluated by monitoring the particle size change after the incubation with PBS (pH 7.4) or serum (50% FBS). (A) The average particle size versus the incubation time profiles of CSA-DOCA/DOX NPs and CSA-DOCA-AMPB/DOX NPs are shown. (B) The representative size distribution diagrams at 0 h (pre-incubation) and 24 h (post-incubation) are presented. Each point represents the mean ± SD (n = 3).

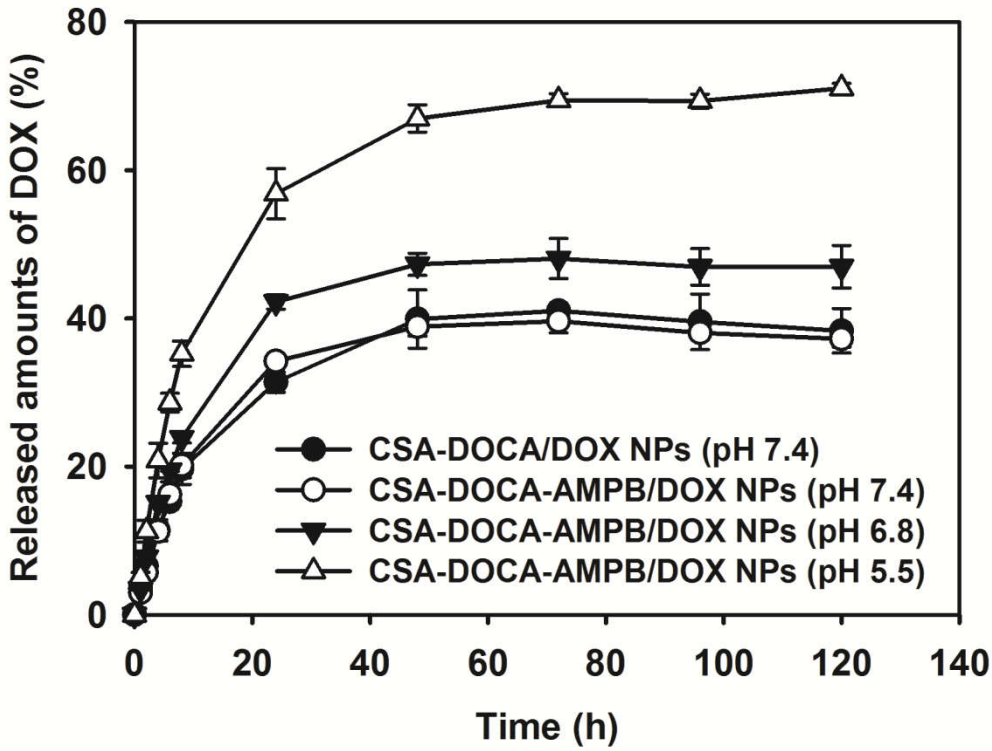

Figure 17 *In vitro* DOX release profiles of the developed NPs. The released amounts of DOX (%) were plotted according to the incubation time. Each point represents the mean ± SD (n = 3).

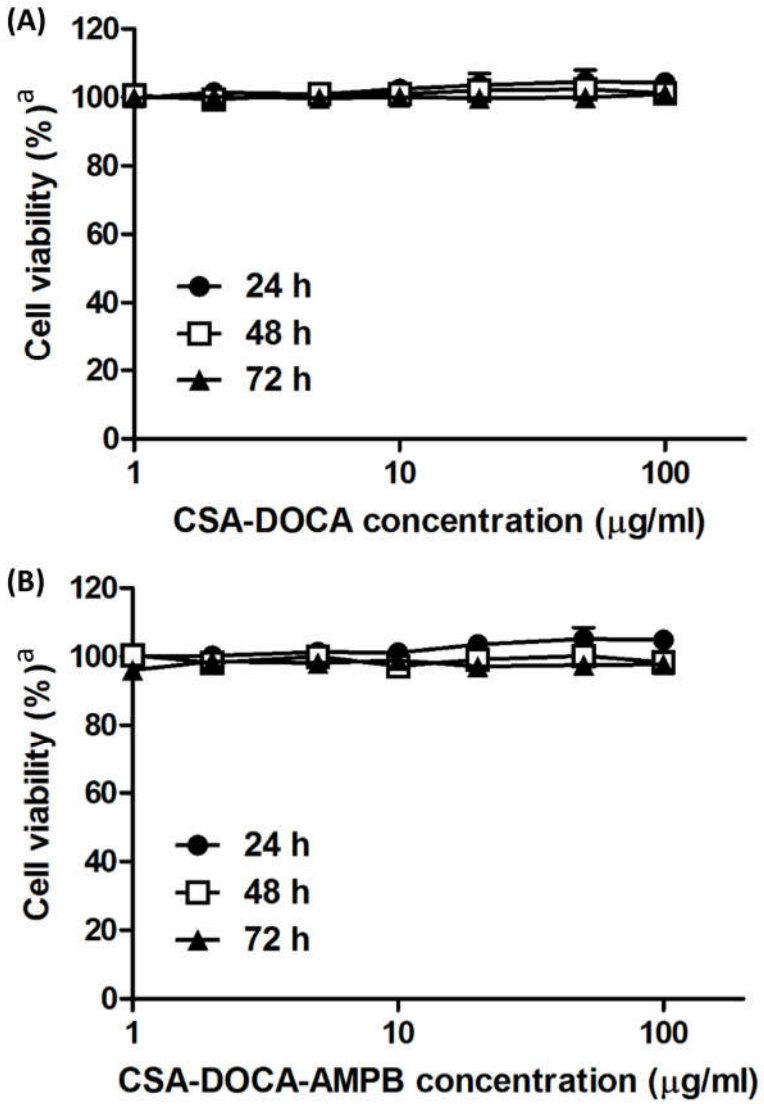

[a]Cell viability (%)$=\frac{\text{Absorbance}^{b}\text{ of NP-treatment group}}{\text{Absorbance}^{b}\text{ of no-treatment group}}$

[b]Absorbance of water-soluble formazan at a wavelength of 490 nm.

Figure 18 Cytotoxicity of the blank NPs in A549 cells. Cell viability (%) was determined by MTS-based assay at various polymer concentrations (1–100 μg/mL) after 24, 48, and 72 h of incubation. Each point represents the mean ± SD (n = 6).

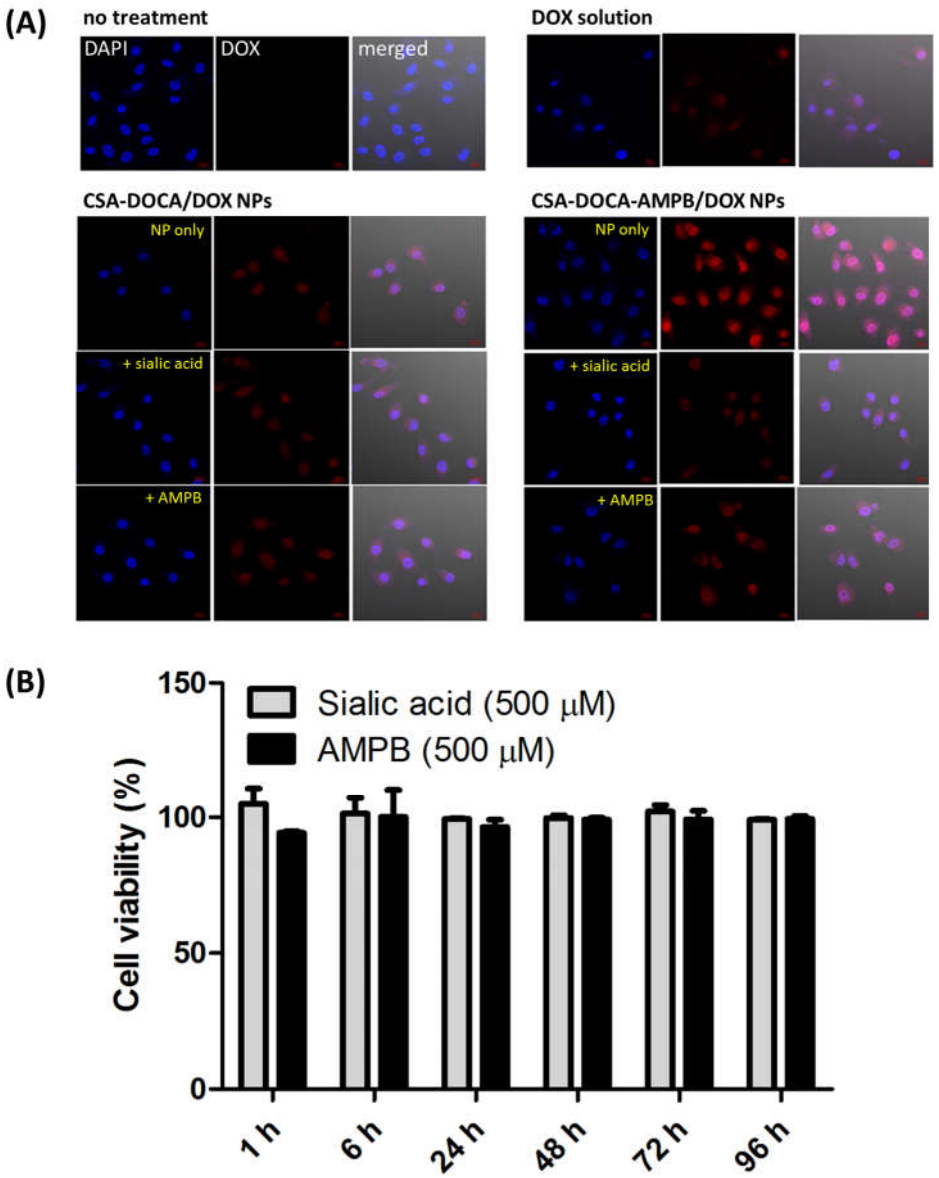

Figure 19 Cellular uptake study in 2D-cultured A549 cells. (A) CLSM images after the incubation with DOX solution, CSA-DOCA/DOX NPs, or CSA-DOCA-AMPB/DOX NPs (as DOX, 100 μM). Sialic acid (500 μM) and AMPB (500 μM) were used as uptake inhibitors to investigate the interaction between AMPB on NP surface and sialic acid on A549 cell surface. DAPI was used to stain the nuclei. The length of the scale bar is 20 μm. (B) Cytotoxicity of sialic acid and AMPB in A549 cells. Cell viability (%) was measured using MTS-based assay at the experimental concentration (500 μM for both compounds) with various incubation periods up to 96 h. Data are presented as the mean ± SD (n = 3).

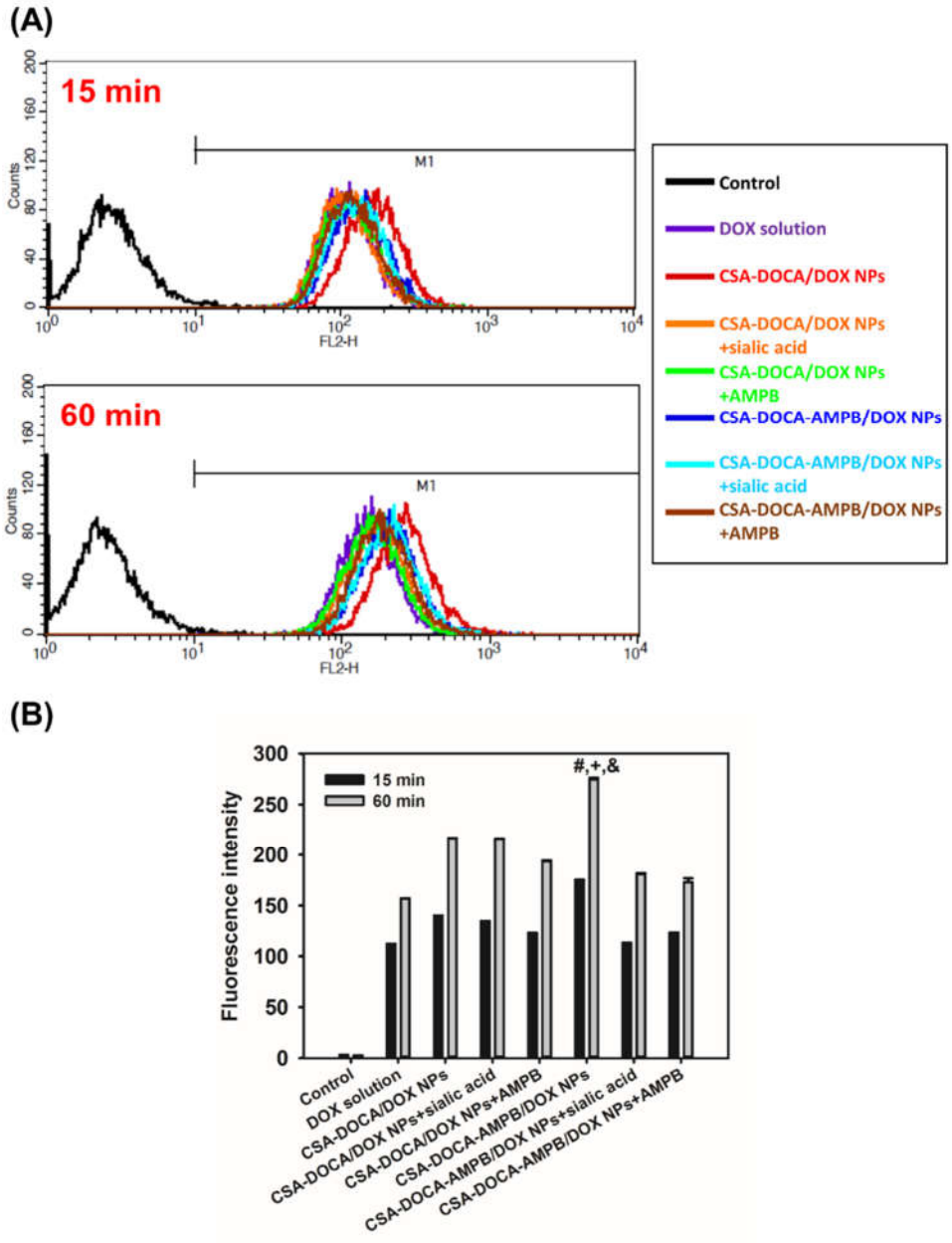

Figure 20 Quantitative analysis of DOX uptake in 2D-cultured A549 cells. Flow cytometry was used to measure the cell counts according to the fluorescence intensity (A) and the mean fluorescence intensity value (B) of each group. Data are presented as the mean ± SD (n = 3). $^{\#}p < 0.05$, compared to CSA-DOCA/DOX NPs group; $^{+}p < 0.05$, compared to CSA-DOCA-AMPB/DOX NPs + sialic acid group; $^{\&}p < 0.05$, compared to CSA-DOCA-AMPB/DOX NPs + AMPB group (at each time point).

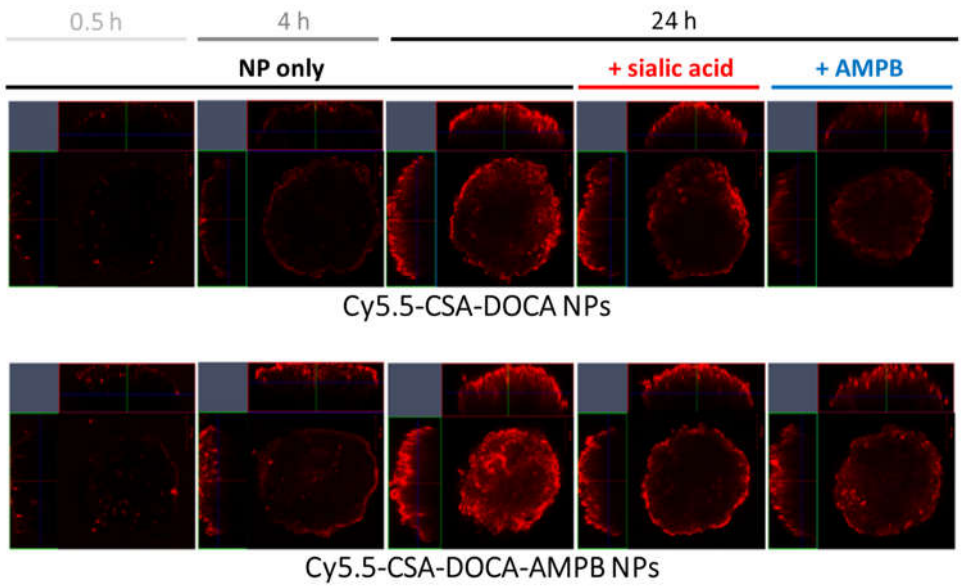

Figure 21 *In vitro* tumor penetration efficiency of the Cy5.5-tagged NPs in the 3D-cultured A549 spheroids. Z-stack CLSM images of A549 spheroids were obtained after incubation with NPs for 0.5, 4, and 24 h. Sialic acid (500 μM) and AMPB (500 μM) were used as inhibitors. The fluorescence intensities of Cy5.5 were observed. The length of scale bar is 100 μm.

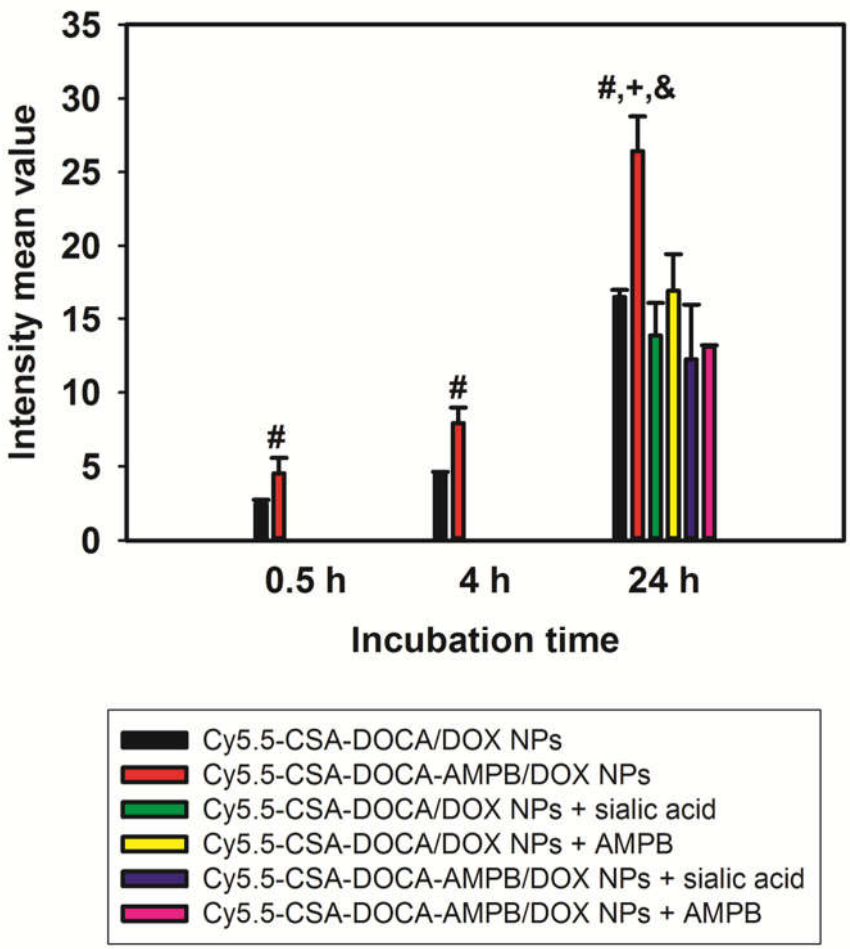

Figure 22 Quantitative analysis of the NP penetration in A549 spheroids using the Z-stack CLSM images. NPs were incubated for 0.5, 4, and 24 h with or without sialic acid (500 μM) or AMPB (500 μM). Fluorescence intensity values were measured from the horizontal section images of spheroids by ZEN2012 (blue edition) software (Carl-Zeiss, Thornwood, NY, USA). Data are presented as the mean ± SD ($n = 3$). $^{\#}p < 0.05$, compared to Cy5.5-CSA-DOCA/DOX NPs group; $^{+}p < 0.05$, compared to Cy5.5-CSA-DOCA-AMPB/DOX NPs + sialic acid group (at 24 h); $^{\&}p < 0.05$, compared to Cy5.5-CSA-DOCA-AMPB/DOX NPs + AMPB group (at 24 h).

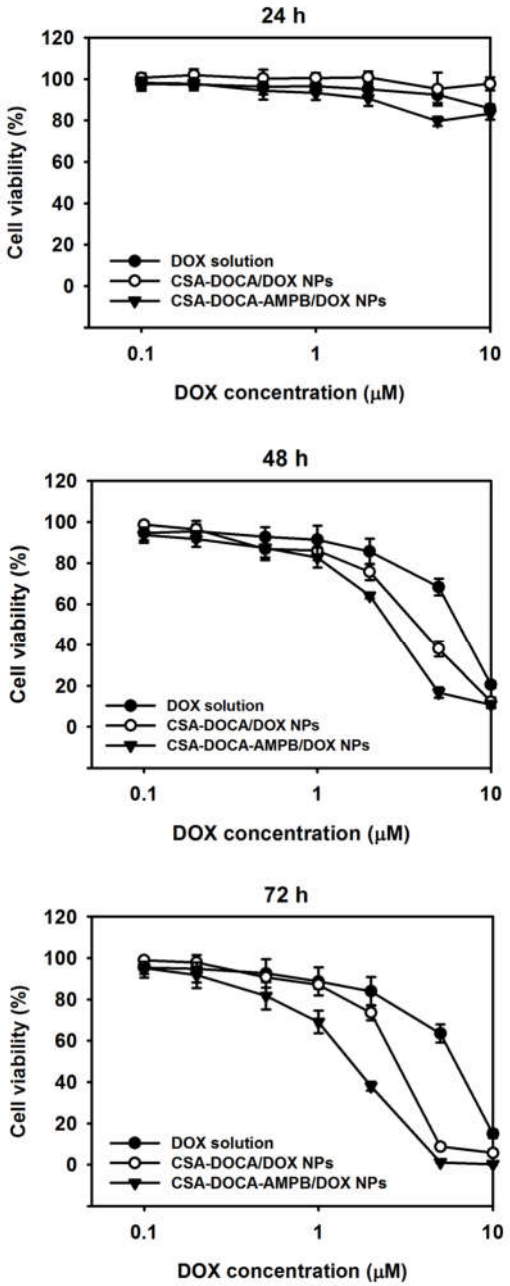

Figure 23 *In vitro* cytotoxicity of the developed DOX-loaded NPs in 2D-cultured A549 cells. The DOX solution and DOX-loaded NPs (as DOX, 0.1–10 μM) were incubated for 24, 48, and 72 in A549 cells. Cell viability (%) was measured using MTS-based assay. Data are presented as the mean ± SD (n = 6).

(A)

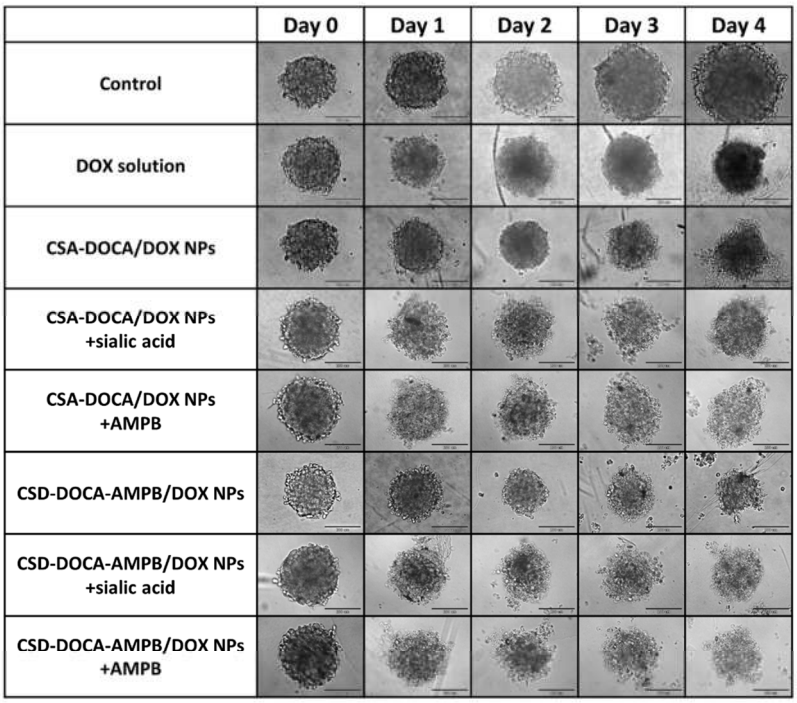

(B)

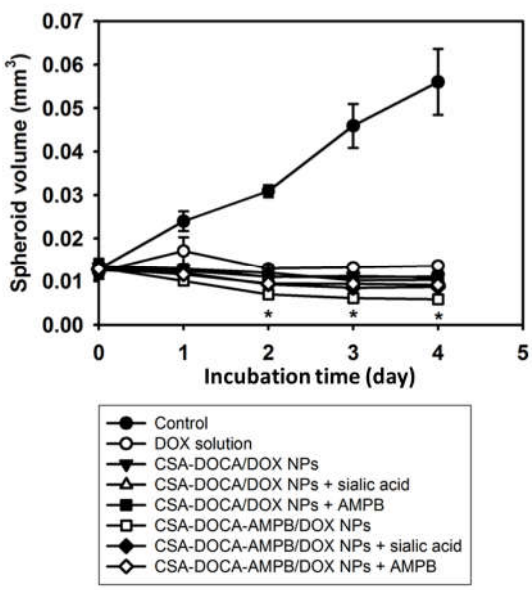

Figure 24 *In vitro* anti-tumor efficacy tests in A549 spheroid model. The DOX solution and DOX-loaded NPs (with or without sialic acid or AMPB) were incubated for 1 day. The spheroids were observed by optical microscopy (A), and their volumes were measured (B) until day 4. The length of scale bar is 200 μm. $^{*}p < 0.05$, compared to the other groups.

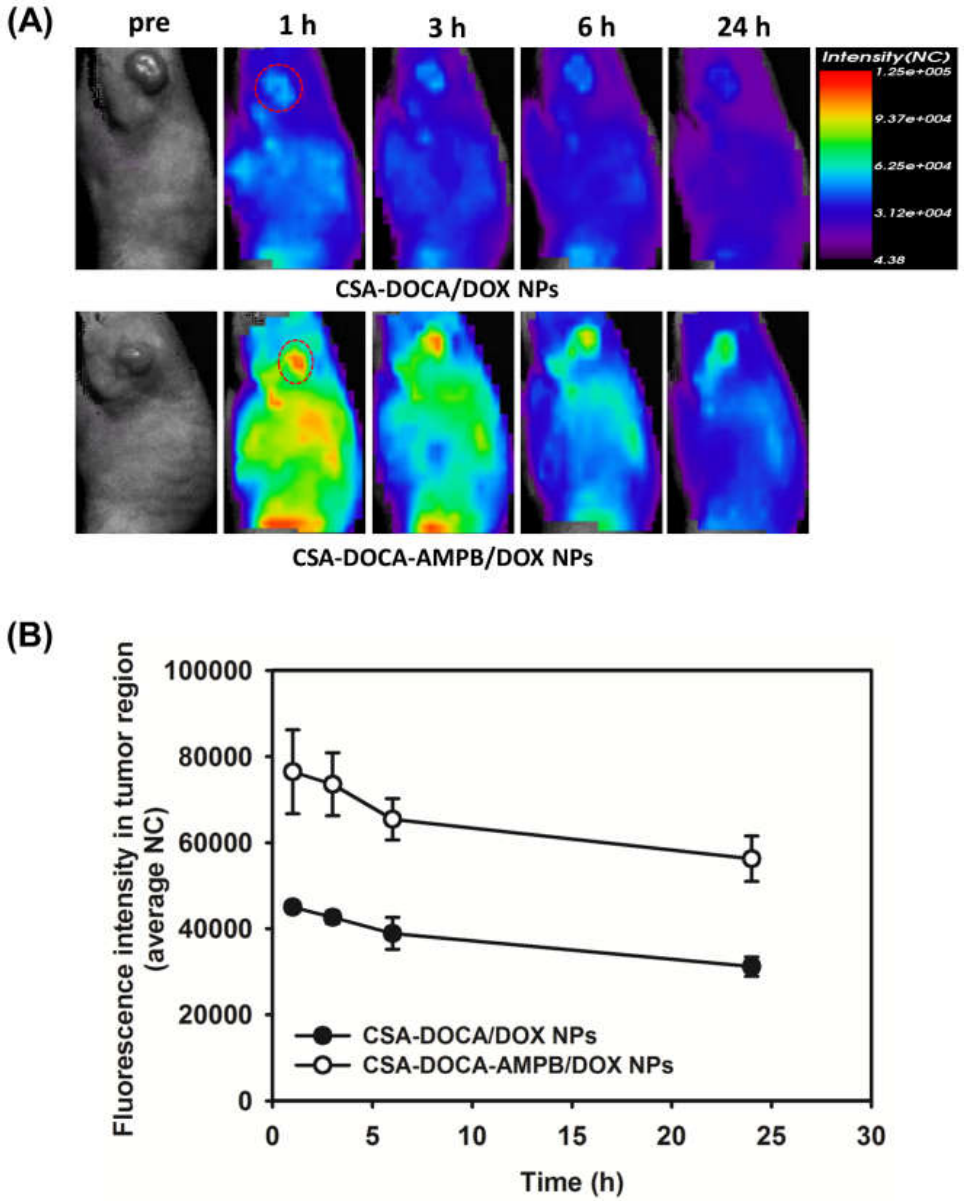

Figure 25 *In vivo* NIRF imaging study after intravenous administration of the Cy5.5-tagged CSA-DOCA/DOX NPs and CSA-DOCA-AMPB/DOX NPs in A549 tumor-xenografted mouse model. (A) Real-time fluorescence images of whole body are presented. Dashed circle indicates tumor region. (B) Profiles of fluorescence intensity in tumor region versus time are shown. Each point represents the mean ± SD (n = 3).

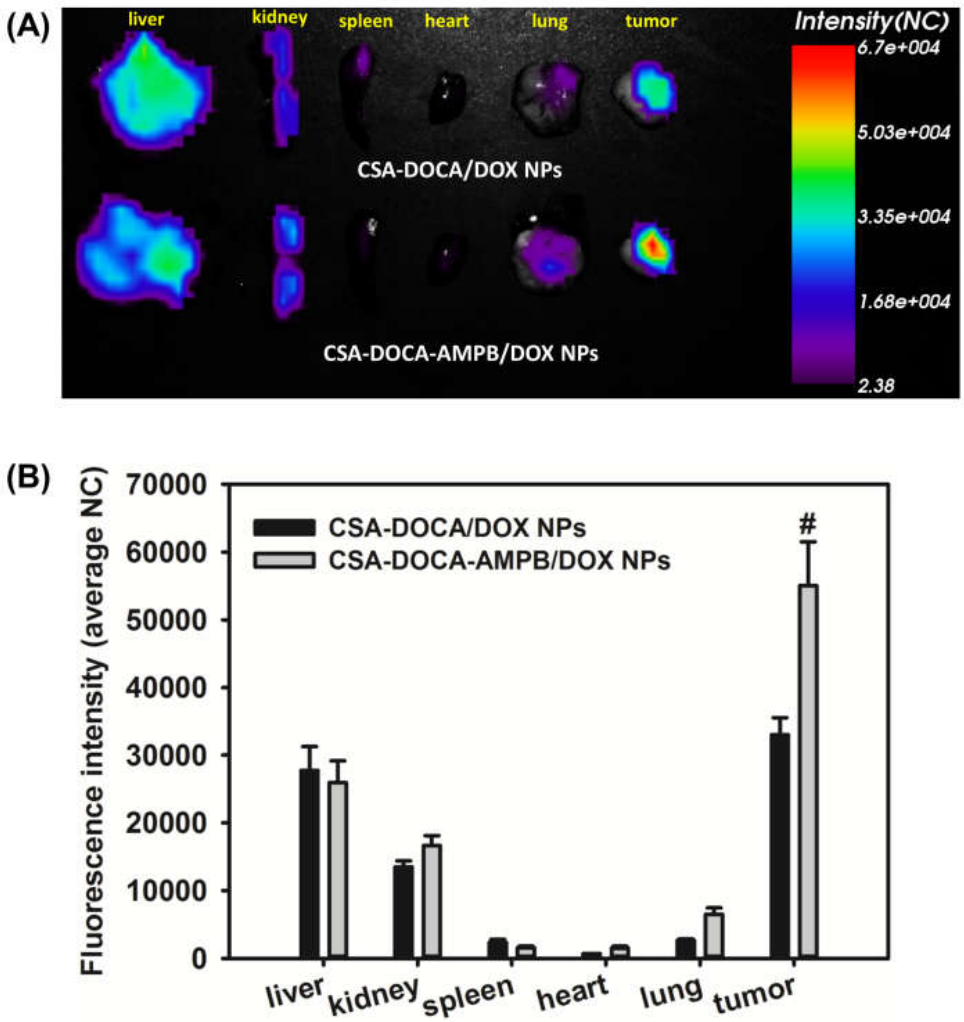

Figure 26 *Ex vivo* NIRF imaging studies in A549 tumor-xenografted mouse model. Biodistribution of the Cy5.5-tagged NPs at 24 h post-injection was investigated. (A) Several organs and tumor tissues were dissected and their NIRF images were obtained. (B) Fluorescence intensities of the organs and tumor tissues were quantitatively analyzed. Data are presented as the mean ± SD ($n = 3$). $^{\#}p < 0.05$, compared to CSA-DOCA/DOX NPs group.

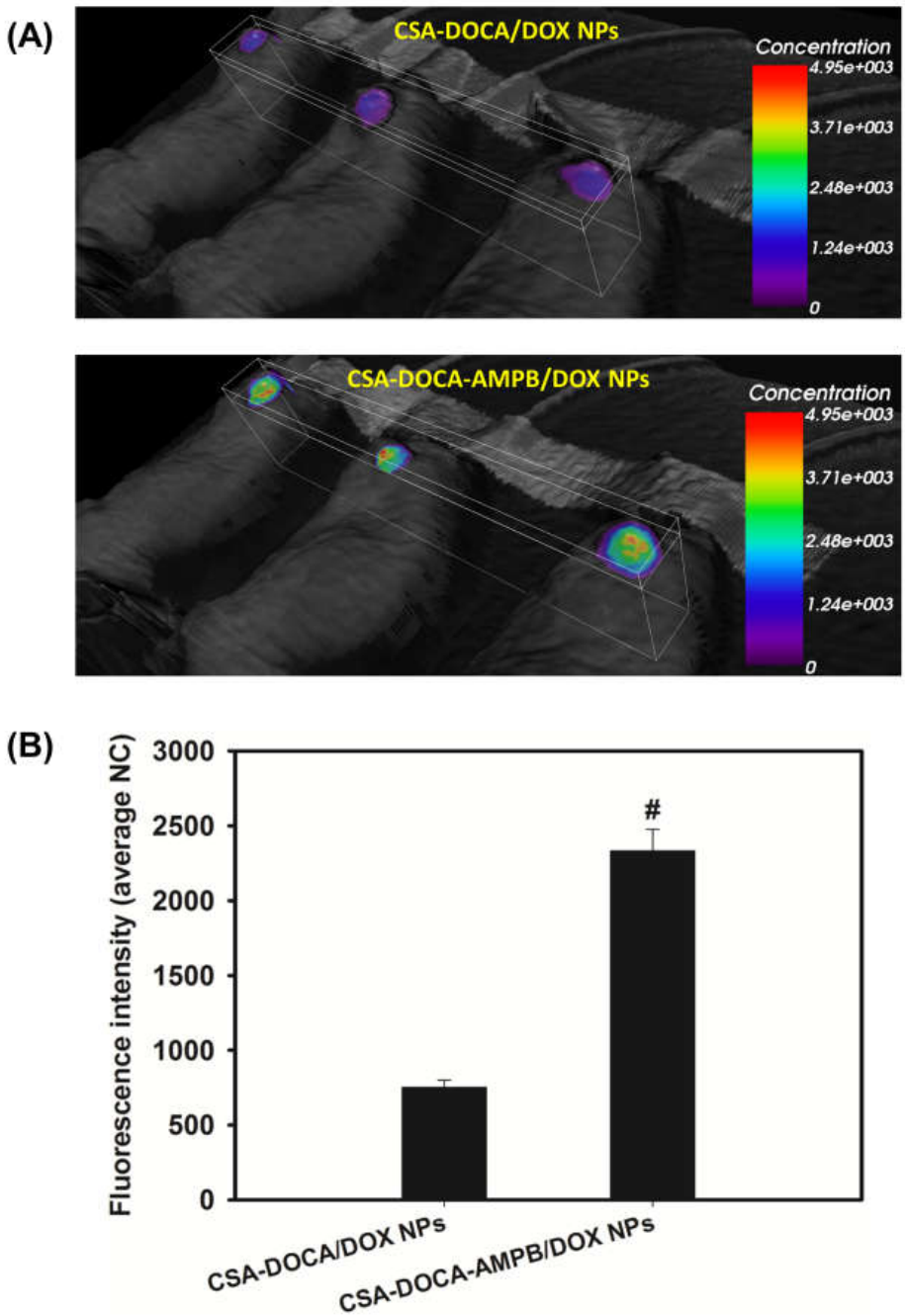

Figure 27 *In vivo* tumor penetration assay of the developed NPs in A549 tumor-xenografted mouse model. (A) Z-stack NIRF images of tumor tissues at 24 h post-injection are presented. (B) Quantitatively analyzed fluorescence intensities in the sliced plane of tumor region of both groups are shown. Data represents the mean ± SD (n = 3). $^{\#}p < 0.05$, compared to CSA-DOCA/DOX NPs group.

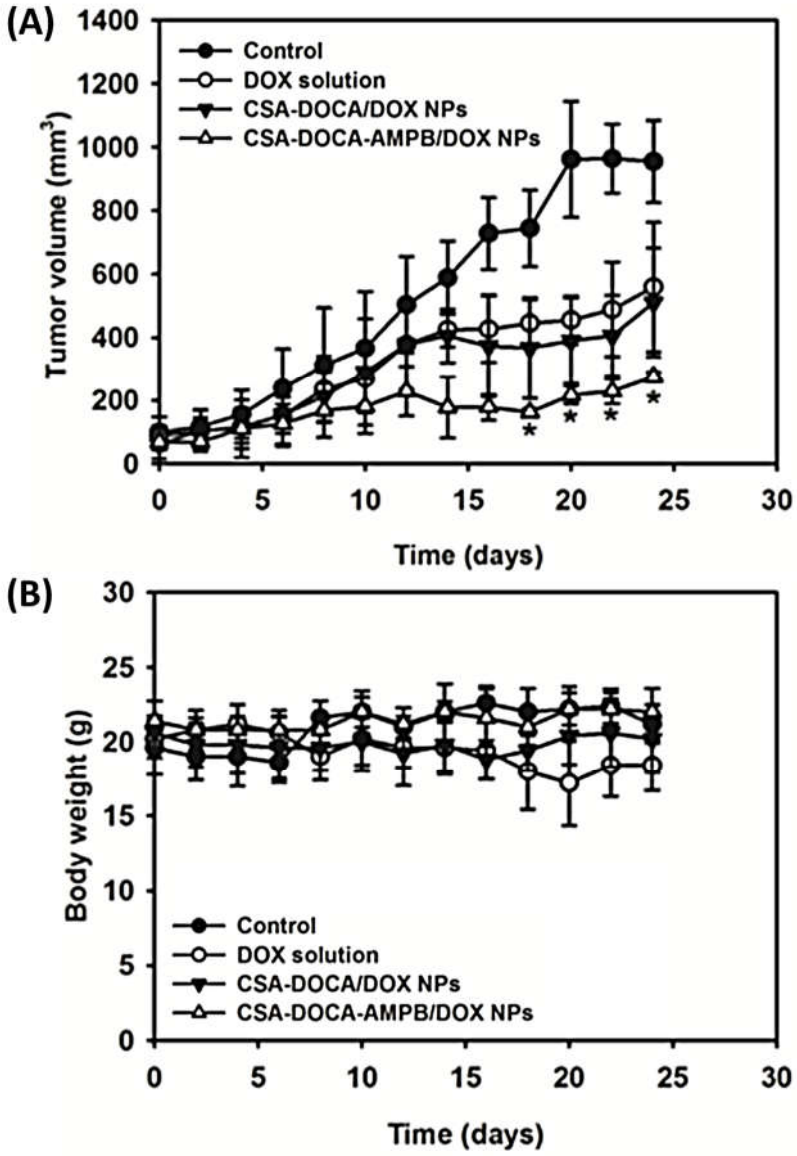

Figure 28 *In vivo* anti-tumor efficacy test in A549 tumor-xenografted mouse model. (A) Tumor growth inhibition after intravenous administration (as DOX, 5 mg/kg; day 4, 7, 9, and 11) of the developed DOX-loaded NPs were evaluated for 24 days by monitoring tumor volume, as well as body weight. Data represent mean ± SD ($n = 4$). $^{*}p < 0.05$, compared to the other groups.

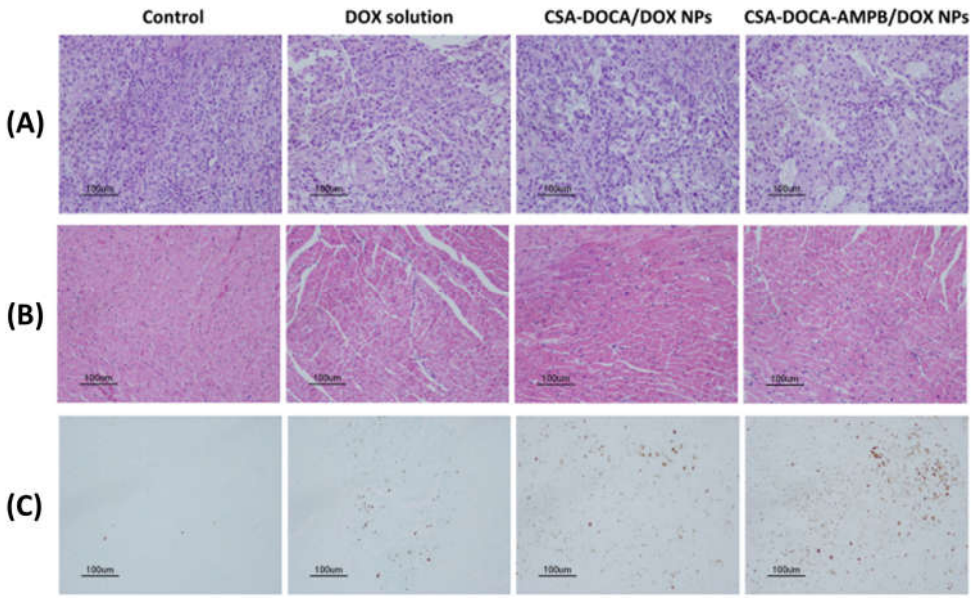

Figure 29 Histological assays of dissected tumor and heart. H&E staining of tumor (A) and heart (B), and TUNEL assay of tumor (C) were carried out at the end of the anti-tumor efficacy test (day 24) with the DOX solution and DOX-loaded NPs. The length of scale bar is 100 μm.

국문초록

종양 표적화 및 침투를 위한 자가조립형 나노입자를 개발하기 위하여 본 연구에서는 소수성 잔기인 deoxycholic acid(DOCA)를 친수성 고분자인 콘드로이틴황산염A(CSA)에 도입하였으며, 이를 (3-aminomethylphenyl)boronic acid(AMPB)로 수식하였다. 합성된 양쪽성 고분자인 CSA-DOCA의 DOCA 함량과 자가조립능을 확인하기 위하여 양성자 핵자기 공명 분석을 실시하고 임계 입자 형성 농도를 산출하였다. 모델 항암제로써 독소루비신을 선정하고 이를 자가조립 과정을 통하여 CSA-DOCA에 봉입함으로써 나노입자를 제조하였다. 완성된 나노입자는 콘드로이틴황산염과 암세포에 과발현 되어 있는 CD44 수용체 간의 상호작용을 통한 종양표적능을 가질 것으로 예상하여, 이를 세포내 도입 실험계와 종양 이종 이식 마우스 모델을 이용하여 검증하였다. 이어서, CSA-DOCA에 AMPB를 수식하여 합성된 CSA-DOCA-AMPB는 양성자 핵자기 공명 및 형광 광도 분석법을 이용하여 AMPB의 도입을 확인하였다. CSA-DOCA-AMPB에 독소루비신을 봉입하여 형성된 나노입자는 구형의 형상을 가지며 200 nm 정도의 평균 입자 지름과 좁은 입도분포, 음의 표면전하를 띠었다. 용출시험을 통하여 CSA-DOCA-AMPB 나노입자로부터 독소루비신이 서방출 되는 것을 확인하였으며 특히 산성 조건에서 그 용출률이 크게 증가되는 것이 관찰 되었다. 종양 침투를 위하여 수식된 AMPB의

작동을 확인하기 위하여 입자 표면의 페닐보론산 과 암세포 표면의 시알산의 상호작용을 2차원 단층 세포 배양 모델 및 3차원 스페로이드 모델에서 검증 하였다. 최종적으로 종양 이종 이식 마우스 모델에서 근적외선형광 이미징을 이용하여 종양 표적화 및 침투를 확인 하였으며 종양의 크기 측정 및 조직 염색을 통하여 항암화학치료효과를 평가하였다. 종합적으로 CSA-DOCA-AMPB 나노입자는 대조군인 CSA-DOCA 나노입자에 비하여 뛰어난 종양 표적·침투능 및 항암화학치료효과를 보여 주었으며 이를 고려할 때, CSA-DOCA-AMPB 나노입자는 항암제의 전달 및 그 치료 효과를 증진시킬 수 있는 제형으로써 사용될 수 있을 것이다.

주요어: 콘드로이틴황산염; 종양 표적능; 종양 침투능; 항암제 전달 시스템; 나노입자

학 번: 2011-21757

APPENDIX

Phenylboronic Acid-Decorated Chondroitin Sulfate A-based Nanoparticles for Solid Tumor Targeting and Penetration

Jae-Young Lee

Department of Pharmaceutical Science
College of Pharmacy
The Graduate School
Seoul National University

HOW TO CURE CANCER?

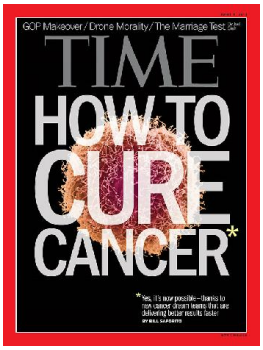

..."This disease is much more complex than we have been treating it," says MIT's Phillip Sharp. "And the complexity is stunning."...

TIME, Apr. 1, 2013

IN VIVO BARRIERS FACING ANTICANCER AGENTS

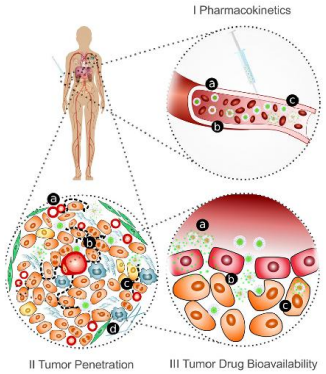

1. blood compartment

2. tumor extravasation and accumulation

3. tumor penetration and tumor drug bioavailability

the Achilles' heel of anticancer drugs that bind to cellular macromolecules

(e.g., **doxorubicin**, paclitaxel, daunomycin, actinomycin D, methotrexate)

Advanced Drug Delivery Reviews 91 (2015) 7–22

MICROENVIRONMENT OF SOLID TUMORS

- **Reduced vascular density**
  - limited delivery of oxygen and nutrients
  - low pH of extracellular region (Warburg effect)
- **Poorly organized vasculature and immature lymphatics**
  - increased interstitial fluid pressure (IFP)
  - reduced convection

➡ **Obstacles for the homogeneous drug delivery** to the cancer cells far from the blood vasculature.

- **Change in ECM structure and composition**
  - cancer-associated fibroblasts (CAF)
  - lysyl oxidase, glycation, or transglutamination
- **Higher packing density of cancer cells**

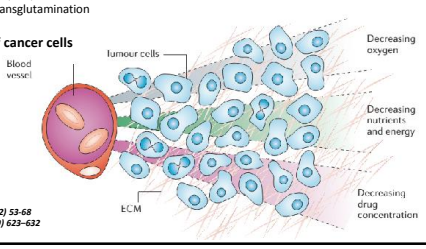

Nature Reviews Cancer. 6 (2006) 583-592
Advanced Drug Delivery Reviews. 64 (2012) 53-68
Advanced Drug Delivery Reviews 61 (2009) 623–632

DOXORUBICIN (DOX), AS A MODEL DRUG (1)

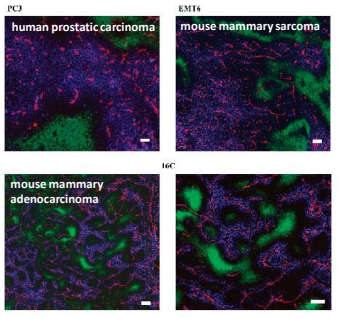

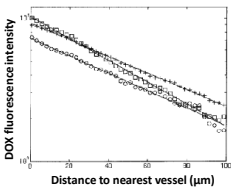

Tumor	Characteristic penetration length "L" (μm)
PC-3	51.4 ± 0.8
16C	39.3 ± 0.08†
EMT6	49 ± 1.6

Clin Cancer Res 11 (2005) 8782-8788

DOXORUBICIN (DOX), AS A MODEL DRUG (2)

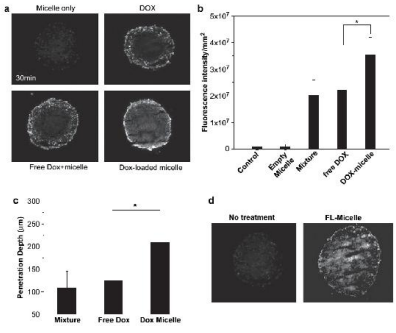

➡ **Poor *in vivo* outcome**
- no pharmacokinetic evaluation

Biomaterials 31 (2010) 7386-7397

DESIGN CRITERIA

1. tumor penetration
2. tumor targeting
3. drug loading & release behavior
4. biocompatibility

KEY FACTORS

- mean diameter
- zeta potential
- targeting moiety
- entrapment efficiency
- sustained release
- toxicity

CHONDROITIN SULFATE (CS) AND CD44 TARGETING

- Sulfated glycosaminoglycan (GAG)
- Biomaterial found in cartilage, skin, corneas, extracellular matrix (ECM), and umbilical cords
- Alternating sugars of N-acetyl-D-galactosamine (GalNAc) and D-glucuronic acid (GlcA)
- Sulfation at either 2-, 4-, or 6-position of GalNAc (4 types): highly polyanionic
- Interaction with cluster of differentiation 44 (CD44): cancer targeting
- High stability, low toxicity, non-immunogenicity, biodegradability, and biocompatibility
- Possibility of chemical modifications (carboxyl and hydroxyl groups)

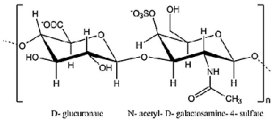

Excellent hydrophilicity
(water solubility ≈ 50 mg/mL)

1. **CS-drug conjugates**
   prednisolone, ketoprofen, ibuprofen, naproxen
2. **Drug-loaded CS derivatives**
   cholesterol, histamine, L-lactide, poly(ε-caprolactone), acetic anhydride

International Immunology 13 (2001) 359–366, Journal of Controlled Release 180 (2014) 81–90, Nanomedicine: Nanotechnology, Biology, and Medicine 9 (2013) 605–626

SELF-ASSEMBLED NANOPARTICLE SYSTEM

- Entrapment of poorly water-soluble drugs in its hydrophobic core(s) ➡ Deoxycholic acid
  - improves apparent aqueous solubility, which enables direct injection into blood circulation system
  - reduces toxic side effects of drug
  - improves stability of drug in vivo

- Nano-sized hydrophilic shell ➡ Chondroitin sulfate A
  - prevent opsonization by reducing the protein interaction
  - decrease clearance by the reticuloendothelial system (RES)
  - prolong the blood circulation (enhanced permeability and retention [EPR] effect; passive targeting)
  - can be modified with targeting ligands (active targeting)

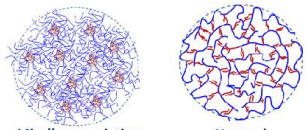

Micellar association | Nanogel

Progress in Polymer Science. 53 (2016) 207–248
Carbohydrate Polymers. 133 (2015) 391–399
Advanced Drug Delivery Reviews 66 (2014) 2–25

SIALIC ACID TARGETING STRATEGY

❖ **Sialic acid (SA)**

- Carbohydrate antigens expressed in all tumor cells (aberrant glycosylation)
- Closely related with cancer progression and poor prognosis
- Increased expression particularly in **hypoxic regions** of solid tumors
- Hypoxia is a product of the **large distance** from functioning blood vessels

➡ SA-targeting could be an efficient tumor penetration strategy

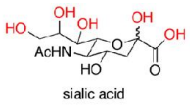

sialic acid

❖ **Saccharide sensors**

- Lectins (Concanavalin A, ricin)
- Glucose oxidase

➡ Limited application (protein-based components)

Polymer 52 (2011) 4631–4643
Biomaterials. 75 (2016) 102–111
Polymer Journal. 46 (2014) 483–491

PHENYLBORONIC ACID (PBA)

- Reversible covalent complexation with *cis*-diol moieties of common sugars
- Glucose sensors, chromatographic separation of carbohydrates, and RNA affinity columns
- Stable, non-toxic, non-immunogenic and inexpensive (cf. lectins)
- PBA-SA binding is stable even at lower pHs
  - multiple metastable binding sites
  - intramolecular stabilization via B-N or B-O
  - stable trigonal binding

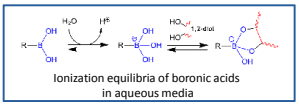

Ionization equilibria of boronic acids in aqueous media

➡ specifically binds to sialylated epitopes at acidic conditions (e.g., tumor and inflammation)

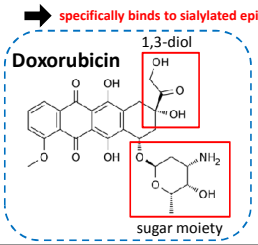

sugar	binding constants (K_b; M^{-1})		K_b 6.5/K_b 7.4
	pH 7.4	pH 6.5	
glucose	1.71	0.39	0.29
mannose	3.95	0.70	0.17
galactose	5.11	1.11	0.21
Neu5Ac (SA)	12.3	12.7	**1.03**

Polymer Journal. 46 (2014) 483–491
Journal of the American Chemical Society. 135 (2013) 15501–15507

HYPOTHESIS

- It was hypothesized that the introduction of phenylboronic acid (PBA) moiety that targets the hypoxic region of tumors, to a tumor-targetable chondroitin sulfate A (CSA)-based NP system may further enhance the tumor-targeting and penetration effects, thereby maximizing the therapeutic efficacy of the loaded drug, doxorubicin.

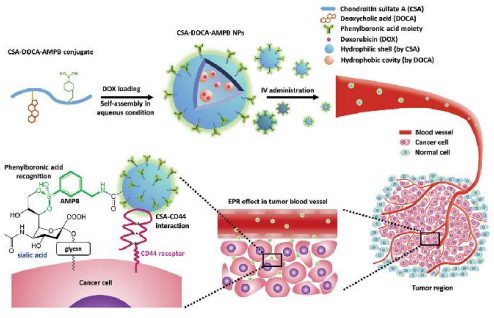

OBJECTIVES

- **Preparation of CSA-based self-assembled nanoparticles (NPs) which can take advantage of the interaction with CD44**
- Preparation of the PBA-decorated CSA-based NPs for the enhanced tumor penetration *via* SA targeting
- *In vitro* and *in vivo* evaluation of the developed NPs focused on the tumor penetration using 3D culture models (multicellular spheroids) and tumor-xenografted mouse model, respectively.

SYNTHETIC SCHEME OF CSA-DOCA

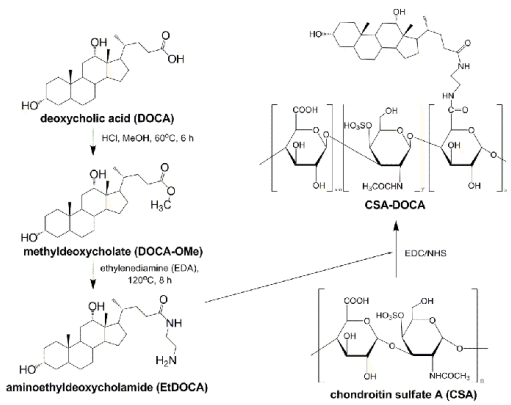

DOCA CONTENT IN CSA-DOCA

❖ NMR spectrum of CSA-DOCA

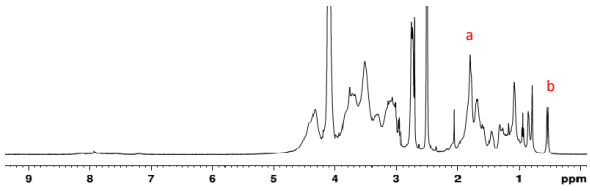

a (1.8 ppm) from CSA and b (0.6 ppm) from DOCA

Product name	Feed ratio (EtDOCA/CSA) weight ratio	Integration ratio	Calculated DOCA/CSA weight ratio	DOCA content in CSA-DOCA (%; w/w)
CSA-DOCA	34.8 mg/100 mg	0.168	0.0979	8.92

CHARACTERIZATION OF DOX-LOADED CSA-DOCA NPS

❖ Size distribution

Blank CSA-DOCA NPs | CSA-DOCA/DOX NPs

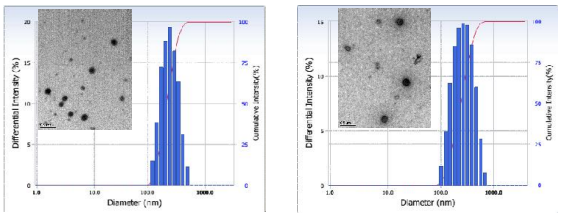

Composition	Mean diameter (nm)	Polydispersity index	Zeta potential (mV)	Entrapment efficiency (%)
Blank CSA-DOCA NPs	228.2 ± 7.6	0.19 ± 0.03	-23.07 ± 1.17	-
CSA-DOCA/DOX NPs	233.7 ± 7.0	0.22 ± 0.02	-21.52 ± 1.06	85.5 ± 7.9

IN VITRO CELLULAR UPTAKE STUDY (CLSM OBSERVATION)

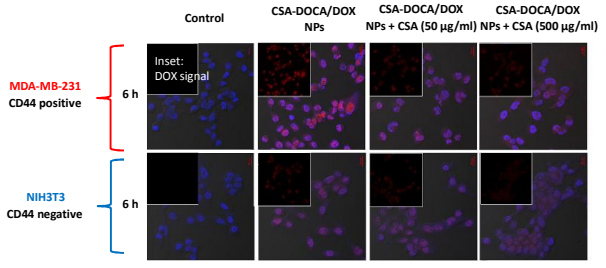

IN VIVO NEAR-INFRARED FLUORESCENCE (NIRF) IMAGING

❖ IV administration of Cy5.5-conjugated CSA-DOCA NPs with or without CSA pre-treatment
- MDA-MB-231 tumor-xenografted mouse model
- sham procedure but the additional CSA pre-treatment (5 mg of CSA per a mouse)

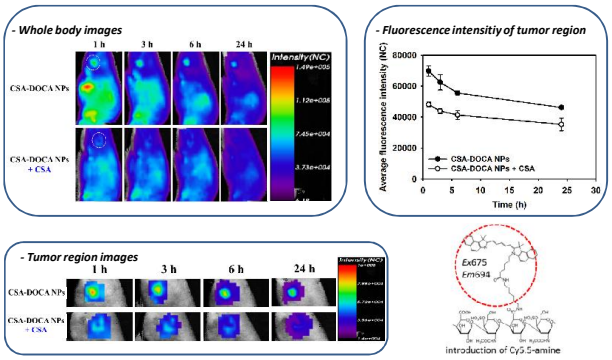

OBJECTIVES

- Preparation of CSA-based self-assembled nanoparticles (NPs) which can take advantage of the interaction with CD44
- **Preparation of the PBA-decorated CSA-based NPs for the enhanced tumor penetration *via* SA targeting**
- ***In vitro* and *in vivo* evaluation of the developed NPs focused on the tumor penetration using 3D culture models (multicellular spheroids) and tumor-xenografted mouse model, respectively.**

IN VITRO 2D (MONOLAYER) VS. 3D CULTURE MODELS

- **2D (monolayer) culture model**
  - exposed to a uniform environment and to a uniform concentration of a drug
  - dose not reflect the microenvironment of solid tumors
- **3D culture model**
  - in vitro multicellular models
  : commonly used tools for qualitative and quantitative evaluation of drug penetration
- **Multicellular spheroids**
  - reflect many of the properties of solid tumors
  : development of an ECM, tight junctions between cells,
  gradients of nutrient and oxygen concentration, and cell contact effect

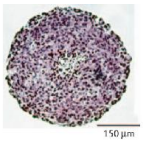

Nature Reviews Cancer 6 (2006) 583-592
International journal of pharmaceutics 464 (2014) 168-177
Biomaterials 31 (2010) 1180-1190

MULTICELLULAR SPHEROIDS

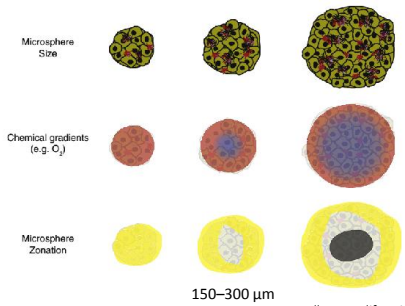

150–300 μm

yellow: proliferating zone
black: necrotic core

Advanced Drug Delivery Reviews 69–70 (2014) 29–41

SYNTHESIS AND CHARACTERIZATION OF CSA-DOCA-AMPB

❖ NMR spectra of CSA-DOCA-AMPB and its AMPB content

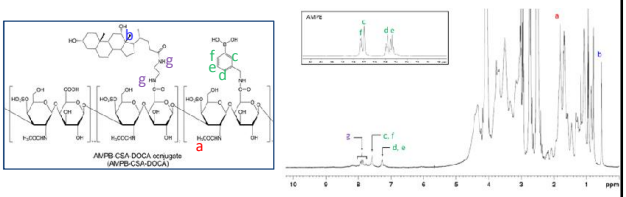

Product name	Feed ratio (AMPB/CSA-DOCA; w/w)	Integration Ratio	Calculated AMPB/CSA-DOCA weight ratio	AMPB content in CSA-DOCA-AMPB (%; w/w)
CSA-DOCA-AMPB	7.5 mg/100 mg	0.265	0.0235	2.30

CHARACTERIZATION OF DOX-LOADED CSA-DOCA-AMPB NPS

❖ Size distribution

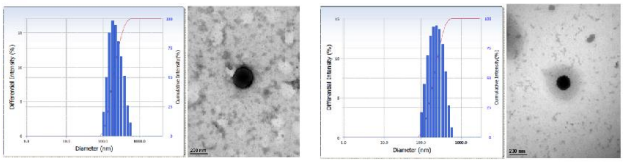

CSA-DOCA/DOX NPs　　CSA-DOCA-AMPB/DOX NPs

Composition	Mean diameter (nm)	Polydispersity index	Zeta potential (mV)	Entrapment efficiency (%)
CSA-DOCA/DOX NPs	228.9 ± 2.0	0.22 ± 0.01	-22.58 ± 1.82	80.9 ± 0.2
CSA-DOCA-AMPB/DOX NPs	205.8 ± 8.2	0.21 ± 0.01	-20.97 ± 0.75	71.7 ± 0.2

zeta potential: +10 mV to -30 mV
mean diameter: EPR vs. interstitial transport

IN VITRO DOX RELEASE TEST

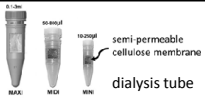

❖ DOX release profile

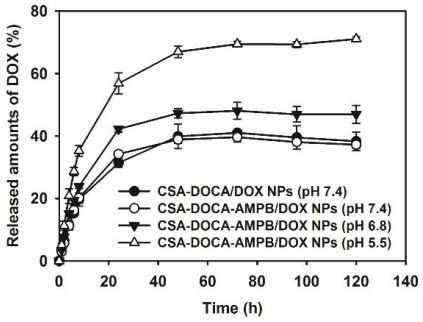

- pH-dependent release pattern was observed
- Each point represents the mean ± SD (n = 3).

In vitro cytotoxicity tests of blank NPs

❖ MTS-based assay in A549 cells

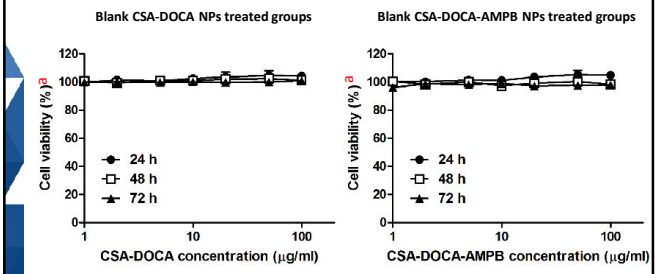

[a] Cell viability (%) = $\frac{\text{Absorbance}^{b} \text{ of NP–treatment group}}{\text{Absorbance of no–treatment group}}$

[b] Absorbance of water–soluble formazan at a wavelength of 490 nm.

In vitro cellular uptake study (CLSM observation) in A549 cells (2D culture)

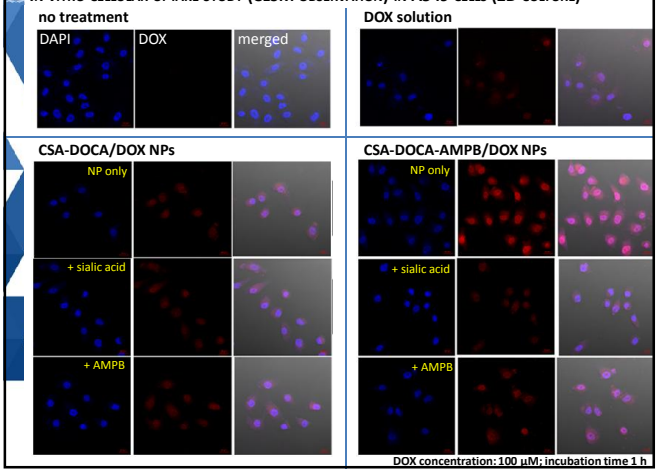

In vitro cellular uptake study (CLSM observation) in A549 spheroids

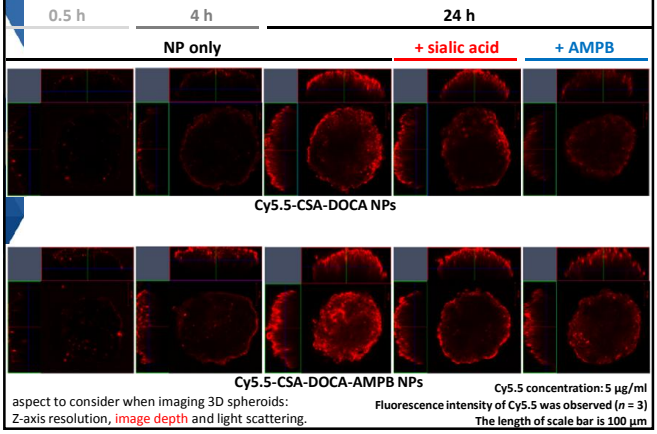

aspect to consider when imaging 3D spheroids:
Z-axis resolution, image depth and light scattering.

Cy5.5 concentration: 5 μg/ml
Fluorescence intensity of Cy5.5 was observed (n = 3)
The length of scale bar is 100 μm

Mean fluorescence intensity values of horizontal section

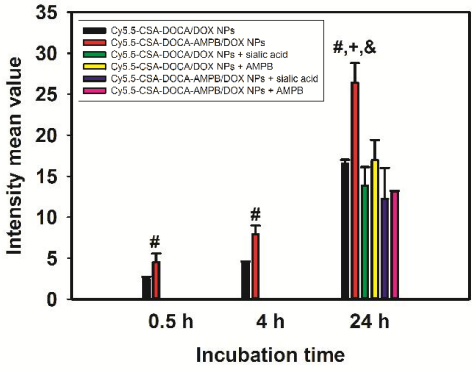

[a] $p < 0.05$, compared to Cy5.5-CSA-DOCA/DOX NPs group

[†] $p < 0.05$, compared to Cy5.5-CSA-DOCA-AMPB/DOX NPs + sialic acid group (at 24 h)

[&] $p < 0.05$, compared to Cy5.5-CSA-DOCA-AMPB/DOX NPs + AMPB group (at 24 h).

In vivo NIRF imaging (1)

❖ IV administration of Cy5.5-CSA-DOCA NPs or Cy5.5-CSA-DOCA-AMPB NPs
- A549 tumor-xenografted mouse model
- as Cy5.5, 0.12 mg/kg

- Whole body images (in vivo)

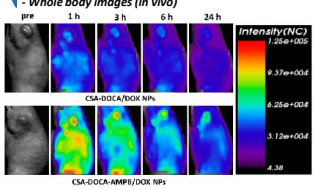

- Ex vivo images

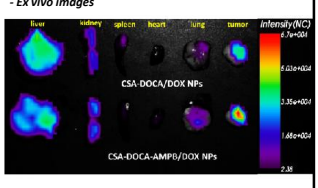

- Fluorescence intensity of tumor region (in vivo)

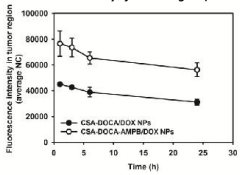

- Fluorescence intensity of dissected organs and tumors

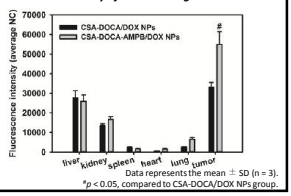

Data represents the mean ± SD (n = 3).
[#] $p < 0.05$, compared to CSA-DOCA/DOX NPs group.

In vivo NIRF imaging (2)

❖ Reconstructed NIRF images for the observation of tumor penetration (Z-stack images)

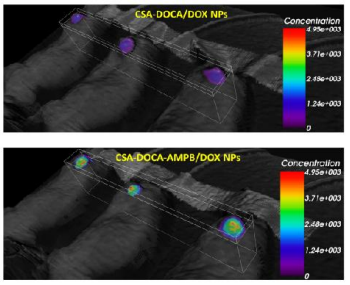

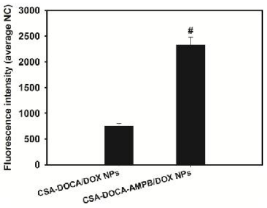

Data represents the mean ± SD (n = 3).
[#] $p < 0.05$, compared to CSA-DOCA/DOX NPs group.

IN VIVO ANTI-TUMOR EFFICACY TEST

- A549 tumor-xenografted mouse model
- dose: as DOX, 5 mg/kg
- iv administration at day 4, 7, 9, and 11.
- $^{*}p < 0.05$, compared to the other groups.

❖ Tumor size and body weights

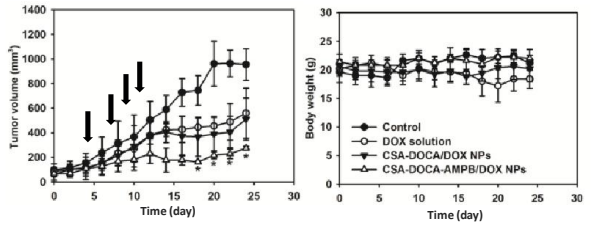

❖ H&E staining of hearts (dissected on day 24)

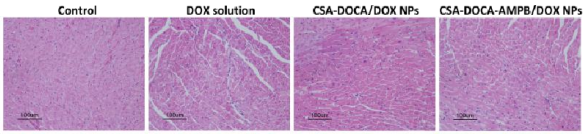

TUMOR-PRIMING EFFECT

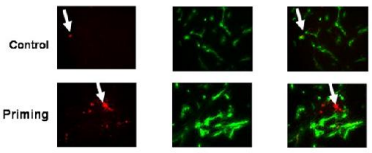

red: NP distribution
green: blood perfusion

DOX -> inducing apoptosis -> reducing tumor cell density and increasing the fraction of interstitial space -> enhancing the diffusive transport

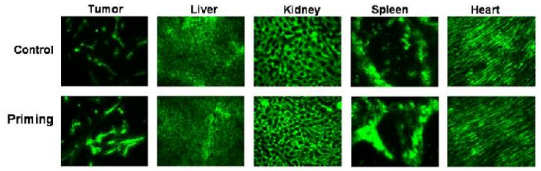

not observed in noncancerous tissues including liver, kidney, heart and spleen

Advanced Drug Delivery Reviews 64 (2012) 29–39

REMAINING CHALLENGES

❖ Complex cellular heterogeneity of tumor

cancer cells coexist with
- cancer-associated fibroblasts (CAFs)
- infiltrating immune cells
- endothelial cell

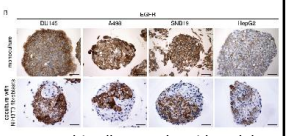

multi-cell-type spheroid models

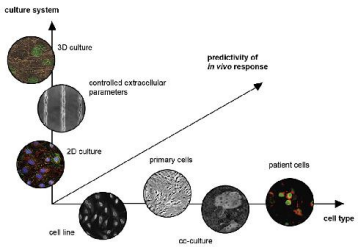

Advanced Drug Delivery Reviews 69–70 (2014) 52–66

REMAINING CHALLENGES

❖ Unrealistic experimental models

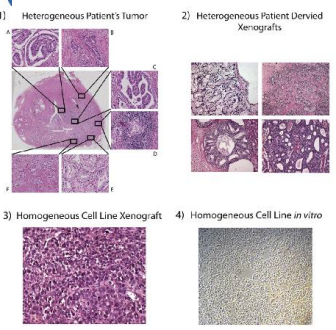

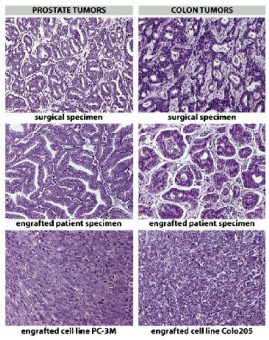

Advanced Drug Delivery Reviews 79–80 (2014) 222–237
Advanced Drug Delivery Reviews 74 (2014) 2–11

FUTURE DIRECTIONS

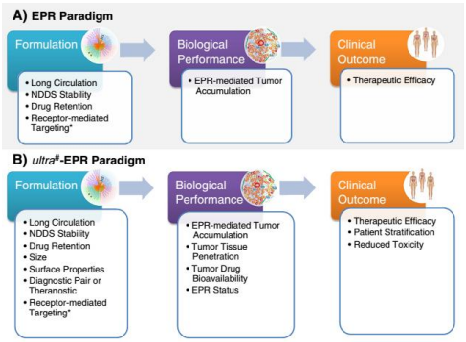

will focus on making **more predictive experimental models and formulations with "*undruggable*" compounds**

Advanced Drug Delivery Reviews 91 (2015) 7–22

THANK YOU

ADVANCED FUNCTIONAL MATERIALS
www.afm-journal.de

Phenylboronic Acid-Decorated Chondroitin Sulfate A-Based Theranostic Nanoparticles for Enhanced Tumor Targeting and Penetration

Jae-Young Lee, Suk-Jae Chung, Hyun-Jong Cho, and Dae-Duk Kim**

Phenylboronic acid-functionalized chondroitin sulfate A (CSA)–deoxycholic-acid (DOCA)-based nanoparticles (NPs) are prepared for tumor targeting and penetration. (3-Aminomethylphenyl)boronic acid (AMPB) is conjugated to CSA–DOCA conjugate via amide bond formation, and its successful synthesis is confirmed using proton nuclear magnetic resonance spectroscopy (^{1}H-NMR). Doxorubicin (DOX)-loaded CSA–DOCA–AMPB NPs with a mean diameter of ≈200 nm, a narrow size distribution, negative zeta potential, and spherical morphology are prepared. DOX release from NPs is enhanced at acidic pH compared to physiological pH. CSA–DOCA–AMPB NPs exhibit improved cellular uptake in A549 (human lung adenocarcinoma) cells and penetration into A549 multicellular spheroids compared to CSA–DOCA NPs as evidenced by confocal laser scanning microscopy and flow cytometry. In vivo tumor targeting and penetrating by CSA–DOCA–AMPB NPs, based on both CSA–CD44 receptor and boronic acid–sialic acid interactions, is revealed using near-infrared fluorescence (NIRF) imaging. Penetration of NPs to the core of the tumor mass is observed in an A549 tumor xenografted mouse model and verified by three-dimensional NIRF imaging. Multiple intravenous injections of DOX-loaded CSA–DOCA–AMPB NPs efficiently inhibit the growth of A549 tumor in the xenografted mouse model and increase apoptosis. These boronic acid-rich NPs are promising candidates for cancer therapy and imaging.

1. Introduction

The selective delivery of high doses of drug to tumors is regarded as the main objective of cancer chemotherapy. The enhanced permeability and retention (EPR) effect can be adopted as a passive tumor targeting strategy and is based on the aberrant vasculature of tumors that results from angiogenesis and an immature lymphatic system.[1] If nanocarriers have suitable physicochemical properties (i.e., particle size, shape, and surface charge), the EPR effect causes them to accumulate in tumors.[2] However, passive tumor targeting based on the EPR effect provides unspecific tumor targeting; therefore, tumor-specific targeting moieties have been introduced to nanocarriers in order to enhance their selective tumor targeting. The conjugation of tumor-specific ligands (i.e., small molecules, peptides, and antibodies) that are able to interact with receptors overexpressed in cancer cells to nanocarriers is called an active tumor targeting strategy,[3–6] and has been widely used in conjunction with passive tumor targeting strategies.

Even though the use of the above mentioned tumor-targeting strategies can result in some anticancer activity, clinically effective therapeutics require homogenous distribution of therapeutic agents across the entire tumor, and this is not easily achieved. The delivery of drugs to solid tumors is hampered by their characteristic features such as increased stiffness of the tumor extracellular matrix (ECM) and high interstitial fluid pressure (IFP).[7,8] The abnormal ECM and high IFP in tumors can prevent the penetration of anticancer agents into the core of tumors. Successful distribution of anticancer drugs to the core of the tumor would allow the establishment of a fully effective cancer therapy and prevent metastasis and relapse. To overcome the stiff ECM and high IFP of solid tumors, there are several strategies that can be employed: the ECM can be degraded with enzymes (i.e., hyaluronidase and collagenase); tumor-targeting ligands can be introduced (i.e., folic acid); and agents that reduce IFP can be used (i.e., vasotargeting agents, vascular disrupting agents, vasodilators, and tumor growth factor-beta inhibitors).[9]

To aid tumor penetration, sialic acid-targeting strategy can be used to enhance intratumoral transport of nanocarriers.[10] It has been reported that sialylated epitopes (glycan chains including *N*-acetylneuraminic acid) are overexpressed on cancer cells, and their presence is implicated in metastasis, progression, apoptosis, and resistance to chemotherapy.[11,12] Phenylboronic acid can selectively recognize the sialic acid expressed on cancer cells and can therefore be used as a tumor-targeting

J.-Y. Lee, Prof. S.-J. Chung, Prof. D.-D. Kim
College of Pharmacy and Research Institute of Pharmaceutical Sciences
Seoul National University
Seoul 151-742, Republic of Korea
E-mail: ddkim@snu.ac.kr
Prof. H.-J. Cho
College of Pharmacy
Kangwon National University
Chuncheon 200-701, Republic of Korea
E-mail: hjcho@kangwon.ac.kr

DOI: 10.1002/adfm.201500680

European Journal of Pharmaceutics and Biopharmaceutics 94 (2015) 532–541

Contents lists available at ScienceDirect

European Journal of Pharmaceutics and Biopharmaceutics

journal homepage: www.elsevier.com/locate/ejpb

Research Paper

Bile acid-conjugated chondroitin sulfate A-based nanoparticles for tumor-targeted anticancer drug delivery

Jae-Young Lee [a], Suk-Jae Chung [a], Hyun-Jong Cho [b,*], Dae-Duk Kim [a,*]

[a] College of Pharmacy and Research Institute of Pharmaceutical Sciences, Seoul National University, Seoul 151-742, Republic of Korea
[b] College of Pharmacy, Kangwon National University, Chuncheon 200-701, Republic of Korea

ARTICLE INFO

Article history:
Received 13 February 2015
Revised 15 May 2015
Accepted in revised form 12 June 2015
Available online 4 July 2015

Keywords:
CD44 receptor
Chondroitin sulfate A
Deoxycholic acid
Nanoparticles
Tumor targeting

ABSTRACT

Chondroitin sulfate A-deoxycholic acid (CSA-DOCA)-based nanoparticles (NPs) were produced for tumor-targeted delivery of doxorubicin (DOX). The hydrophobic deoxycholic acid (DOCA) derivative was conjugated to the hydrophilic chondroitin sulfate A (CSA) backbone *via* amide bond formation, and the structure was confirmed by ^{1}H-nuclear magnetic resonance (NMR) analysis. Loading the DOX to the CSA-DOCA NPs resulted in NPs with an approximately 230 nm mean diameter, narrow size distribution, negative zeta potential, and relatively high drug encapsulation efficiency (up to 85%). The release of DOX from the NPs exhibited sustained and pH-dependent release profiles. The cellular uptake of DOX from the CSA-DOCA NPs in CD44 receptor-positive human breast adenocarcinoma MDA-MB-231 cells was reduced when co-treated with free CSA, indicating the interaction between CSA and the CD44 receptor. The lower IC_{50} value of DOX from the CSA-DOCA NPs compared to the DOX solution was also probably due to this interaction. Moreover, the ability of the developed NPs to target tumors could be inferred from the *in vivo* and *ex vivo* near-infrared fluorescence (NIRF) imaging results in the MDA-MB-231 tumor-xenografted mouse model. Both passive and active strategies appear to have contributed to the *in vivo* tumor targetability of the CSA-DOCA NPs. Therefore, these CSA-DOCA NPs could further be developed into a theranostic nanoplatform for CD44 receptor-positive cancers.

1. Introduction

Anticancer agents ranged from small chemicals to biomacromolecules, targeting a wide range of cancer types, have been developed [1–4]. The intravenous route has been favored for most of these agents due to the rapid onset time, negligible drug loss during administration, and higher accessibility to the tumor region. However, drug administration without carriers has induced unwanted toxicity to normal tissues and organs. Therefore, efforts have been made to formulate anticancer drugs that can be delivered to the tumor site selectively [5–7].

Studies have shown that abnormal tumor vasculatures, such as the high ratio of proliferating endothelial cells, lack of pericyte, and unusual formation of basement membrane, can lead to enhanced vascular permeability [8]. This is also related to the immatured lymphatic system in the tumor region, resulting in insufficient drainage. Enhanced permeability and retention (EPR), which is a passive tumor targeting strategy, has thus been proposed based on the fact that nano-sized carriers can enter the tumor region and easily accumulate at that site [9]. EPR is based on the biological factors of tumor tissues and the physicochemical properties of the nanocarriers such as size, charge, and shape [10]. However, the lack of specificity for cancer targeting calls for selective ligands that have been adopted for interactions with receptors expressed in cancer tissues, as an active tumor targeting strategy [10,11].

An example of this active tumor targeting strategy is CD44 receptor-mediated targeting, which has been widely investigated in preparing nano-sized carriers [6,12,13]. The CD44 receptor is a cell surface molecule involved in the proliferation, differentiation, migration, and survival of cells. Ligands that have been reported for the CD44 receptor include hyaluronic acid (HA), osteopontin, collagens, and matrix metalloproteinases. For example [6,14,15], hyaluronic acid-ceramide (HACE)-based nanocarriers have been produced, and their functions *via* HA and CD44 receptor interaction for cancer diagnosis and therapy have been evaluated.

Chondroitin sulfate is classified as a linear, sulfated, and negatively charged glycosaminoglycan (GAG) [16]. Due to its similarity in structure to HA, chondroitin sulfate can also be used as a ligand for the CD44 receptor [17]. It is abundant in tendons, ligaments,

* Corresponding authors. Tel.: +82 33 250 6916; fax: +82 33 259 5631 (H.-J. Cho). Tel.: +82 2 880 7870; fax: +82 2 873 9177 (D.-D. Kim).
E-mail addresses: hjcho@kangwon.ac.kr (H.-J. Cho), ddkim@snu.ac.kr (D.-D. Kim).

http://dx.doi.org/10.1016/j.ejpb.2015.06.011
0939-6411/

Journal of Controlled Release 236 (2016) 38–46

Contents lists available at ScienceDirect

Journal of Controlled Release

journal homepage: www.elsevier.com/locate/jconrel

Dual CD44 and folate receptor-targeted nanoparticles for cancer diagnosis and anticancer drug delivery

Jae-Young Lee [a,1], Ubonvan Termsarasab [a,1], Ju-Hwan Park [a], Song Yi Lee [b], Seung-Hak Ko [c], Jae-Seong Shim [c,d], Suk-Jae Chung [a], Hyun-Jong Cho [b,*], Dae-Duk Kim [a,*]

[a] College of Pharmacy and Research Institute of Pharmaceutical Sciences, Seoul National University, Seoul 151-742, Republic of Korea
[b] College of Pharmacy, Kangwon National University, Chuncheon 200-701, Republic of Korea
[c] Biogenics Inc., Daejeon 305-510, Republic of Korea
[d] Skin & Tech Inc., Seongnam 461-713, Republic of Korea

ARTICLE INFO

Article history:
Received 21 July 2015
Received in revised form 23 May 2016
Accepted 10 June 2016
Available online 16 June 2016

Keywords:
CD44 receptor
Dual targeting
Folate receptor
Hyaluronic acid-ceramide-folic acid
Nanoparticles

ABSTRACT

Dual CD44 and folate receptor targetable nanoparticles (NPs) based on hyaluronic acid-ceramide-folic acid (HACE-FA) were fabricated for improving tumor targetability. HACE-FA was synthesized *via* esterification between the carboxylic group of FA and hydroxyl group of HA. Doxorubicin (DOX)-loaded HACE-FA NPs, with a mean diameter of 120–130 nm, narrow size distribution, and negative zeta potential, were prepared. The drug release from HACE-FA NPs were significantly increased in acidic pH (pH 5.5) compared with physiological pH (7.4) ($p < 0.05$). The cellular accumulation of the drug in HACE-FA NPs group was higher than that of HACE NPs group in SKOV-3 cells (human ovarian cancer cells; CD44 and folate receptor (FR)-positive cells). Dual targetability of HACE-FA NPs, compared to HACE NPs, was also verified in the SKOV-3 tumor-xenografted mouse model by near-infrared fluorescence (NIRF) imaging. Twenty-four hours after injection, HACE-FA NPs were accumulated mainly in tumor regions and their fluorescence intensity was 4.82-fold higher than that of HACE NPs ($p < 0.05$). These findings suggest successful application of HACE-FA NPs for the accurate delivery of anticancer drugs to ovarian cancer.

1. Introduction

Recently, numerous approaches have been attempted to deliver anticancer drugs to tumor regions and to diagnose their status [1–5]. For intravenous administration of anticancer drugs, nano-sized carriers have been used widely to deliver them efficiently. Intravenously administered drug carriers may exhibit physicochemical characteristics (*i.e.* particle size, surface charge, morphological shape)-dependent fate *in vivo* [6,7]. Nano-sized particles are favored to avoid elimination and to ensure longer retention in the blood stream [6,8,9]. Particles bound with serum proteins can be also taken up by macrophages in the reticuloendothelial system (RES) of the liver and spleen [10]. In addition, because solid tumors have defective blood-vessel architectures, nano-sized carriers can enhance vascular permeability. Along with an immature lymphatic system, macromolecules are prone to accumulation in tumor regions and stay longer due to the "enhanced permeability and retention [EPR] effect" [11]. This EPR effect, as a passive targeting strategy, causes the macromolecules or nano-sized drug carriers to easily move to tumor regions. But since the passive targeting lacks tumor selectivity, active targeting strategies for introducing tumor-targeting moieties to the anticancer drug or nanocarrier have been investigated [8].

For the fabrication of biocompatible nanocarriers, several natural and synthetic materials have been introduced [12–16] among which hyaluronic acid (HA) is a biodegradable and biocompatible natural material with advantages as a matrix for drug delivery systems. With HA, several types of nano-sized systems including nanoparticles (NPs), micelles, liposomes, chemical conjugates, and hybrid systems can be prepared [17–20].

In our previous studies, hyaluronic acid-ceramide (HACE) (Fig. 1), as an amphiphilic HA oligomer derivative, was synthesized and self-assembled NPs were developed [12,17,20,21]. Diverse physiological functions of HA, according to its molecular weight, have been reported [22]. As far as toxicity is concerned, HACE which consists of an HA oligomer did not reveal severe systemic toxicities [12,17,21]. Since HA can bind to the CD44 receptor which is overexpressed in many cancer cells, it can be used as a tumor-targeting ligand for active targeting of tumors [23]. It has been reported that HACE-based nanocarriers acquire tumor targetability based on HA–CD44 receptor interactions and *in vitro* and *in vivo* anti-tumor efficacies have been demonstrated [12,17,21]. HACE showed sufficient potentials as a nanosystem for drug delivery and

* Corresponding authors.
E-mail addresses: hjcho@kangwon.ac.kr (H.-J. Cho), ddkim@snu.ac.kr (D.-D. Kim).
[1] These authors have equally contributed to this work.

http://dx.doi.org/10.1016/j.jconrel.2016.06.021
0168-3659/

Carbohydrate Polymers 151 (2016) 68–77

Contents lists available at ScienceDirect

Carbohydrate Polymers

journal homepage: www.elsevier.com/locate/carbpol

Polyethylene glycol-conjugated chondroitin sulfate A derivative nanoparticles for tumor-targeted delivery of anticancer drugs

Jae-Young Lee[a], Ju-Hwan Park[a], Jeong-Jun Lee[b], Song Yi Lee[b], Suk-Jae Chung[a], Hyun-Jong Cho[b,*], Dae-Duk Kim[a,*]

[a] College of Pharmacy and Research Institute of Pharmaceutical Sciences, Seoul National University, Seoul 151-742, Republic of Korea
[b] College of Pharmacy, Kangwon National University, Chuncheon 200-701, Republic of Korea

ARTICLE INFO

Article history:
Received 16 November 2015
Received in revised form 12 May 2016
Accepted 13 May 2016
Available online 18 May 2016

Keywords:
Chondroitin sulfate A
PEGylation
Nanoparticles
Tumor targeting
Pharmacokinetics

ABSTRACT

Polyethylene glycol (PEG)-decorated chondroitin sulfate A-deoxycholic acid (CSD) nanoparticles (NPs) were fabricated for the selective delivery of doxorubicin (DOX) to ovarian cancer. CSD-PEG was synthesized *via* amide bond formation between the —NH_2 group of methoxypolyethylene glycol amine and the —COOH group of CSD. CSD-PEG/DOX NPs with a 247 nm mean diameter, negative zeta potential, and >90% drug encapsulation efficiency were prepared. Sustained and pH-dependent DOX release profiles from CSD-PEG NPs were observed in dissolution tests. Endocytosis of NPs by SKOV-3 cells (CD44 receptor-positive human ovarian cancer cells), based on the CSA-CD44 receptor interaction, was determined by flow cytometry and confocal laser scanning microscopy (CLSM) studies. PEGylation of NPs also resulted in reduced drug clearance (CL) *in vivo* and improved relative bioavailability, compared to non-PEGylated NPs, as determined by the pharmacokinetic study performed after intravenous administration in rats. Developed CSD-PEG NPs can be a promising delivery vehicle for the therapy of CD44 receptor-expressing ovarian cancers.

1. Introduction

Different types of nano-sized carriers have been investigated for the targeted delivery of anticancer agents to tumor regions (Gong, Chen, Zheng, Wang, & Wang, 2012; Jhaveri, Deshpande, & Torchilin, 2014; Schroeder et al., 2011). The biological properties of cancer, abnormal tumor vasculatures, characterized by a high portion of proliferating endothelial cells, lack of pericytes, unusual formation of basement membrane, and an immature lymphatic system, result in an enhanced permeability and retention (EPR) effect (Maeda, Wu, Sawa, Matsumura, & Hori, 2000). Because the EPR effect can increase the accumulation of nanoparticles (NPs) of a particular size and macromolecules in the tumor region, it has been used as a passive tumor targeting strategy. The physicochemical properties of nanocarriers (*i.e.* size, surface charge, shape) are related to the EPR effect and they can determine the tumor targeting efficiency of nanocarriers. However, due to the intrinsic unspecificity of passive tumor targeting, active tumor targeting strategies have been introduced to deliver anticancer drugs more selectively and precisely to tumor tissues. Ligands (*i.e.*, small chemicals, peptides, proteins), interacting with the receptors overexpressed in cancer, can be attached to nanocarriers to improve tumor targetability (Bertrand, Wu, Xu, Kamaly, & Farokhzad, 2014; Zhong, Meng, Deng, & Zhong, 2014). The combination of passive and active tumor targeting strategies may produce more improved antitumor efficacy and minimize unwanted effects of anticancer drugs.

An example of active tumor targeting is the interaction between CD44 receptor and its ligands. It is known that CD44 receptor is linked to the proliferation, differentiation, migration, and survival of cells and is highly expressed in various types of cancer cells (Naor, Nedvetzki, Golan, Melnik, & Faitelson, 2002; Negi et al., 2012). One of the principal CD44 receptor ligands is hyaluronic acid, a component of the extracellular matrix. Collagen, fibronectin, laminin, osteopontin, and serglycin can also act as ligands for the CD44 receptor (Goodison, Urquidi, & Tarin, 1999). The tumor targetability of hyaluronic acid derivative-based nanocarriers for CD44 receptor-expressed cancers has already been reported (Cho et al., 2011; Cho, Yoon, Koo et al., 2012; Cho, Yoon, Yoon et al., 2012; Park, Cho, Termsarasab et al., 2014; Park, Cho, Yoon et al., 2014; Park, Lee et al., 2014). Due to structural similarity with hyaluronic acid, chondroitin sulfate A (CSA) can be also used as a ligand for CD44 receptor.

* Corresponding authors.
E-mail addresses: hjcho@kangwon.ac.kr (H.-J. Cho), ddkim@snu.ac.kr (D.-D. Kim).

http://dx.doi.org/10.1016/j.carbpol.2016.05.043
0144-8617/

Biomaterials 85 (2016) 218–231

Contents lists available at ScienceDirect

Biomaterials

journal homepage: www.elsevier.com/locate/biomaterials

Iodinated hyaluronic acid oligomer-based nanoassemblies for tumor-targeted drug delivery and cancer imaging

Jae-Young Lee [a], Suk-Jae Chung [a], Hyun-Jong Cho [b, *], Dae-Duk Kim [a, *]

[a] College of Pharmacy and Research Institute of Pharmaceutical Sciences, Seoul National University, Seoul 151-742, Republic of Korea
[b] College of Pharmacy, Kangwon National University, Chuncheon 200-701, Republic of Korea

ARTICLE INFO

Article history:
Received 30 December 2015
Received in revised form
23 January 2016
Accepted 27 January 2016
Available online 29 January 2016

Keywords:
Hyaluronic acid
In vivo imaging
Nanoassemblies
Triiodobenzoic acid
Tumor-targeted therapy

ABSTRACT

Nano-sized self-assemblies based on amphiphilic iodinated hyaluronic acid (HA) were developed for use in cancer diagnosis and therapy. 2,3,5-Triiodobenzoic acid (TIBA) was conjugated to an HA oligomer as a computed tomography (CT) imaging modality and a hydrophobic residue. Nanoassembly based on HA-TIBA was fabricated for tumor-targeted delivery of doxorubicin (DOX). Cellular uptake of DOX from nanoassembly, compared to a DOX solution group, was enhanced *via* an HA-CD44 receptor interaction, and subsequently, the *in vitro* antitumor efficacy of DOX-loaded nanoassembly was improved in SCC7 (CD44 receptor positive squamous cell carcinoma) cells. Cy5.5, a near-infrared fluorescence (NIRF) dye, was attached to the HA-TIBA conjugate and the *in vivo* tumor targetability of HA-TIBA nanoassembly, which is based on the interaction between HA and CD44 receptor, was demonstrated in a NIRF imaging study using an SCC7 tumor-xenografted mouse model. Tumor targeting and cancer diagnosis with HA-TIBA nanoassembly were verified in a CT imaging study using the SCC7 tumor-xenografted mouse model. In addition to efficient cancer diagnosis using NIRF and CT imaging modalities, improved antitumor efficacies were shown. HA and TIBA can be used to produce HA-TIBA nanoassembly that may be a promising theranostic nanosystem for cancers that express the CD44 receptor.

1. Introduction

Diverse approaches have been employed to selectively deliver anticancer agents to tumor sites and simultaneously diagnose cancers [1–3]. To minimize the distribution of anticancer drugs to normal tissues and organs, tumor targeting strategies, including passive and active targeting, have been introduced in drug delivery systems [4,5]. Due to the aberrant vasculature of tumors that result from angiogenesis and an immature lymphatic system, nano-sized particles and macromolecules are prone to be retained in the tumor region. This enhanced permeability and retention (EPR) effect is linked to the physicochemical properties of carriers (*i.e.*, size, shape, and surface charge), and it has been used as a passive tumor targeting strategy [6]. Intrinsic limitation to its selectivity and specificity can be overcome by active targeting strategies using tumor targeting moieties (*i.e.*, small chemicals, peptides, antibodies) as ligands for receptors that are overexpressed in cancer cells [7,8]. A combination of passive and active targeting strategies can provide improved tumor targeting and chemotherapeutic effects. Recently, a number of imaging compounds for X-ray computed tomography (CT), magnetic resonance (MR), positron emission tomography (PET), and optical imaging have been chemically conjugated to polymers to produce nano-sized particles or physically loaded into the particles [9,10]. Simultaneous cancer diagnosis and chemotherapy can improve patient compliance and therapeutic efficacies.

Among the various nano-sized delivery systems, self-assembled nanoparticles (NPs) have been widely investigated for tumor-targeted drug delivery and cancer imaging [11,15]. Hydrophobic residues with specialized diagnostic and therapeutic functions can be chemically conjugated to the hydrophilic backbone [16]. In this study, 2,3,5-triiodobenzoic acid (TIBA) (a hydrophobic residue) was grafted to a hyaluronic acid (HA) oligomer (a hydrophilic backbone). TIBA is poorly soluble in water but soluble in alkaline solutions (NaOH, KOH) and in several organic solvents (ethanol, dimethyl sulfoxide (DMSO) and ether). As hydrophobic TIBA contains iodine atoms, it can be used as a CT contrast agent for *in vivo* imaging. TIBA is structurally similar to the commercial contrast imaging agent iohexol (Omnipaque, GE Healthcare), which is approved by the U.S. Food and Drug Administration (FDA) for

* Corresponding authors.
E-mail addresses: hjcho@kangwon.ac.kr (H.-J. Cho), ddkim@snu.ac.kr (D.-D. Kim).

http://dx.doi.org/10.1016/j.biomaterials.2016.01.060
0142-9612/

BIOPHARMACEUTICS & DRUG DISPOSITION
Biopharm. Drug Dispos. **37**: 156–167 (2016)
Published online in Wiley Online Library
(wileyonlinelibrary.com) **DOI**: 10.1002/bdd.2005

High body clearance and low oral bioavailability of alantolactone, isolated from *Inula helenium*, in rats: extensive hepatic metabolism and low stability in gastrointestinal fluids

Jae-Young Lee[a], Sang-Bum Kim[a], Jaemoo Chun[b], Kwang Ho Song[b], Yeong Shik Kim[b], Suk-Jae Chung[a], Hyun-Jong Cho[c], In-Soo Yoon[d,*], and Dae-Duk Kim[a,*]

[a]*College of Pharmacy and Research Institute of Pharmaceutical Sciences, Seoul National University, Seoul, Republic of Korea*
[b]*Natural Products Research Institute, College of Pharmacy, Seoul National University, Seoul, Republic of Korea*
[c]*College of Pharmacy, Kangwon National University, Gangwon, Republic of Korea*
[d]*College of Pharmacy and Natural Medicine Research Institute, Mokpo National University, Jeonnam, Republic of Korea*

ABSTRACT: Alantolactone (ALA) is a major bioactive sesquiterpene lactone present in the roots of *Inula helenium* L. (Asteraceae) which has been used widely in traditional medicine against various diseases such as asthma, cancer and tuberculosis. The pharmacologic activities of alantolactone have been well characterized, yet information on the physicochemical and pharmacokinetic properties of alantolactone and their mechanistic elucidation are still limited. Thus, this study aims to investigate the oral absorption and disposition of alantolactone and their relevant mechanisms. Log *P* values of alantolactone ranged from 1.52 to 1.84, and alantolactone was unstable in biological samples such as plasma, urine, bile, rat liver microsomes (RLM) and simulated gastrointestinal fluids. The metabolic rate of alantolactone was markedly higher in rat liver homogenates than in the other tissue homogenates. A saturable and concentration-dependent metabolic rate profile of alantolactone was observed in RLM, and rat cytochrome P450 (CYP) 1 A, 2C, 2D and 3 A subfamilies were significantly involved in its hepatic metabolism. Based on the well-stirred model, the hepatic extraction ratio (HER) was estimated to be 0.890–0.933, classifying alantolactone as a drug with high HER. Moreover, high total body clearance (111 ± 41 ml/min/kg) and low oral bioavailability (0.323%) of alantolactone were observed in rats. Taken together, the present study demonstrates that the extensive hepatic metabolism, at least partially mediated by CYP, is primarily responsible for the high total body clearance of alantolactone, and that the low oral bioavailability of alantolactone could be attributed to its low stability in gastrointestinal fluids and a hepatic first-pass effect in rats. Copyright © 2016 John Wiley & Sons, Ltd.

Key words: Alantolactone; GI stability; cytochrome P450; hepatic metabolism; oral bioavailability

Introduction

Inula helenium L. (Asteraceae), also known as elecampane, is a perennial herb commonly distributed in East Asia, Europe and North America [1]. Its extracts have been used widely in traditional medicine against various diseases such as asthma, cancer, bronchitis, chronic enterogastritis and tuberculosis [2–5]. Previous studies also reported that *I. helenium* possesses anti-inflammatory, anticancer and antimicrobial activities [6–8]. The major bioactive compound of *I. helenium* is well known to be sesquiterpene lactones including alantolactone (ALA; Figure 1; IUPAC name: (3a(R),5(S),8a(R),9a(R))-5,8a-

*Correspondence to: College of Pharmacy and Natural Medicine Research Institute, Mokpo National University, 1666 Youngsan-ro, Muan-gun, Jeonnam 58554, Republic of Korea.
E-mail: isyoon@mokpo.ac.kr
College of Pharmacy and Research Institute of Pharmaceutical Sciences, 1 Gwanak-ro, Gwanak-gu, Seoul 08826, Republic of Korea.
E-mail: ddkim@snu.ac.kr

Received 28 October 2015
Revised 10 January 2016
Accepted 30 January 2016

Journal of Chromatography B, 1011 (2016) 121–127

Contents lists available at ScienceDirect

Journal of Chromatography B

journal homepage: www.elsevier.com/locate/chromb

Determination of manassantin B in rat plasma using a high performance liquid chromatography with fluorescence detection and its quantitative application to pharmacokinetic study

Jae-Young Lee[a,1], Jae-Hyoung Song[b,1], In-Soo Yoon[c], Hyun-Jeong Ko[b], Dae-Duk Kim[a], Hyun-Jong Cho[b,*]

[a] College of Pharmacy and Research Institute of Pharmaceutical Sciences, Seoul National University, Seoul 151-742, Republic of Korea
[b] College of Pharmacy, Kangwon National University, Chuncheon 200-701, Republic of Korea
[c] College of Pharmacy and Natural Medicine Research Institute, Mokpo National University, Jeonnam 534-729, Republic of Korea

ARTICLE INFO

Article history:
Received 23 April 2015
Received in revised form
22 December 2015
Accepted 28 December 2015
Available online 2 January 2016

Keywords:
Manassantin B
Validation
HPLC
Fluorescence detection
Pharmacokinetics

ABSTRACT

A simple, sensitive, rapid, and reproducible analytical method of manassantin B in rat plasma by high performance liquid chromatography with fluorescence detection (HPLC-FL) was developed for its application to pharmacokinetic study in rats. Valsartan (VST) was used as an internal standard (IS) in this quantitative analytical method. Manassantin B and VST were extracted by simple and efficient protein precipitation method. Manassantin B was detected at 282/322 nm (excitation/emission) wavelengths using FL detector. The chromatographic separation was obtained with reverse phase C18 column and the mobile phase composed of potassium phosphate buffer containing 0.025% trifluoroacetic acid (pH 2.5; 5 mM) and acetonitrile including 0.025% trifluoroacetic acid (20:80, v/v) at 1.0 mL/min flow rate. The linearity was established at 25.0–10000 ng/mL and the lower limit of detection (LLOD) was 7 ng/mL. The intra- and inter-day accuracy and precision values of manassantin B were within ± 15% of the theroretical values and <9% from the nominal concentrations, respectively. Accuracy and precision values of manassantin B after stability tests were also within the acceptable ranges. Developed assay was also successfully applied to pharmacokinetic study after intravenous administration of manassantin B in rats.

1. Introduction

Saururus is a genus of plants belongs to the family Saururaceae and it has two species, such as *Saururus cernuus* and *Saururus chinensis*. *S. cernuus* is a medicinal plant native to North America and *S. chinensis* is a perennial plant mainly distributed in China and South Korea, respectively. Diverse therapeutic potentials of *Saururus* for the treatment of inflammation, diuretic, edema, gonorrhea, and jaundice have been reported [1,2]. Several compounds, such as lignans, alkaloids, phenolic acids, terpenoids, steroids, and fatty acids, have been isolated and identified from these herbs and they were known to have various biological efficacies [2–12]. Among them, it was reported that manassantin isomers have anti-inflammatory, anti-plasmodial, anti-angiogenic, anti-melanogenic, anti-viral, and hypoxia-inducible factor 1 (HIF-1) inhibitory effects [12–16].

Manassantin B, (1*R*,2*R*)-1-(1,3-benzodioxol-5-yl)-2-{4-[(2*S*,3*R*,4*R*,5*S*)-5-(4-{[(1*R*,2*R*)-1-(3,4-dimethoxyphenyl)-1-hydroxypropan-2-yl]oxy}-3-methoxyphenyl)-3,4-dimethyltetrahydrofuran-2-yl]-2-methoxyphenoxy}propan-1-ol, is a dilignan isolated from *S. cernuus* and *S. chinensis* and its molecular weight is 716.81 (Fig. 1). Considering the known pharmacological efficacies and its traditional use in a few countries, the development and establishment of analytical method for manassantin B are required. Although analytical methods for the detection of several major compounds of *S. chinensis* using high performance liquid chromatography-diode array detector (HPLC-DAD), high performance liquid chromatography-diode array detector-electrospray ionization mass spectrometry (HPLC-DAD-ESI-MS), and capillary electrophoresis with electrochemical detection have been developed [17–19], the quantitative analytical method of manassantin B was not reported yet, to the best of our knowledge.

HPLC with fluorescence (FL) detector has been widely used for the quantitative analysis of drug in the biological fluids. Although

* Corresponding author at: College of Pharmacy, Kangwon National University, 1 Kangwondaehak-gil, Chuncheon 200-701, Republic of Korea. Fax: +82 33 259 5631.
E-mail address: hjcho@kangwon.ac.kr (H.-J. Cho).
[1] These authors are equally contributed to this work.

http://dx.doi.org/10.1016/j.jchromb.2015.12.058
1570-0232/

Journal of Chromatography B, 1000 (2015) 155–162

Contents lists available at ScienceDirect

Journal of Chromatography B

journal homepage: www.elsevier.com/locate/chromb

Determination and validation of psammaplin A and its derivatives in rat plasma by liquid chromatography–tandem mass spectrometry and its application in pharmacokinetic study

Jae-Young Lee[a], Mee Yeon Lee[a], Min Woo Ha[a], Tae Hyung Won[a], Hyun-Jong Cho[b], Jongheon Shin[a], Hyeung-geun Park[a], Dae-Duk Kim[a,*]

[a] College of Pharmacy and Research Institute of Pharmaceutical Sciences, Seoul National University, Seoul 151-742, Republic of Korea
[b] College of Pharmacy, Kangwon National University, Chuncheon 200-701, Republic of Korea

ARTICLE INFO

Article history:
Received 11 April 2015
Received in revised form 1 July 2015
Accepted 5 July 2015
Available online 19 July 2015

Keywords:
Psammaplin A
Psammaplin A derivatives
Validation
LC–MS/MS
Pharmacokinetics

ABSTRACT

A liquid chromatography–tandem mass (LC–MS/MS) method was developed for the determination of psammaplin A (PsA) and its newly synthesized derivatives (PsA 107, PsA 109, and PsA 123) in rat plasma using bupropion as an internal standard (IS). The plasma samples were deproteinized with acetonitrile. Chromatographic separation was performed on hydro-RP column (75 × 2.0 mm, 80 Å, 4 μm) with isocratic elution using 5 mM ammonium formate buffer/acetonitrile (30:70, v/v) at a flow rate of 0.4 mL/min and the total run time was 5 min. Mass spectrometric detection was performed with positive electrospray ionization (ESI) in multiple reaction monitoring (MRM) mode. The ion transitions monitored were m/z 663.2 → 331.0, 687.2 → 343.1, 587.3 → 293.1, 563.3 → 281.0, and 240.0 → 184.0 for PsA, PsA 107, PsA 109, PsA 123, and IS, respectively. All analytes showed good linearity over the concentration range of 5.00–5000 ng/mL ($r^2 \geq 0.994$). The lower limit of quantification was 5 ng/mL for PsA and its three PsA derivatives. Within- and between-run precisions (relative standard deviation, RSD) were less than 9.66% and accuracy (relative error, RE) ranged from −9.34% to 7.25%. Established method was successfully applied to the investigation of pharmacokinetic properties of PsA and its derivatives in rats after intravenous administration at a dose of 2 mg/kg.

1. Introduction

Psammaplin A (PsA) is a natural bromotyrosine derivative, which was first isolated from Psammaplysilla sponge in 1987 [1,2]. PsA has a structure of symmetrical dimer connected by disulfide bond derived from the condensation of modified tyrosine and cysteine units (Fig. 1) [3]. It was reported that PsA has diverse bioactivities such as inhibition of DNA gyrase, topoisomerase II, farnesyl protein transferase, leucine aminopeptidase, chitinase, Pol α-primase, PPAR-γ, and mammalian aminopeptidase *N* [4–11]. The potent cytotoxicity against several cancer cells including lung cancer, ovarian cancer and colon cancer with dual inhibition of histone deacetylase (HDAC) and DNA methyltransferase (DNMT) is also a therapeutically appealing property of the compound [12,13].

HDAC and DNMT epigenetically catalyze the covalent modification of histone proteins and DNA in chromatin of tumor suppressor gene, thereby being considered as new targets for the cancer therapy [14–18]. Though the exact mechanism of histone acetylation/deacetylation was poorly understood, acetylation in evolutionally conserved lysine residue in histone *N*-terminus is crucial to change chromatin into transcriptionally competent state [19]. The inhibition of HDAC, by leaving the histone acetylated, subsequently contribute to an activation of tumor suppressor gene [19]. Some anticancer agents which take advantage of this mechanism have been used clinically (Zolinza® and Istodax®) for the treatment of cutaneous T-cell lymphoma [20].

Methylation to the C5 position of cytosine within the CpG-rich islands in DNA by DMNT represses the chromatin state and inhibits transcription [21,22]. In tumors, several tumor suppressor genes are hypermethylated, which means anti-cancer efficacy can be achieved with inhibition of DNMT [23]. The DNMT inhibitors (Vidaza® and Dacogen®) are already in clinical use for the treatment of myelodysplastic syndrome [24].

Notwithstanding the promising pharmacological activities, PsA has two major drawbacks making itself a poor lead compound. First, the low-abundance of PsA in marine products hinders its

* Corresponding author. Fax: 82 2 873 9177.
E-mail address: ddkim@snu.ac.kr (D.-D. Kim).

http://dx.doi.org/10.1016/j.jchromb.2015.07.014
1570-0232/

Drug Design, Development and Therapy

Dovepress
open access to scientific and medical research

Open Access Full Text Article

ORIGINAL RESEARCH

Soluplus®/TPGS-based solid dispersions prepared by hot-melt extrusion equipped with twin-screw systems for enhancing oral bioavailability of valsartan

This article was published in the following Dove Press journal:
Drug Design, Development and Therapy
22 May 2015
Number of times this article has been viewed

Jae-Young Lee[1,*]
Wie-Soo Kang[2,*]
Jingpei Piao[2]
In-Soo Yoon[3]
Dae-Duk Kim[1]
Hyun-Jong Cho[4]

[1]College of Pharmacy and Research Institute of Pharmaceutical Sciences, Seoul National University, Seoul, [2]School of Bioscience and Biotechnology, Kangwon National University, Chuncheon, [3]College of Pharmacy and Natural Medicine Research Institute, Mokpo National University, Jeonnam, [4]College of Pharmacy, Kangwon National University, Chuncheon, Republic of Korea

*These authors contributed equally to this work

Background: Soluplus® (SP) and D-alpha-tocopherol polyethylene glycol 1000 succinate (TPGS)–based solid dispersion (SD) formulations were developed by hot-melt extrusion (HME) to improve oral bioavailability of valsartan (VST).

Methods: HME process with twin-screw configuration for generating a high shear stress was used to prepare VST SD formulations. The thermodynamic state of the drug and its dispersion in the polymers were evaluated by solid-state studies, including Fourier-transform infrared, X-ray diffraction, and differential scanning calorimetry. Drug release from the SD formulations was assessed at pH values of 1.2, 4.0, and 6.8. Pharmacokinetic study was performed in rats to estimate the oral absorption of VST.

Results: HME with a high shear rate produced by the twin-screw system was successfully applied to prepare VST-loaded SD formulations. Drug amorphization and its molecular dispersion in the polymer matrix were verified by several solid-state studies. Drug release from SD formulations was improved, compared to the pure drug, particularly at pH 6.8. Oral absorption of drug in rats was also enhanced in SP and TPGS-based SD groups compared to that in the pure drug group.

Conclusion: SP and TPGS-based SDs, prepared by the HME process, could be used to improve aqueous solubility, dissolution, and oral absorption of poorly water-soluble drugs.

Keywords: hot-melt extrusion, oral bioavailability, solid dispersion, valsartan

Introduction

Many approaches have been used to prepare oral formulations of poorly water-soluble drugs to improve oral bioavailability.[1–3] Among them, solid dispersion (SD), in which the drug molecule is dispersed in a polymeric matrix, has been shown to improve the aqueous solubility and oral absorption of drugs.[4,5] SD produces these effects on poorly water-soluble drugs by increasing wettability, decreasing agglomeration, and altering the physical state of the drugs. Although SD formulations can be prepared by several methods, hot-melt extrusion (HME) is an attractive and emerging method for the production of SDs.[6,7] The HME process has the advantage of being a continuous, solvent-free, dust-free (environmentally friendly), and robust manufacturing process, as well as possessing the ability to yield several solid dosage forms (eg, pellets or tablets).[8] During the HME process, shear stress generated by extruder screws can be applied to overcome the crystal lattice energy of crystalline drugs and soften polymers. The mixing and dispersing of the drugs and polymers

Correspondence: Dae-Duk Kim
College of Pharmacy and Research Institute of Pharmaceutical Sciences, Seoul National University, 1 Gwanak-ro, Gwanak-gu, Seoul 151-742, Republic of Korea
Tel +82 2 880 7870
Fax +82 2 873 9177
Email ddkim@snu.ac.kr

Hyun-Jong Cho
College of Pharmacy, Kangwon National University, 1 Kangwondaehak-gil, Chuncheon 200-701, Republic of Korea
Tel +82 33 250 6916
Fax +82 33 259 5631
Email hjcho@kangwon.ac.kr

submit your manuscript | www.dovepress.com
Dovepress
http://dx.doi.org/10.2147/DDDT.S84070

RESEARCH ARTICLE – *Pharmaceutical Nanotechnology*

Nanocomplexes Based on Amphiphilic Hyaluronic Acid Derivative and Polyethylene Glycol–Lipid for Ginsenoside Rg3 Delivery

JAE-YOUNG LEE,[1] HEEJUNG YANG,[2] IN-SOO YOON,[3] SANG-BUM KIM,[1] SEUNG-HAK KO,[4] JAE-SEONG SHIM,[4,5] SANG HYUN SUNG,[1] HYUN-JONG CHO,[2] DAE-DUK KIM[1]

[1]College of Pharmacy and Research Institute of Pharmaceutical Sciences, Seoul National University, Seoul 151-742, Republic of Korea
[2]College of Pharmacy, Kangwon National University, Chuncheon 200-701, Republic of Korea
[3]College of Pharmacy and Natural Medicine Research Institute, Mokpo National University, Jeonnam 534-729, Republic of Korea
[4]Biogenics Inc., Daejeon 305-510, Republic of Korea
[5]Skin and Tech Inc., Seongnam 461-713, Republic of Korea

Received 8 March 2014; revised 5 June 2014; accepted 15 July 2014

Published online 11 August 2014 in Wiley Online Library (wileyonlinelibrary.com). DOI 10.1002/jps.24111

ABSTRACT: Hybrid nanocomplex formulations, based on amphiphilic hyaluronic acid–ceramide (HACE) and lipids, were fabricated for the delivery of 20(*S*)-ginsenoside Rg 3 [(*S*)-Rg3]. Nanocomplexes with less than 200 nm mean diameter, narrow size distribution, spherical shape, and negative zeta potential were prepared. The maintenance of the structural stability of the hybrid nanocomplexes in the blood stream was demonstrated by measuring their particle size in serum. Nanocomplexes based on HACE, phosphatidylcholine (PC), and 1,2-distearoyl-*sn*-glycero-3-phosphoethanolamine-N-[methoxy(polyethyleneglycol)-2000] (DSPE-PEG) showed a sustained drug release profile compared with other formulations. Blank nanocomplexes exhibited negligible cytotoxicity within the tested concentration range in A549 human lung adenocarcinoma cells. The cellular uptake efficiency of hybrid nanocomplexes was improved compared with the HACE-based nanoparticles probably because of interactions between lipids and the cellular membrane. The results of a pharmacokinetic study in rats revealed decreased *in vivo* clearance of (*S*)-Rg3, especially in the HACE/PC/DSPE-PEG-based hybrid nanocomplex (F3) group. The hybrid nanostructure and the outer PEG chain likely contributed to improve *in vivo* performance of the F3 group. Thus, these developed hybrid nanocomplexes could serve as good candidates for tumor-targeted delivery of anticancer agents. © 2014 Wiley Periodicals, Inc. and the American Pharmacists Association J Pharm Sci 103:3254–3262, 2014

Keywords: Biocompatibility; cancer; controlled release; ginsenoside Rg 3; hyaluronic acid–ceramide; nanocomplex; pharmacokinetics; polyethylene glycol–lipid; targeted drug delivery

INTRODUCTION

Tumor-targeted drug delivery via nanocarriers has been considered a particularly promising method among many approaches that have been developed for the efficient delivery of anticancer agents.[1–3] Drugs that have been used for this purpose include natural products with antiproliferative, antioxidative, and apoptotic effects.[4] Various formulations that have been developed for natural products include nanosized delivery vehicles for administration via oral or injection routes.[5–9]

Among many of the therapeutic reagents from natural resources, ginsenosides have been widely investigated for their antiallergic, antiatherosclerotic, anticancer, antidiabetic, antihypertensive, antiinflammatory, and immunomodulatory effects.[10] Ginsenosides, as active constituents of *Panax ginseng*, can be generally classified into four groups: protopanaxadiol (Rb1, Rb2, Rb3, Rc, Rd, Rg3, Rh2, etc.), protopanaxatriol (Rg1, Rg2, Re, Rf, Rh1, etc.), ocotillol, and oleanolic acid.[11] Over 150 subtypes of ginsenosides have been isolated and verified. Among them, Rg3 possesses pharmacological efficacies as an anticancer agent in hepatocarcinoma, lung adenocarcinoma, and glioblastoma cells.[9,12,13] The stereo-selective structures of Rg3 can alter its pharmacological effects, and 20(*S*)-Rg3 exhibited higher cytotoxicity in certain cancer cell types.[14–16] However, in spite of the therapeutic potential of (*S*)-Rg3 in cancer therapy, a system for its delivery has not been developed. Rg3 is a poorly water-soluble drug and its half-life, after intravenous administration, is not sufficient to exert its antitumor effects.[9] Prolonged circulation in the blood stream using a nanocomplex system could be the principal approach for improving its pharmacological efficacy.

In the development of nanovehicles for drug delivery to tumor regions, self-assembled nanoparticles based on amphiphilic polymers have been used for tumor-targeted drug delivery.[17,18] Amphiphilic hyaluronic acid (HA) derivative-based nanoparticles were fabricated for cancer diagnosis and therapy in our previous studies.[19–22] Hyaluronic acid–ceramide (HACE)-based nanoparticles can encapsulate hydrophobic drugs because of self-assembling nanostructures and move to the tumor region via an enhanced permeability and retention (EPR) effect (passive targeting) and an HA–CD44 receptor interaction (active targeting). The introduction of a lipid moiety into the HACE-based nanostructure and the fabrication of hybrid nanocomplexes based on HACE and lipids are expected to improve cellular uptake efficiency and maintain structural stability in the blood stream. Moreover, the addition of lipid–polyethylene glycol (PEG) conjugate can produce a PEG chain-anchored hybrid nanocomplex system that may exert prolonged circulation time in the blood stream. Herein, we report

Correspondence to: Hyun-Jong Cho (Telephone: +82-33-250-6916; Fax: +82-33-259-5631; E-mail: hjcho@kangwon.ac.kr); Dae-Duk Kim (Telephone: +82-2-880-7870; Fax: +82-2-873-9177; E-mail: ddkim@snu.ac.kr)

Journal of Pharmaceutical Sciences, Vol. 103, 3254–3262 (2014)

International Journal of Nanomedicine

Dovepress
open access to scientific and medical research

Open Access Full Text Article

ORIGINAL RESEARCH

Poly(styrene)-b-poly(DL-lactide) copolymer-based nanoparticles for anticancer drug delivery

This article was published in the following Dove Press journal:
International Journal of Nanomedicine
3 June 2014
Number of times this article has been viewed

Jae-Young Lee[1]
Jung Sun Kim[2]
Hyun-Jong Cho[3]
Dae-Duk Kim[1]

[1]College of Pharmacy and Research Institute of Pharmaceutical Sciences, Seoul National University, Seoul, Republic of Korea; [2]Division of Health Sciences, Dongseo University, Busan, Republic of Korea; [3]College of Pharmacy, Kangwon National University, Chuncheon, Republic of Korea

Abstract: Poly(styrene)-b-poly(DL-lactide) (PS-PDLLA) copolymer-based nanoparticles (NPs) of a narrow size distribution, negative zeta potential, and spherical shape were fabricated for the delivery of docetaxel (DCT). The particle size was consistently maintained in serum for 24 hours and a sustained drug release pattern was observed for 10 days in the tested formulations. The cytotoxicity of the developed blank NPs was negligible in prostate cancer (PC-3) cells. Cellular uptake and distribution of the constructed NPs containing a hydrophobic fluorescent dye was monitored by confocal laser scanning microscopy (CLSM) for 24 hours. Anti-tumor efficacy of the PS-PDLLA/DCT NPs in PC-3 cells was significantly more potent than that of the group treated with commercially available DCT, Taxotere® ($P<0.05$). Blood biochemistry tests showed that no serious toxicity was observed with the blank NPs in the liver and kidney. In a pharmacokinetic study of DCT in rats, in vivo clearance of PS-PDLLA/DCT NPs decreased while the half-life in blood increased compared to the Taxotere-treated group ($P<0.05$). The PS-PDLLA NPs are expected to be a biocompatible and efficient nano-delivery system for anticancer drugs.

Keywords: docetaxel, prolonged blood circulation, prostate cancer

Introduction

Diverse approaches for cancer therapy and diagnosis continue to be pursued.[1–3] Among the various formulation types, intravenous administration is the primary choice for cancer treatment, and several injectable formulations for anticancer drug delivery have recently been developed.[4–7] In most of these cases, improving aqueous solubility and tumor targeting of anticancer agents have been the primary objectives in the formulation development. Nanovehicles, known to produce sufficient aqueous solubility, sustained release, and tumor targeting of anticancer drugs, have been developed based on diverse materials as one of these injectable formulations. Nevertheless, only a few among those developed have been approved for clinical applications due to toxicity of the materials and insufficient biodistribution of the nanovehicles to the tumors. Although the in vitro and in vivo toxicity of many organic and inorganic materials have been evaluated, a limited number of substances have been selected for clinical application so far.

In the current investigation, a poly(styrene)-b-poly(DL-lactide) (PS-PDLLA) copolymer (Figure 1A) was used for the preparation of nanoparticles (NPs) for docetaxel (DCT) delivery. Both PS and PDLLA have been used in various biomedical applications.[8,9,15–17] PS is a synthetic aromatic polymer composed of the monomer styrene. Nano-sized vehicles based on PS have been widely investigated as a drug delivery

Correspondence: Hyun-Jong Cho
College of Pharmacy, Kangwon National University, 1 Kangwondaehak-gil, Chuncheon 200-701, Republic of Korea
Tel +82 33 250 6916
Fax +82 33 259 5631
Email hjcho@kangwon.ac.kr

Dae-Duk Kim
College of Pharmacy and Research Institute of Pharmaceutical Sciences, Seoul National University, Seoul 151-742, Republic of Korea
Tel +82 2 880 7870
Fax +82 2 873 9177
Email ddkim@snu.ac.kr

submit your manuscript | www.dovepress.com
Dovepress
http://dx.doi.org/10.2147/IJN.S62806

Journal of Pharmaceutical Investigation
Vol. 41, No. 3, 125-142 (2011)

Solid Dispersions as a Drug Delivery System

Ki Taek Kim*, Jae Young Lee*, Mee Yeon Lee, Chung Kil Song, Joonho Choi and Dae-Duk Kim†

College of Pharmacy and Research Institute of Pharmaceutical Sciences, Seoul National University, Seoul 151-742, Korea

(Received March 15, 2011 · Revised March 28, 2011 · Accepted March 29, 2011)

ABSTRACT – Solid dispersion, defined as the dispersion of one or more active ingredient in a carrier or matrix at solid state, is an efficient strategy for improving dissolution of poorly water-soluble drugs for enhancement of their bioavailability. Compared to other conventional formulations such as tablets or capsules, solid dispersion which can be prepared by various methods has many advantages. However, despite numerous studies which have been carried out, limitations for commercializing these products remain to be solved. For example, during the manufacturing process or storage, amorphous form of solid dispersion can be converted into crystalline form. That is, the dissolution rate of solid dispersion would continuously decrease during storage, resulting in a product of no value. To resolve these problems, studies have been conducted on the effects of excipients. In fact, modification of the solid dispersions to overcome these disadvantages has progressed from the first generation to the recent third generation products. In this review, an overview on solid dispersions in general will be given with emphasis on the various manufacturing processes which include the use of polymers and on the stabilization strategies which include methods to prevent crystallization.

Key words – Solid dispersion, Polymeric carrier, Bioavailability, Crystallization, Stabilization

With the discovery of many novel drug candidates, the importance of finding appropriate formulations and treatment routes for these bioactive entities is emphasized more than ever. There are various factors that need to be considered to make these drugs into the right dosage formulation. The initial developmental direction is whether the drug has hydrophilic or hydrophobic properties because drugs have to have an adequate effect at the target site. These properties are important in terms of stable delivery until they reach the exact target site.

The focus of this review will be on oral drug formulations which need to pass through the gastrointestinal site while being transported to target. As a matter of fact, most of the newly-discovered drugs have poor water solubility (van Drooge, 2006; Vasconcelos and Sarmento et al., 2007). Since the gastrointestinal membrane has lipophilic components, these hydrophobic drugs can easily permeate through the gastrointestinal membrane (Gardner, 1997; Streubel, 2006). However these drugs lack an essential factor for enhancing drug's bioavailability which is water solubility in the hydrophilic gastrointestinal fluid (Ohara, 2005; Desai, 2006; Streubel, 2006; Vippagunta and Wang et al., 2007). Reducing the drug particle size or modifying the drug's structure to become more water soluble is a few examples of methods that can be utilized to make the drug more soluble in the GI fluid. However, altering the drug particle itself carries obvious limitations which are inadequate for enhancement of bioavailability. Therefore, additional physical changes including control of drug release from their formulations should be taken into consideration.

Solid dispersion is one of the most successful strategies for improving the drug release profile. A broad range of newly discovered drugs are formulated using this solid dispersion technique. Moreover, several useful carriers which have been discovered make solid dispersion one of the most efficient pharmaceutical formulations. Therefore, despite the remaining problem of stability, the development of polymers and surface active carriers are revealing promising results in improving the dispersion formulations. An overview on solid dispersions in general will be given in this review with emphasis on the various manufacturing processes and on the stabilization strategies.

Definition of Solid Dispersion

Solid dispersion, as implied in its name, refers to the solid state where one substance is dispersed into another material. The substances can be mixed completely or partially, containing several phases. In general, solid dispersion is defined as

*These authors contributed equally to this work.
†Corresponding Author :
Tel : +82-2-880-7870, E-mail : ddkim@snu.ac.kr
DOI : 10.4333/KPS.2011.41.3.125

Article

Journal of
Nanoscience and Nanotechnology

www.aspbs.com/jnn

Capmul MCM/Solutol HS15-Based Microemulsion for Enhanced Oral Bioavailability of Rebamipide

Ki Taek Kim[1], Jae-Young Lee[1], Ju-Hwan Park[1], Hyun-Jong Cho[2], In-Soo Yoon[3,*] and Dae-Duk Kim[1,*]

[1]*College of Pharmacy and Research Institute of Pharmaceutical Sciences, Seoul National University, Seoul 08826, Republic of Korea*
[2]*College of Pharmacy, Kangwon National University, Gangwon 24341, Republic of Korea*
[3]*College of Pharmacy and Natural Medicine Research Institute, Mokpo National University, Jeonnam 58554, Republic of Korea*

Rebamipide (RBP) is a potent anti-ulcer and anti-oxidative agent, which is a BCS class IV drug with a low oral bioavailability of less than 10%. Thus, the systemic absorption of RBP into the blood circulation is an essential prerequisite for exerting its pharmacological activities after oral dosing. Herein, we report on microemulsion (ME) systems for the enhancement of oral RBP bioavailability. In this study, MEs consisting of Capmul MCM (oil), Solutol HS15 (surfactant), and ethanol (co-surfactant) were prepared by the construction of pseudo-ternary phase diagram. The RBP-loaded MEs had spherical nano-sized droplets with narrow size distribution and neutral zeta potential. Moreover, the prepared MEs significantly enhanced the dissolution and oral bioavailability of RBP with no discernible intestinal toxicity. These results suggest that the present ME system could be further developed as an alternative oral formulation for RBP.

Keywords: Rebamipide, Bioavailability, Microemulsion, Solutol HS 15, Capmul MCM.

1. INTRODUCTION

Rebamipide (RBP) is a potent anti-ulcer and anti-oxidative agent, which acts by stimulating prostaglandin production in the gastric mucosa and inhibiting several inflammation mechanisms including neutrophil activation in the blood capillary.[1] Thus, following the oral dosing of RBP, its systemic absorption into the blood circulation is an essential prerequisite for exerting its pharmacological activities.

However, RBP, classified as a BCS class IV drug, has a low oral bioavailability of less than 10%, which may cause difficulties in optimizing RBP-based therapy.[2] Thus, in recent studies, solid dispersions and nano-crystal tablets were prepared to enhance the solubility/dissolution and oral bioavailability of RBP.[3, 4] However, there still exists the necessity of further attempts to develop more efficient oral formulations for RBP.

Amongst various drug delivery systems, microemulsion (ME) has been reported to significantly enhance the solubility/dissolution and oral bioavailability of several BCS class IV drugs including docetaxel, paclitaxel, and cefpodoxime.[5–7] However, to the best of our knowledge, there are few studies on the development of ME systems for the oral delivery of RBP. In this study, the RBP-loaded MEs were prepared by the construction of phase diagram and evaluated in terms of particle size/morphology, drug dissolution, and *in vivo* oral bioavailability and toxicity in rats.

*Corresponding author.
(D. D. Kim). Tel: +82 2 880 7870; fax: +82 2 873 9177.
E-mail address: ddkim@snu.ac.kr
(I. S. Yoon). Tel: +82 61 450 2688; fax: +82 61 450 2689.
E-mail address: isyoon@mokpo.ac.kr

Journal of Pharmaceutical Investigation (2016) 46:363–375
DOI 10.1007/s40005-016-0258-8

Online ISSN 2093-6214
Print ISSN 2093-5552

REVIEW

Application of montmorillonite in bentonite as a pharmaceutical excipient in drug delivery systems

Ju-Hwan Park[1] · Hyeon-Jong Shin[1] · Min Hwan Kim[1] · Ji-Su Kim[1] · Naewon Kang[1] · Jae-Young Lee[1] · Ki-Taek Kim[1] · Jangik Ike Lee[1] · Dae-Duk Kim[1]

Received: 13 April 2016 / Accepted: 9 May 2016 / Published online: 21 May 2016

Abstract Montmorillonite is a multifunctional clay mineral and a major component of bentonite. Montmorillonite has been used in various industrial and pharmaceutical fields due to its unique characteristics, which include swelling and adsorption. The high adsorption capacity of montmorillonite contributes to increase drug entrapment and sustained-release of drugs. Montmorillonite generally sustains drug release in many formulations by strongly adsorbing to the drug. In addition, montmorillonite enhances the dissolution rate and bioavailability of hydrophobic drugs. Moreover, montmorillonite was applied to form composites with other polymer-based delivery systems. Thus, montmorillonite could be applied to formulate diverse drug delivery systems to control and/or improve the pharmaceutical properties of drugs, including solubility, dissolution rate, and absorption. In this review, perspectives of applying montmorillonite as a pharmaceutical excipient in drug delivery systems are discussed.

Keywords Bentonite · Montmorillonite · Adsorption · Cationic exchange · Sustained release · Delivery system · Drug release

✉ Dae-Duk Kim
ddkim@snu.ac.kr

[1] College of Pharmacy and Research Institute of Pharmaceutical Sciences, Seoul National University, Seoul 08826, Republic of Korea

Introduction

Montmorillonite is a major active component of bentonite and a multifunctional clay mineral with unique properties, such as swelling and adsorption. These characteristics, have allowed montmorillonite to be widely used in medical and industrial applications (Eisenhour and Brown 2009; Carretero and Pozo 2010). Moreover, it has been applied to develop diverse drug delivery systems to overcome the pharmaceutical disadvantages of drugs, including low solubility and poor pharmacokinetic properties (low bioavailability and short biological half-life) (McNerny et al. 2010; Savjani et al. 2012; Griffin et al. 2013; Mould et al. 2015). Considering these characteristics of montmorillonite, applying this clay mineral to drug delivery systems could be a promising approach to improve the therapeutic efficacy of drugs in the body via sustained release of hydrophilic drugs or solubilization of hydrophobic drugs. Moreover, montmorillonite enhances the function of original formulations of various drug carriers. In this review, basic information about montmorillonite, including its physicochemical characteristics, will be introduced, and perspectives for various applications of montmorillonite as a pharmaceutical excipient in drug delivery systems will be discussed in more detail.

Bentonite and montmorillonite

Bentonite is a natural clay containing clay minerals in the smectite group that was formed by devitrification of volcanic ash that fell into water (Eisenhour and Brown 2009). Bentonite was named after Fort Benton near Rock River, Wyoming, USA where it was originally found, by W.C. Knight in 1898. This clay has excellent swelling,

Colloids and Surfaces B: Biointerfaces 145 (2016) 267–274

Contents lists available at ScienceDirect

Colloids and Surfaces B: Biointerfaces

journal homepage: www.elsevier.com/locate/colsurfb

Electrosprayed nanocomposites based on hyaluronic acid derivative and Soluplus for tumor-targeted drug delivery

Song Yi Lee[a,1], Jeong-Jun Lee[a,1], Ju-Hwan Park[b], Jae-Young Lee[b], Seung-Hak Ko[c], Jae-Seong Shim[c,d], Jongkook Lee[a], Moon Young Heo[a], Dae-Duk Kim[b], Hyun-Jong Cho[a,*]

[a] College of Pharmacy, Kangwon National University, Chuncheon 200-701, Republic of Korea
[b] College of Pharmacy and Research Institute of Pharmaceutical Sciences, Seoul National University, Seoul 151-742, Republic of Korea
[c] Biogenics Inc., Daejeon 305-510, Republic of Korea
[d] Skin & Tech Inc., Seongnam 461-713, Republic of Korea

ARTICLE INFO

Article history:
Received 17 February 2016
Received in revised form 8 April 2016
Accepted 3 May 2016
Available online 6 May 2016

Keywords:
CD44 receptor
Electrospraying
Nanocomposite
Resveratrol
Tumor targeting

ABSTRACT

Nanocomposite (NC) based on hyaluronic acid-ceramide (HACE) and Soluplus (SP) was fabricated by electrospraying for the tumor-targeted delivery of resveratrol (RSV). Amphiphilic property of both HACE and SP has been used to entrap RSV in the internal cavity of NC. Electrospraying with established experimental conditions produced HACE/SP/RSV NC with 230 nm mean diameter, narrow size distribution, negative zeta potential, and >80% drug entrapment efficiency. Sustained and pH-dependent drug release profiles were observed in drug release test. Cellular uptake efficiency of HACE/SP NC was higher than that of SP NC, mainly based on HA-CD44 receptor interaction, in MDA-MB-231 (CD44 receptor-positive human breast cancer) cells. Selective tumor targetability of HACE/SP NC, compared to SP NC, was also confirmed in MDA-MB-231 tumor-xenograted mouse model using a near-infrared fluorescence (NIRF) imaging. According to the results of pharmacokinetic study in rats, decreased *in vivo* clearance and increased half-life of RSV in NC group, compared to drug solution group, were shown. Given that these experimental results, developed HACE/SP NC can be a promising theranostic nanosystem for CD44 receptor-expressed cancers.

1. Introduction

Currently, diverse chemotherapeutic agents have been developed, but their clinical uses are restricted due to their random distribution to normal tissues and organs (non-tumor region) and subsequent toxicities to those tissues and organs. To deliver drug payload to cancer selectively, tumor targeting strategies have been introduced [1–3]. Solid tumors have an enhanced vascular permeability, due to high ratio of proliferating endothelial cells, deficiency of pericytes, and abnormal formation of basement membrane, and insufficient lymphatic drainage caused by the immature lymphatic systems [4,5]. Therefore, macromolecules are prone to leak out from the tumor blood vessels and accumulate in the tumor tissue. This enhanced permeability and retention (EPR) effect does not occur in normal tissues, thus it has been used as a passive tumor targeting strategy. However, as a passive tumor targeting lacks a sufficient tumor targetability, introduction of tumor targeting ligands (*i.e.* small chemicals, peptides, antibodies) to delivery systems has been used as an active tumor targeting strategy [4]. After reaching the tumor region *via* an EPR effect (as a passive tumor targeting), nano-sized drug delivery systems can be easily internalized into the cancer cells by ligand-receptor interaction (as an active tumor targeting).

As one of active tumor targeting strategies, hyaluronic acid (HA)-CD44 receptor interaction has been adopted and it has been used for the development of anticancer drug delivery systems [6–8]. In our previous reports [9–15], hyaluronic acid-ceramide (HACE)-based nanocarriers were fabricated for tumor-targeted drug delivery and cancer diagnosis. In this investigation, HACE with Soluplus (SP) were used to make nanocomposites (NCs) for anticancer drug delivery. Compared to our previous studies [9–15], electrospraying process, instead of solvent evaporation method, was applied to fabricate HACE/SP NC as a theranostic nanosystem. Electrospraying, as one of electrohydrodynamic techniques, can generate nano-sized particles by one-step process [16]. If the Coulomb force (electrostatic force inside the droplet) overcomes the cohesive force of the droplet, the droplet may break into the smaller ones. Dur-

* Corresponding author.
E-mail address: hjcho@kangwon.ac.kr (H.-J. Cho).
[1] These authors have equally contributed to this work

http://dx.doi.org/10.1016/j.colsurfb.2016.05.009
0927-7765/

ISSN 0377-9556 (PRINT) ISSN 2383-9457 (ONLINE)
약학회지 제 60 권 제 2 호 73~77 (2016)
Yakhak Hoeji Vol. 60, No. 2
DOI 10.17480/psk.2016.60.2.73

藥學會誌

시판중인 메트릭스 정제의 팽윤력 비교 연구

김기택 · 김지수 · 박주환 · 이재영 · 조영우* · 양재권* · 장준희* · 최은선* · 김대덕#
서울대학교 약학대학, *대화제약(주)
(Received February 16, 2016; Revised February 26, 2016; Accepted March 1, 2016)

Swelling of Commercial Matrix Tablets Based on Carboxymethyl Cellulose Sodium and Alginic Acid

Ki Taek Kim, Ji Su Kim, Ju-Hwan Park, Jae-Young Lee, Yeong Woo Jo*, Jae-Gwon Yang*, Jun Hee Jang*, Eun-Sun Choi* and Dae-Duk Kim#
College of Pharmacy, Seoul National University, Seoul 08826, Korea
**Daehwa Pharmaceutical Co., Ltd., Seoul 08805, Korea*

Abstract — Alginic acid and carboxymethyl cellulose sodium are dietary fibers from plants. They have a swelling property and delay the gastric emptying time, thereby resulting in feeling satiated after oral administration, which may eventually contribute to loss of body weight. The goal of this study was to compare swelling property of three commercial matrix tablets based on alginic acid and carboxymethyl cellulose sodium. When the swelling was determined by the Korean Ministry of Food and Drug Safety (MFDS) guideline, the tablet prepared by direct compression method with highly viscous swelling agent showed the highest swelling in acidic conditions. Water uptake of these tablets was rapid and completed within 30 min. Moreover, when the pH was changed from 2.5 to 6.8 buffer, the water uptake was not significantly changed in all tablets.

Keywords □ alginic acid, carboxymethyl cellulose sodium, tablet, swelling, water uptake

식이섬유의 섭취는 질병 예방과 건강 증진을 위한 식사지침으로 세계적으로 추천되고 있으며, 이것이 비만의 관리 및 체중 감량을 위한 유용한 방법이 될 수 있다는 연구 또한 계속적으로 보고되고 있다.[1,2] 식이섬유는 식물에서 유래된, 소화가 일어나지 않는 탄수화물류 및 리그닌을 포함하는 것으로 점성을 갖는 식이섬유는 음식물의 위 통과시간을 지연시켜 포만감을 느끼게 한다.[3] 알긴산은 갈조류로부터 추출되는 식이섬유 중 하나로서 점성을 갖고, 위 내의 산성 환경에서 겔을 형성하여 위 통과시간을 지연시키게 된다.[4] 최근의 연구에서, 일주일 동안 식사 전 알긴산 섭취를 한 실험군이 대조군에 비해 열량섭취가 유의적으로 낮았음을 보고하였다.[5] 카르복시메틸셀룰로오스나트륨 또한 점성을 갖는 식이섬유 중 하나로, 식물세포벽의 구성성분인 셀룰로오스 유래의 성분이다.[3] 이것 역시 위 내에서 물을 흡수하여 팽윤하고, 위 통과시간을 지연시킨다는 연구가 보고되어 있다.[6] 국내에는 일반의약품으로서 위의 두 가지의 팽윤성 고분자를 주성분으로 하는 메트릭스 정제가 음식물 섭취감소를 통한 체중감량의 보조요법 목적으로 시판되고 있는데, 한 개의 정제 당 200 mg의 알긴산과 100 mg의 카르복시메틸셀룰로오스나트륨을 함유하고 있다. 본 연구의 목적은, 알긴산과 카르복시메틸셀룰로오스나트륨을 주성분으로 하여 시판중인 세 가지 메트릭스 정제의 팽윤력을 비교 평가하고, 팽윤제의 분자량과 점도 및 제조공정이 팽윤에 미치는 영향을 고찰하는 것이다.

#**Corresponding Author**
Dae-Duk Kim
College of Pharmacy, Seoul National University, Seoul 08826, Korea
Tel.: 02-880-7870 Fax.: 02-873-9177
E-mail: ddkim@snu.ac.kr

실험 방법

시약

시판 중인 세 가지 팽윤성 메트릭스 정제(각각 A정, B정, C정으로 명명, C정은 대화제약(주)의 마론정)는 시중의 약국에서 구입하였다. 알긴산과 카르복시메틸셀룰로오스나트륨, 기타 부형제 및 실험에 사용된 모든 시료는 대화제약(주)로부터 공급받았다.

Colloids and Surfaces B: Biointerfaces 140 (2016) 239–245

Contents lists available at ScienceDirect

Colloids and Surfaces B: Biointerfaces

journal homepage: www.elsevier.com/locate/colsurfb

Omega-3 fatty acids incorporated colloidal systems for the delivery of *Angelica gigas* Nakai extract

Jeong-Jun Lee[a], Ju-Hwan Park[b], Jae-Young Lee[b], Jae Young Jeong[a], Song Yi Lee[a], In-Soo Yoon[c], Wie-Soo Kang[d], Dae-Duk Kim[b], Hyun-Jong Cho[a,*]

[a] College of Pharmacy, Kangwon National University, Chuncheon 200-701, Republic of Korea
[b] College of Pharmacy and Research Institute of Pharmaceutical Sciences, Seoul National University, Seoul 151-742, Republic of Korea
[c] College of Pharmacy and Natural Medicine Research Institute, Mokpo National University, Jeonnam 534-729, Republic of Korea
[d] School of Bioscience and Biotechnology, Kangwon National University, Chuncheon 200-701, Republic of Korea

ARTICLE INFO

Article history:
Received 11 September 2015
Received in revised form
26 November 2015
Accepted 24 December 2015
Available online 29 December 2015

Keywords:
Angelica gigas Nakai
Colloidal carrier
Omega-3
Oral formulation
TPGS

ABSTRACT

Omega-3 (ω-3) fish oil-enriched colloidal systems were developed for the oral delivery of *Angelica gigas* Nakai (AGN) extract (ext). By constructing a pseudo-ternary phase diagram, the composition of oil-in-water (o/w) microemulsion (ME) systems based on ω-3 (oil), Labrasol (surfactant), and water was determined. AGN ext was dissolved into the ME system and D-α-tocopherol polyethylene glycol 1000 succinate (TPGS) was added to the ME formulation in order to enhance the mucosal absorption of the pharmacologically active ingredients in the AGN ext. The droplet size of AGN-loaded MEs was 205–277 nm and their morphology was spherical. The release of major components of AGN, decursin (D) and decursinol angelate (DA), from ME formulations in pH 1.2 and 6.8 buffers was significantly greater ($P < 0.05$) than that from the AGN suspension group. The pharmacokinetic properties of AGN-loaded MEs in rats were evaluated by measuring decursinol (DOH) concentrations in plasma after oral administration. TPGS-included ME (F2) resulted in significantly greater ($P < 0.05$) systemic exposure of DOH than that with ME without TPGS (F1), AGN ext + TPGS, and AGN in suspension. Severe toxicity of F1 and F2 on the intestinal epithelium was not observed by histological staining. The colloidal carriers described herein are promising delivery systems for oral administration of AGN ext.

1. Introduction

Dang-Gui (*Angelica gigas*) is a biennial or short-lived perennial plant cultured in Northeast Asia, such as China, Japan, and Korea. Cham-Dang-Gui, the dried root of *A. gigas* Nakai (AGN), has been cultivated in Korea and used as a medicinal herb. Chemical compounds included in the roots, stems, and leaves of AGN are pyranocoumarins, simple coumarins, furocoumarins, phthalides, volatile compounds, polyacetylenes, flavonoids, organic acids, polysaccharides, and phenolics [1]. Among these, pyranocoumarins are the major chemical substances of alcoholic extracts of AGN. Decursin (D), decursinol angelate (DA), and decursinol (DOH) are abundant components of coumarins obtained from AGN extract (ext). Various therapeutic properties of these major compounds have been identified, such as analgesic, anticancer, anti-inflammatory, anti-obesity, anti-diabetic, and cognitive enhancing effects [1–6]. However, the poor aqueous solubility of these compounds can restrict dietary and medicinal applications [7,8].

Diverse approaches regarding formulation development have been tried to improve the solubility and bioavailability of pharmacologically active ingredients from natural products [8–11]. Colloidal dispersion systems, which have a nanoscale particle size, can be used in natural product formulations. Microemulsions (MEs) are clear, thermodynamically stable, and isotropic liquid mixtures based on oil, surfactant, and water. MEs have been widely used to increase the solubility and mucosal absorption of drugs [12,13].

In this investigation, omega-3 (ω-3)-based ME systems were developed for the oral delivery of an ethanol extract of AGN (AGN EtOH ext). Polyunsaturated fatty acids (PUFAs) containing a double bond located at the third carbon atom from the end of the carbon chain are called ω-3 fatty acids (FAs). The ω-3 FA types that are physiologically relevant to humans include α-linolenic acid (ALA, found in plant oils, 18:3), eicosapentaenoic acid (EPA, found in fish oils, 20:5), and docosahexaenoic acid (DHA, found in fish oils, 22:6). It is known that fish oil EPA and DHA have beneficial effects for

* Corresponding author. Tel.: +82 33 250 6916; fax: +82 33 259 5631.
E-mail address: hjcho@kangwon.ac.kr (H.-J. Cho).

http://dx.doi.org/10.1016/j.colsurfb.2015.12.047
0927-7765/

Journal of Medicinal Chemistry

Brief Article

pubs.acs.org/jmc

Selenoacyclovir and Selenoganciclovir: Discovery of a New Template for Antiviral Agents

Pramod K. Sahu,[†,§] Tamima Umme,[‡,§] Jinha Yu,[†] Akshata Nayak,[†,‡] Gyudong Kim,[†] Minsoo Noh,[†] Jae-Young Lee,[†] Dae-Duk Kim,[†] and Lak Shin Jeong*[,†]

[†]Research Institute of Pharmaceutical Sciences, College of Pharmacy, Seoul National University, Seoul 151-742, Korea

[‡]College of Pharmacy, Ewha Womans University, Seoul 120-750, Korea

Supporting Information

ABSTRACT: On the basis of the potent antiviral activity of acyclovir and ganciclovir, selenoacyclovir (**2a**) and selenoganciclovir (**2b**) were designed based on bioisoteric rationale and synthesized via the diselenide **7** as the key intermediate. Compound **2a** exhibited potent anti-HSV-1 and -2 activities while **2b** exerted moderate anti-HCMV activity, indicating that these nucleosides can serve as a novel template for the development of new antiviral agents.

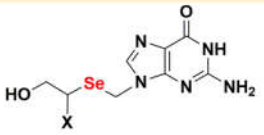

2a (X = H, seleno-acyclovir): anti-HSV activity
2b (X = CH_2OH, seleno-ganciclovir): anti-HCMV activity

INTRODUCTION

Therapy against viral infections still remains one of the substantial challenges to modern medicine because of appearances of resistance, latency, cytotoxicity, and so on.[1] The herpesviridae family including herpes simplex virus (HSV), varicella-zoster virus (VZV), cytomegalovirus (CMV), and Epstein−Barr virus (EBV) causes severe viral diseases in humans, which should be treated with antiviral chemotherapeutic agents.[1]

Acyclovir (**1a**),[2,3] which is a prototype of acyclic nucleosides, has been a drug of choice for the treatments of herpetic infections (Figure 1). This compound is converted into the triphosphate, which inhibits viral DNA polymerase.[4,5] Compound **1a** shows a high selectivity index because it is monophosphorylated only by viral encoded thymidine kinase but also has many drawbacks such as low oral bioavailability and poor solubility.[4,5] To overcome these disadvantages, its prodrug valacyclovir[6] has been developed and clinically used for the treatment of shingles. Ganciclovir (**1b**), another prototypical acyclic nucleoside, and its prodrug valganciclovir have been clinically developed against CMV infection.[7−9] In CMV infected cell, **1b** is converted to the monophosphate by a virus kinase encoded by the CMV gene UL97 (phosphotransferase), which is then subsequently converted into the diphosphate by cellular guanylate kinase and into the triphosphate by a number of cellular enzymes.[10] Ganciclovir triphosphate competitively inhibits CMV polymerase and competes with the natural 2′-deoxyguanosine 5′-triphosphate (dGTP) for incorporation into viral DNA. It can be also used as a substrate for CMV DNA polymerase and is incorporated into the viral DNA chain, resulting in the prevention of viral DNA synthesis.[10] However, this drug is also associated with high cytotoxicity such as bone marrow suppression,[11] hepatotoxicity,[12] and nephrotoxicity.[13] These drawbacks prompted us to design a new template for acyclic nucleoside drug development.

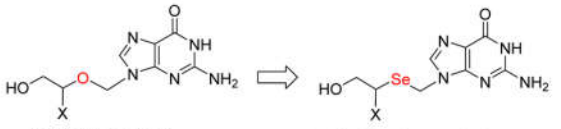

1a (X = H, acyclovir)
1b (X = CH_2OH, ganciclovir)

2a (X = H, seleno-acyclovir)
2b (X = CH_2OH, seleno-ganciclovir)

Figure 1. Rationale for the design of selenoacyclic nucleosides **2a** and **2b**.

Selenium is essential for cellular function in many organisms as a trace element. This element is a component of the antioxidant enzymes glutathione peroxidase and thioredoxin reductase, which protect the organism from oxidative damage.[14] In view of new drug developments, selenium possess several advantages such as the antioxidant properties and high lipophilicity which might enhance the penetration across the cell membrane, resulting in higher oral bioavailability. Selenium also exists in a bioisosteric relationship with oxygen, and it is expected to exhibit similar biological activity. Thus, based on these results, we designed and synthesized selenoacyclovir (**2a**) and selenoganciclovir (**2b**), which replaced the oxygens of acyclovir (**1a**) and ganciclovir (**1b**) with selenium, respectively, using novel selenium chemistry. Herein, we report the concise and efficient synthesis of the selenoacyclic nucleosides **2a** and **2b** and their antiviral activity.

RESULTS AND DISCUSSION

Chemistry. Scheme 1 illustrates the retrosynthetic analysis to final nucleosides **2a** and **2b**. The final compounds can be synthesized via two routes.

Received: May 27, 2015
Published: October 13, 2015

DOI: 10.1021/acs.jmedchem.5b00804
J. Med. Chem. 2015, 58, 8734−8738

PLOS | ONE

RESEARCH ARTICLE

Angelica gigas Nakai and Soluplus-Based Solid Formulations Prepared by Hot-Melting Extrusion: Oral Absorption Enhancing and Memory Ameliorating Effects

Jingpei Piao[1], Jae-Young Lee[2], Jin Bae Weon[3], Choong Je Ma[3,4], Hyun-Jeong Ko[5], Dae-Duk Kim[2], Wie-Soo Kang[1]*, Hyun-Jong Cho[5]*

1 School of Bioscience and Biotechnology, Kangwon National University, Chuncheon, 200–701, Republic of Korea, **2** College of Pharmacy and Research Institute of Pharmaceutical Sciences, Seoul National University, Seoul, 151–742, Republic of Korea, **3** Department of Medical Biomaterials Engineering, College of Biomedical science, Kangwon National University, Chuncheon, 200–701, Republic of Korea, **4** Research Institute of Biotechnology, Kangwon National University, Chuncheon, 200–701, Republic of Korea, **5** College of Pharmacy, Kangwon National University, Chuncheon, 200–701, Republic of Korea

* kangwiso@kangwon.ac.kr (WSK); hjcho@kangwon.ac.kr (HJC)

OPEN ACCESS

Citation: Piao J, Lee J-Y, Weon JB, Ma CJ, Ko H-J, Kim D-D, et al. (2015) *Angelica gigas* Nakai and Soluplus-Based Solid Formulations Prepared by Hot-Melting Extrusion: Oral Absorption Enhancing and Memory Ameliorating Effects. PLoS ONE 10(4): e0124447. doi:10.1371/journal.pone.0124447

Academic Editor: Junxuan Lu, Texas Tech Univ School of Pharmacy, UNITED STATES

Received: September 16, 2014

Accepted: March 13, 2015

Published: April 27, 2015

Data Availability Statement: All relevant data are within the paper and its Supporting Information files.

Funding: This study is supported by Kangwon National University (http://www.kangwon.ac.kr) and the National Research Foundation of Korea (NRF), funded by the Korean government (MSIP) (No. NRF-2012R1A1A1038944, URL http://www.nrf.re.kr/nrf_tot_cms/index.jsp?pmi-sso-return2=none&pmi-sso-return2=none).

Competing Interests: The authors have declared that no competing interests exist.

Abstract

Oral solid formulations based on *Angelica gigas* Nakai (AGN) and Soluplus were prepared by the hot-melting extrusion (HME) method. AGN was pulverized into coarse and ultrafine particles, and their particle size and morphology were investigated. Ultrafine AGN particles were used in the HME process with high shear to produce AGN-based formulations. In simulated gastrointestinal fluids (pH 1.2 and pH 6.8) and water, significantly higher amounts of the major active components of AGN, decursin (D) and decursinol angelate (DA), were extracted from the HME-processed AGN/Soluplus (F8) group than the AGN EtOH extract (ext) group ($p < 0.05$). Based on an *in vivo* pharmacokinetic study in rats, the relative oral bioavailability of decursinol (DOH), a hepatic metabolite of D and DA, in F8-administered mice was 8.75-fold higher than in AGN EtOH ext-treated group. In scopolamine-induced memory-impaired mice, F8 exhibited a more potent cognitive enhancing effect than AGN EtOH ext in both a Morris water maze test and a passive avoidance test. These findings suggest that HME-processed AGN/Soluplus formulation (F8) could be a promising therapeutic candidate for memory impairment.

Introduction

Angelica gigas (Dang-Gui) is a biennial or short lived perennial plant found in China, Japan, and Korea. The root of *Angelica gigas* has been used in oriental traditional medicine and is marketed as a functional food product in Europe and North America [1]. Cham-Dang-Gui (Korean Angelica, the dried root of *Angelica gigas* Nakai (AGN)) has been principally cultivated in Korea and used as a Korean medicinal herb. It contains several chemicals, such as

International Journal of Nanomedicine

Dovepress
open access to scientific and medical research

Open Access Full Text Article

ORIGINAL RESEARCH

Preparation and characterization of self-assembled nanoparticles based on low-molecular-weight heparin and stearylamine conjugates for controlled delivery of docetaxel

This article was published in the following Dove Press journal:
International Journal of Nanomedicine
8 December 2014
Number of times this article has been viewed

Dong-Hwan Kim[1]
Ubonvan Termsarasab[1]
Hyun-Jong Cho[2]
In-Soo Yoon[3]
Jae-Young Lee[1]
Hyun Tae Moon[1]
Dae-Duk Kim[1]

[1]College of Pharmacy and Research Institute of Pharmaceutical Sciences, Seoul National University, Seoul, Republic of Korea; [2]College of Pharmacy, Kangwon National University, Chuncheon, Republic of Korea; [3]College of Pharmacy and Natural Medicine Research Institute, Mokpo National University, Jeonnam, Republic of Korea

Abstract: Low-molecular-weight heparin (LMWH)–stearylamine (SA) conjugates (LHSA)-based self-assembled nanoparticles were prepared for intravenous delivery of docetaxel (DCT). 1-Ethyl-3-(3-dimethylaminopropyl) carbodiimide and *N*-hydroxysuccinimide were used as coupling agents for synthesis of LHSA conjugates. The physicochemical properties, in vitro antitumor efficacy, in vitro cellular uptake efficiency, in vivo antitumor efficacy, and in vivo pharmacokinetics of LHSA nanoparticles were investigated. The LHSA nanoparticles exhibited a spherical shape with a mean diameter of 140–180 nm and a negative surface charge. According to in vitro release and in vivo pharmacokinetic test results, the docetaxel-loaded LHSA5 (LMWH:SA =1:5) nanoparticles exhibited sustained drug release profiles. The blank LHSA nanoparticles demonstrated only an insignificant cytotoxicity in MCF-7 and MDAMB 231 human breast cancer cells; additionally, higher cellular uptake of coumarin 6 (C6) in MCF-7 and MDAMB 231 cells was observed in the LHSA5 nanoparticles group than that in the C6 solution group. The in vivo tumor growth inhibition efficacy of docetaxel-loaded LHSA5 nanoparticles was also significantly higher than the Taxotere®-treated group in the MDAMB 231 tumor-xenografted mouse model. These results indicated that the LHSA5-based nanoparticles could be a promising anticancer drug delivery system.

Keywords: amphiphilic polymer, docetaxel, drug delivery, low-molecular-weight heparin, self-assembled nanoparticle

Introduction

Over the past decade, nanoparticulate drug delivery systems containing anticancer agents have been investigated extensively due to their specific accumulation behavior at the tumor site.[1,2] Nanoparticulate drugs can be distributed to tumor vasculatures by the enhanced permeability and retention (EPR) effect, taking advantage of the leaky vascular nature of tumor tissues that provides for passive tumor targeting.[3,4] Additionally, these nanoparticulate drugs offer the advantages of prolonged systemic circulation by avoiding phagocytosis, improved efficacy, and reduced toxicity. Numerous biocompatible and biodegradable materials, such as poly(lactic acid),[5,6] poly(glycolic acid),[7] polycaprolactone,[8,9] polysaccharides,[10] proteins,[11] and polypeptides,[12] have been used for the preparation of polymeric nanoparticles. Among them, polysaccharides have been used extensively to prepare nanoparticles for drug delivery.[2] Polysaccharides are natural biomaterials; thus, they are generally safe, nontoxic, biocompatible, and biodegradable. They have various derivable groups that can be modified with other

Correspondence: Dae-Duk Kim
College of Pharmacy and Research Institute of Pharmaceutical Sciences, Seoul National University, Seoul 151-742, Republic of Korea
Tel +82 2 8807 870
Fax +82 2 8739 177
Email ddkim@snu.ac.kr

submit your manuscript | www.dovepress.com
Dovepress
http://dx.doi.org/10.2147/IJN.S74353

International Journal of Pharmaceutics 473 (2014) 426–433

Contents lists available at ScienceDirect

International Journal of Pharmaceutics

journal homepage: www.elsevier.com/locate/ijpharm

Pharmaceutical nanotechnology

Development of poly(lactic-co-glycolic) acid nanoparticles-embedded hyaluronic acid–ceramide-based nanostructure for tumor-targeted drug delivery

Ju-Hwan Park [a], Jae-Young Lee [a], Ubonvan Termsarasab [a], In-Soo Yoon [b], Seung-Hak Ko [c], Jae-Seong Shim [c,d], Hyun-Jong Cho [e,*], Dae-Duk Kim [a,**]

[a] College of Pharmacy and Research Institute of Pharmaceutical Sciences, Seoul National University, Seoul 151-742, Republic of Korea
[b] College of Pharmacy and Natural Medicine Research Institute, Mokpo National University, Jeonnam 534-729, Republic of Korea
[c] Biogenics Inc., Daejeon 305-510, Republic of Korea
[d] Skin & Tech Inc., Seongnam 461-713, Republic of Korea
[e] College of Pharmacy, Kangwon National University, Chuncheon 200-701, Republic of Korea

ARTICLE INFO

Article history:
Received 15 March 2014
Received in revised form 21 May 2014
Accepted 25 July 2014
Available online 28 July 2014

Keywords:
Cancer diagnosis
Docetaxel
Embedding
Hyaluronic acid–ceramide
PLGA nanoparticle
Tumor targeting

ABSTRACT

A hyaluronic acid–ceramide (HACE) nanostructure embedded with docetaxel (DCT)-loaded poly(D,L-lactide-co-glycolide) (PLGA) nanoparticles (NPs) was fabricated for tumor-targeted drug delivery. NPs with a narrow size distribution and negative zeta potential were prepared by embedding DCT-loaded PLGA NPs into a HACE nanostructure (DCT/PLGA/HACE). DCT-loaded PLGA and DCT/PLGA/HACE NPs were characterized by solid-state techniques, including Fourier-transform infrared (FT-IR) spectroscopy, differential scanning calorimetry (DSC), and powder X-ray diffraction (PXRD). A sustained drug release pattern from the NPs developed was observed and negligible cytotoxicity was seen in NIH3T3 cells (normal fibroblast, CD44 receptor negative) and MDA-MB-231 cells (breast cancer cells, CD44 receptor positive). PLGA/HACE NPs containing coumarin 6, used as a fluorescent dye, exhibited improved cellular uptake efficiency, based on the HA-CD44 receptor interaction, compared to plain PLGA NPs. Cyanine 5.5 (Cy5.5)-labeled PLGA/HACE NPs were injected intravenously into a MDA-MB-231 tumor xenograft mouse model and demonstrated enhanced tumor targetability, compared with Cy5.5-PLGA NPs, according to a near-infrared fluorescence (NIRF) imaging study. Considering these experimental results, the DCT/PLGA/HACE NPs developed may be useful as a tumor-targeted drug delivery system.

1. Introduction

Nano-sized vehicles have attracted much interest for anticancer drug delivery and cancer diagnosis (Cho and Kwon, 2011; Koo et al., 2012; Termsarasab et al., 2013a,b; Yoon et al., 2013a,b; Zhang et al., 2013). Due to the innate cytotoxicity of anticancer drugs to normal tissues and organs, tumor targeting has long been regarded as desirable for anticancer drug delivery. Numerous approaches to tumor targeting have been developed and some have been used successfully in clinical cancer therapy (Cheng et al., 2012; Ma et al., 2011).

Tumor targeting strategies are generally classified into passive and active targeting (Danhier et al., 2010; Lammers et al., 2012; Maeda et al., 2013). Passive tumor targeting is based on the "enhanced permeability and retention" (EPR) effect, which may be caused by large clefts in the endothelium of blood vessels and an impaired lymphatic drainage system in tumors. Thus, macromolecules can readily accumulate in the tumor region and drug-loaded nanovehicles may exert improved anti-cancer efficacy. Major drawbacks of the passive targeting strategy are insufficient tumor targetability and the continuing toxic potential to normal cells. To address this limitation, specific ligands (small molecules, peptides, proteins) that have a high binding affinity for receptors overexpressed on cancer cells have been introduced to nanovehicles to improve tumor targeting efficiency (Danhier et al., 2012; Kamaly et al., 2012).

For anticancer drug delivery and cancer diagnosis, diverse biocompatible materials have been used to fabricate nanovehicles (Bunschoten et al., 2012; Lee et al., 2011; Yoon et al., 2013a,b).

* Corresponding author. Tel.: +82 33 250 6916; fax: +82 33 259 5631.
** Corresponding author. Tel.: +82 2 880 7870; fax: +82 2 873 9177.
E-mail addresses: hjcho@kangwon.ac.kr (H.-J. Cho), ddkim@snu.ac.kr (D.-D. Kim).

http://dx.doi.org/10.1016/j.ijpharm.2014.07.038
0378-5173/

Colloids and Surfaces B: Biointerfaces 121 (2014) 380–387

Contents lists available at ScienceDirect

Colloids and Surfaces B: Biointerfaces

journal homepage: www.elsevier.com/locate/colsurfb

Interconnected hyaluronic acid derivative-based nanoparticles for anticancer drug delivery

Ju-Hwan Park[a,1], Hyun-Jong Cho[b,1], Ubonvan Termsarasab[a], Jae-Young Lee[a], Seung-Hak Ko[c], Jae-Seong Shim[c,d], In-Soo Yoon[e], Dae-Duk Kim[a,*]

[a] College of Pharmacy and Research Institute of Pharmaceutical Sciences, Seoul National University, Seoul 151-742, Republic of Korea
[b] College of Pharmacy, Kangwon National University, Chuncheon 200-701, Republic of Korea
[c] Biogenics Inc., Daejeon 305-510, Republic of Korea
[d] Skin & Tech Inc., Seongnam 461-713, Republic of Korea
[e] College of Pharmacy and Natural Medicine Research Institute, Mokpo National University, Jeonnam 534-729, Republic of Korea

ARTICLE INFO

Article history:
Received 25 February 2014
Received in revised form 8 June 2014
Accepted 9 June 2014
Available online 16 June 2014

Keywords:
Interconnected structure
Hyaluronic acid-ceramide
Doxorubicin
High drug payload
Tumor targeting

ABSTRACT

Doxorubicin (DOX)-loaded nanoparticles (NPs) based on interconnected hyaluronic acid-ceramide (HACE) structure were fabricated and their anti-tumor efficacy was evaluated *in vitro*. Interconnected HACE was synthesized by cross-linking HACE with adipic acid dihydrazide (ADH) and its synthesis was identified by ^{1}H NMR analysis. DOX-loaded NPs with <200 nm mean diameter, negative zeta potential, and spherical shape were prepared. Interconnected HACE-based NPs increased drug-loading capacity and *in vitro* drug release, compared to HACE-based NPs. DOX release was dependent on the environmental pH, implying the feasibility of enhancing drug release in tumor region and endosomal compartments. Synthesized interconnected HACE did not show cytotoxic effect up to 1000 μg/ml concentration in NIH3T3 and MDA-MB-231 cells. In cellular uptake studies using confocal laser scanning microscopy (CLSM) and flow cytometry in MDA-MB-231 cells, higher uptake of DOX was observed in the interconnected HACE-based NPs than HACE NPs. *In vitro* anti-tumor efficacy was assessed by MTS-based assay, in which cytotoxic effect of DOX-loaded interconnected HACE NPs was higher than that of DOX-loaded HACE NPs. Thus, these results suggest the feasibility of interconnected HACE-based NPs to be used for efficient tumor-targeted delivery of anticancer drugs.

1. Introduction

Administration of unfabricated anticancer drugs may result in treatment failure due to the following reasons: short half-life in the body, poor tumor selectivity, unwanted accumulation in normal organs and tissues, and susceptibility to acquire multidrug resistance in cancer cells. To overcome these obstacles, various approaches with drug delivery systems have been tried. Particularly, nano-sized systems have gained substantial interests for anticancer drug delivery [1–3].

Nanocarriers can avoid uptake by reticuloendothelial system (RES), thus prolonging the drug circulation in the blood stream. However, those with specific mean diameter and surface properties are not eliminated easily and subsequently could be accumulated in leaky tumor region. Enhanced permeability and retention (EPR) effect is based on the unique characteristics of the tumor region, such as dysfunctional lymphatic drainage and leaky vasculature [4,5]. However, passive targeting strategy, usually represented by EPR effect, has its intrinsic drawbacks, including low tumor specificity. Therefore, diverse active targeting strategies have been tried to overcome the limitation of passive targeting strategy.

Hyaluronic acid (HA) is known as a tumor-targeting ligand for the CD44 receptor which is overexpressed in various kinds of cancers [6–8]. Specific ligands, including peptides and proteins or small molecules, can be conjugated directly to the drug itself or to nanocarriers [9–11]. On the other hand, carriers have been prepared by using biomaterials (i.e. HA) that can act as tumor-targeting ligands. HA can thus seek tumor tissue actively and deliver anticancer drugs to the particular region selectively, reducing adverse reactions which may occur in normal organs and tissues.

Diverse biopolymer-based nanocarriers based on these targeting strategies have been developed [12,13]. In spite of their biocompatibility, they may also have several shortcomings such

* Corresponding author. Tel.: +82 2 880 7870; fax: +82 2 873 9177.
E-mail address: ddkim@snu.ac.kr (D.-D. Kim).
[1] These authors have contributed equally.

http://dx.doi.org/10.1016/j.colsurfb.2014.06.025
0927-7765/